

Chapter 2

Basic Principles

2.1 Introduction

In this chapter the process group of forming will be described in detail. First, a series of basic problems in forming engineering will be discussed in order to understand, classify and evaluate the relevant technological idiosyncrasies involved. Thereby, the material to be formed along with its plastic behaviour under mechanical stress and under the effects of temperature will be in focus. This chapter serves to help understanding the material properties under various stresses which arise within the sphere of forming engineering. Thereby, the basic insights of metallurgy and plasticity theory will be explicated as well as the tribological relations between the tool and the workpiece. Furthermore, different ways to determine the material data of the workpiece materials will be described and various computational solution possibilities for problems in theory of plasticity will be shown.

2.2 Metallurgical Foundations for Determining the Condition of the Material

2.2.1 *Crystal Structure*

Metals make up the largest group among the workpiece materials. They consist of atoms that are metallically bonded. The common property of all ferrous and non-ferrous metals is their crystalline structure, i.e. their regular, definite arrangement of atoms. Metal physics has developed models of crystal structure as shown in Fig. 2.1 in atomic and macroscopic views using the unit cell of α -iron as an example.

Most metals have either a cubic or hexagonal crystal system. In the case of cubic crystal systems, we distinguish between a body-centred and a face-centred lattice structure.

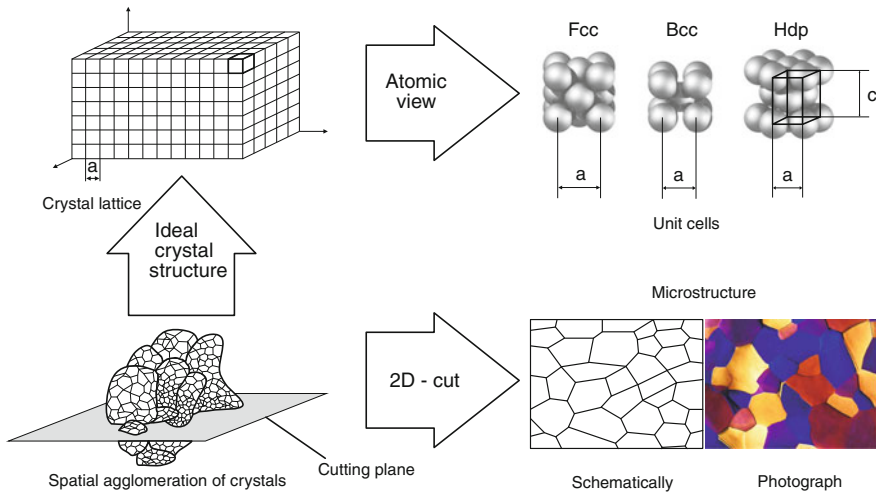


Fig. 2.1 Atomic and macroscopic views of metal structure; *bottom right*: grain structure, schematic and real

Examples for body-centred cubic (bcc) lattices are ferritic steel, chrome (Cr), tungsten (W), molybdenum (Mo), vanadium (V), niobium (Nb) and tantalum (Ta). Austenitic steel, aluminium (Al), copper (Cu), nickel (Ni), silver (Ag), platinum (Pt), gold (Au) and lead (Pb) are examples of face-centred cubic (fcc) crystal structures. Magnesium (Mg), zinc (Zn) and beryllium (Be) are hexagonally (hcp) structured. Many metals can exhibit different lattice structures. For example, titanium (Ti) is hexagonally oriented below 1,155 K, while above this temperature it transforms into a body-centred cubic structure. Iron (Fe) has a similar behaviour. At room temperature, iron has a bcc lattice structure, and at 1,184 K (911 °C) it changes to a fcc lattice structure. Iron reverts back to a body-centred cubic crystal structure above 1,665 K (1,392 °C).

The unit cell is the smallest geometrically cohesive unit of a crystal lattice. The lattice constants are in the range of 0.2–0.5 nm for a large number of metals. If theoretically unit cells are put together in all three spatial coordinates, a crystal lattice is formed (see Fig. 2.1, top left). Basically, the unit cell already contains the most important regularities and properties of the entire crystal. By geometrically stringing together unit cells, ideal crystals are created, i.e. faultless crystals which do not occur in practice. The real space lattice of the metals exhibit a variety of deviations (lattice defects). Fundamentally, we distinguish between three types of lattice fault:

- **Zero-dimensional lattice faults (point-shaped lattice faults):** if the atoms are embedded at interstitial sites, we speak of interstitial atoms. If the atom sites are occupied by foreign atoms, we refer to them as exchange or substitute atoms. If foreign atoms are located at interstitial sites, they are called interstitial impurity atoms. Sites, that are not occupied by atoms are called vacancies. Lattice

vacancies, or vacancy density, are especially important for thermally activated processes such as diffusion.

- One-dimensional lattice faults: one-dimensional lattice faults are linear structural faults (dislocations), see Fig. 2.3. The most important dislocations are edge dislocations and screw dislocations. Figure 2.3 provides a schematic view of an edge dislocation. Dislocations make plastic forming possible and are therefore of especial importance.
- Two-dimensional lattice faults: two-dimensional lattice faults result from surface effects. The most important two-dimensional lattice faults are grain boundaries and phase interfaces. Crystallization from the fluid state generally initiates at many different locations. Proceeding from seeds, the crystals grow towards each other. If a crystal encounters a second crystal during the growth phase (either from the fluid phase or during recrystallization), the lattice planes generally form a larger angle to each other. Large angle grain boundaries are formed, or in general usage: grain boundaries.

Due to lattice faults, real crystals differ from ideal ones considerably. For example, the tensile strength of iron is more than two orders of magnitude below that of the theoretically possible strength of the ideal crystal. An explanation for this phenomenon was only made possible when the effects of lattice defects were fundamentally understood so that corresponding model representations could be made, which will be considered more closely in the following chapter.

In the unit cells, the distances of the atoms to each other varies in different directions (Fig. 2.1 top right). Therefore, the fact can be already derived that certain properties of metals depend on the direction. This direction dependence is called anisotropy. Iron monocrystals have a modulus of elasticity between 130 and 290 GPa depending on the crystal orientation. In polycrystalline materials, the crystallites are frequently distributed in a statistically random fashion. From the outside, the material then generally appears isotropic (quasi-isotropic).

When technical melts solidify, impurities are for the most part pushed in front of the solidification front and collect at the grain boundaries. Figure 2.1 (bottom right) shows schematic representation of a grain structure and a real grain structure as seen in a metallographic specimen through a light microscope. We can recognize the shape, size and arrangement of the crystals, but not their internal structure.

2.2.2 Elastic and Plastic Deformation of Crystals

Deformation of a body occurs due to external forces affecting the body. Such deformation is subdivided in elastic and plastic strain.

If the deformed body returns completely to the initial shape and dimensions after the external strain is removed, it is referred to as an elastic strain. This results from a shifting of the atoms from their stable position of equilibrium where they

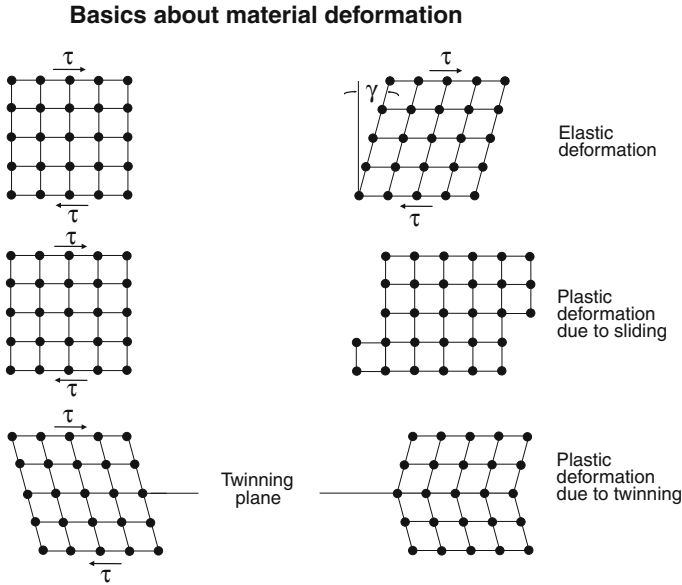


Fig. 2.2 Atomic representation of elastic and plastic deformation of the crystal lattice

exhibit a minimum of potential energy (Fig. 2.2). The respective amount of shifting is smaller than one interatomic distance. From materials mechanics, Hooke's law for tensile and compressive stress is well-known for the functional description of this process.

$$\sigma = E \cdot \varepsilon \quad (2.1)$$

Given a shear stress of τ , the following linear relation results for the resulting displacement γ :

$$\tau = G \cdot \gamma \quad (2.2)$$

In forming technology, elastic deformation is generally very small compared to plastic deformation. For this reason, elastic deformation can often be neglected. One undesirable property of elastic behaviour during forming processes is known as spring-back. This phenomenon occurs especially when deep drawing large-scale components and will be considered in more detail in Sect. 4.1.

In the case of plastic deformation, there is a dislocation of atoms into a new position of stable equilibrium. The amount of dislocation can be much larger than one atomic distance and the deformation remains after the external forces have been removed. Metallurgy recognizes essentially two mechanisms of plastic deformation: sliding (translation) and twinning (Fig. 2.2). In considering these processes, one first proceeds from a monocrystal so that varying orientations and grain boundaries can be neglected. Mechanical twinning involves a shifting of atoms that lie on planes parallel to the twin plane.

The amount of dislocation is proportional to the distance of these planes from the twin plane. The lattice area deformed by twinning appears as a reflection of the non-deformed area on the twin plane. In comparison to sliding, it requires relatively large external stresses to trigger the twinning process. It is therefore more rarely seen. Hexagonal and body-centred cubic metals and metals under abrupt stress are exceptions in this regard.

On the other hand, the mechanism of sliding is of higher importance in forming engineering. According to the atomic interpretation of this process, entire lattice areas are shifted relative to one another along a sliding plane. The amount of dislocation can be much larger than the atomic distance, sometimes by a large whole number multiple. To this end, a shear stress must be applied that is sufficient to overcome the elastic reset forces.

Interatomic bonding forces are lowest in the lattice areas that are the most densely occupied. Given an external force, sliding will therefore begin first where the resulting shear stress is largest (e.g. in the uniaxial tensile test below 45° to the direction of tension) while at the same time there are favourably oriented, densely occupied slide planes. The number and orientation of the potential slide planes vary in different crystal systems. For example, a hexagonal lattice has only one slide plane, a face-centred cubic lattice structure has four non-parallel slide planes. Slide planes and sliding directions together comprise the slide system (fcc: 12; bcc: 12; hcp: 3). This can explain, for example, how iron, copper and aluminium (i.e. metals with a cubic crystal structure) are more easily deformable than zinc and magnesium, which have hexagonal lattice structures.

Dislocation migration is assumed to be a basic mechanism of sliding in metal physics. Figure 2.3 left provides as an example a cross-section of an edge dislocation, which is characterized by the fact that atom row “2” is additionally inserted into the otherwise regular cubic lattice structure. Now already a small shear stress is sufficient to dislocate atom “A” with the underlying atoms into row “2”. The discontinuity is thus pushed to the left. This process repeats itself several times until the discontinuity has left the lattice area under consideration and all atoms of the slide plane have shifted places.

Since in this case all individual atomic rows and not an entire plane migrates, the critical shear stress required to initiate sliding is small, the theoretically calculated value of which agrees well with experimental results.

For the purposes of forming engineering, a clearer conception is often useful, in which the material volume is understood as a card deck made of lattice layers and inter-adjacent slide planes. Figure 2.4 shows material behaviour under tension, pressure and shear strain for this model conception.

In the process of cold forming, metals have been observed to undergo a change in their strength values (Fig. 2.5). Tensile strength (R_m), elastic limit (R_p) and hardness (HB) are increased, while reduction in area (Z) and uniform elongation (A_{10}) are reduced.

This behaviour is called strain hardening. The dislocations migrating through the lattice mutually impede each other or accumulate at the grain boundaries and

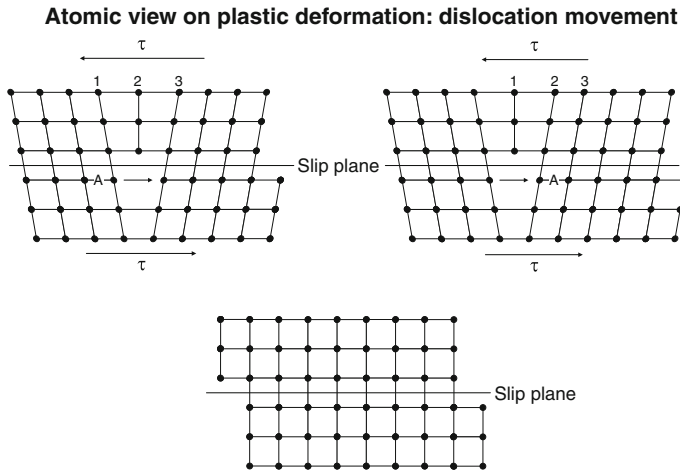


Fig. 2.3 Atomic representation of plastic deformation as dislocation migration

Schematic description of sliding processes of a single crystal

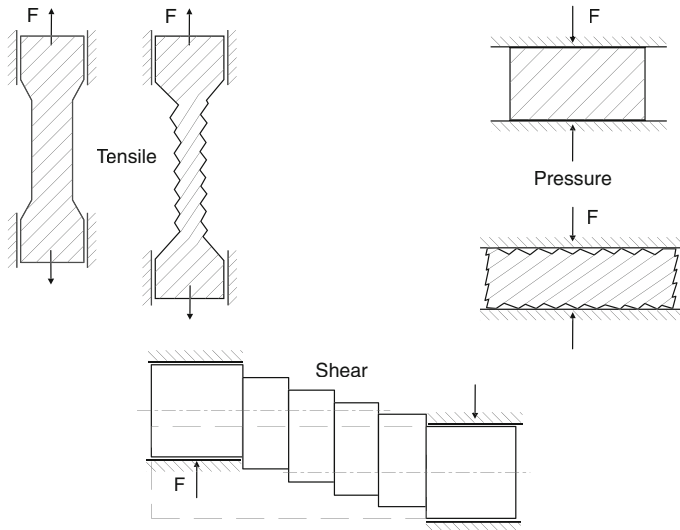


Fig. 2.4 Simplified representation of sliding processes in the monocrystal

phase interfaces. Moreover, the dislocation density is increased with progressive forming. In order to maintain plastic flow nonetheless, less favourable slide systems must also be activated. The force requirement is increased and the slide possibilities (ductility) are reduced. When the failure limit of the workpiece material is reached, cracks appear or fracture occurs. The metal is embrittled. The dependence of the stress required for flow k_f on the true strain described by the

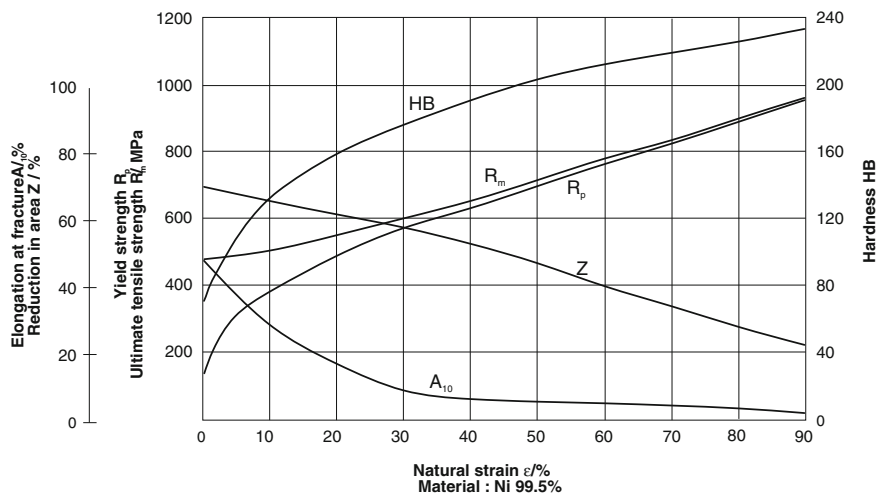


Fig. 2.5 Effect of true strain on strength and deformation parameters

flow curve. The flow stress is the stress that has to be applied for initiating plastic flow and for overcoming hardening (Fig. 2.6). Besides true strain the flow stress also depends on the crystal lattice type and orientation (Fig. 2.7) as well as on the strain rate and the forming temperature. The dependence on strain rate and forming temperature will be described in detail in later chapters. The gradient of the flow curve is a measure for hardening. It depends on the lattice type and is considerably affected by the alloying elements. In the case of certain materials, change in the crystal lattice can also be initiated by the forming process, changes which intensify strain hardening. This occurs for example when forming martensite is created by the occurring sliding processes.

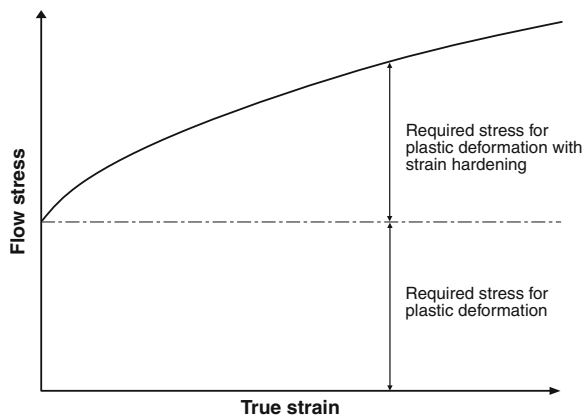


Fig. 2.6 Schematic sequence of the flow curve of a monocrystal

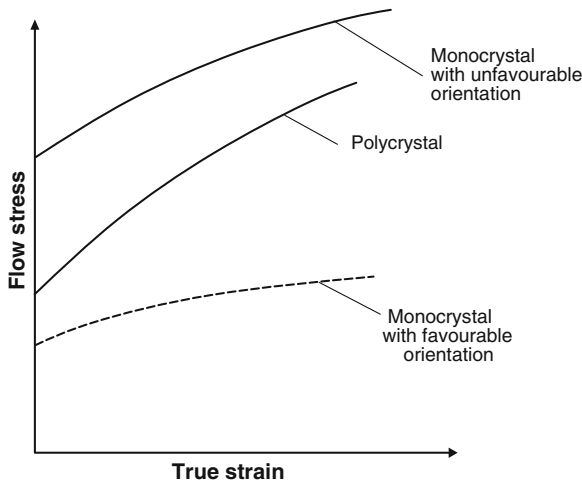


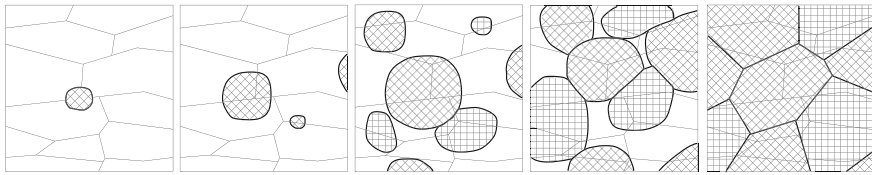
Fig. 2.7 Influence of the type and orientation of the crystals on flow behaviour

2.2.3 Recrystallization

From the technical point of view, a forming process is described by the flow capability, the deformability of the material and the therefor required energy. For a correct evaluation of the technological parameters involved in forming, the most important material processes on the atomic level must be also understood. An especially important role play thermally activated processes and changes in the metal lattice at high temperatures. A material system no longer changes in equilibrium. Plastic forming raises the energy content of the material considerably. Elastic distortions of the lattice are primarily brought about by dislocations. With progressive forming, i.e. as the dislocation density is increased, an increasing state of disequilibrium is produced. When heated up, the atoms strive again towards the state of equilibrium—the higher the temperature, the more quickly this process takes place. Fundamentally, two processes should be distinguished: crystal regeneration and recrystallization (Fig. 2.8). Both processes involve a thermally activated change of location in the lattice. In order to initiate these processes, a certain energy threshold must be exceeded, which is called activation energy.

The energy applied in plastic forming is converted for the most part into heat. The rest remains stored in the lattice as internal energy, as potential energy of elastic deformation. Of interest for forming are twins and dislocations as well as lattice vacancies and interstitial atoms. The largest amount of elastic deformation energy can be attributed to dislocations, the number of which is significantly increased in the case of cold forming. When the activation energy is exceeded, the lattice defects are recovered and rearranged.

Lattice defects also react with each other, for example opposing dislocations in one slide plane cancel each other. Aligned dislocations migrate into lower-energy



Schematic course of recrystallisation of cold formed microstructure

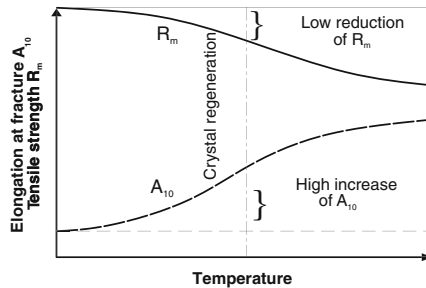


Fig. 2.8 Effect of crystal regeneration and recrystallization on tensile strength and strain of a cold-formed material

positions and form sub-grain boundaries. The randomly distributed dislocations become ordered in rows, and in this way small-angle grain boundaries are created within the grains. This process is also known as polygonization. Important for technical applications is the fact that while these processes take place on the atomic level, they nonetheless already cause changes in important macroscopic properties of the material (Fig. 2.8). Internal stresses are reduced and the elongation at fracture and tensile strength are slightly reduced. However, the deformation structure basically remains the same during crystal regeneration. The characteristics of crystal regeneration is essentially determined by the existence of impurity atoms, true strain, dislocation density (strain hardening) and temperature. When the temperature is increased, the regeneration processes proceed further because dislocations now become capable of climbing due to the onset of diffusion. While mechanical properties are only relatively slightly changed during crystal regeneration, other material properties such as electric conductivity and resistance practically reach their initial values already in the regeneration phase. Moreover, residual stresses are significantly reduced by crystal regeneration.

If temperature is further increased, these areas serve as the seeds of a complete reorganization of the microstructure. Now, new grain areas become visible, the old grains and the forming structure are completely consumed (Fig. 2.8). A completely new, unstressed and undeformed initial structure is formed. The crystallization fronts growing towards each other from different locations form new grain boundaries, grain sizes and grain forms. The most important process in this respect is the movement of the grain boundaries. The grain size is a function of true strain and the recrystallization temperature (Fig. 2.9). From this diagram we can derive the following basic facts regarding forming and recrystallization:

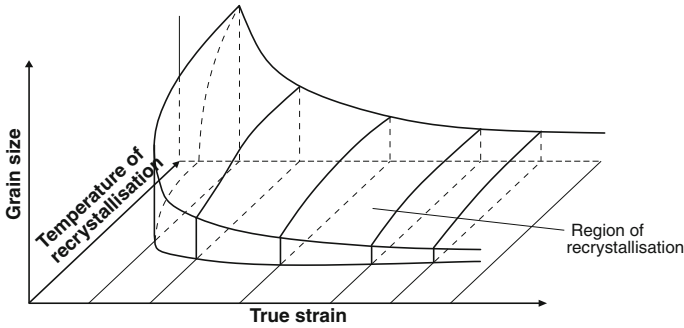


Fig. 2.9 The effect of the deformation level and temperature on the grain size during recrystallization [EISE66]

- The deformation level must exceed a certain minimum.
- Under otherwise identical conditions, low deformation levels lead to coarser grain sizes; high deformation levels lead to fine-grained structures.
- The temperature of recrystallization must exceed a certain minimum.
- In the case of higher deformation levels, recrystallization takes place at lower temperatures.

This summary makes it clear that the recrystallization temperature T_R is not a fixed characteristic value of the material. Nevertheless, we can proceed from the following relation as a reference value [GOTT98]:

$$T_R \approx 0.4 \cdot T_s, \quad (2.3)$$

into which the melting point T_s of the metal is to be inserted in Kelvin.

Often, previous deformation textures are dismantled after recrystallization. Under certain conditions of deformation and with certain materials however, it is also possible that the deformation texture remains intact even after recrystallization. These are called recrystallization textures. In general, textures are undesirable because they result in anisotropic properties. However, they are of great importance in a practical application from engine technology. In FeSi magnetic sheets, textures are created by annealing which later result in lower re-magnetization losses.

In forming technology, recrystallization is of central importance. In many cases, forming cannot advance up to the level predetermined by the manufacturing task because either the pressing force available is insufficient for sustaining plastic flow in the case of progressing strain hardening or because the forming capacity of the material is depleted and the first cracks appear.

It is then possible to recreate the original undeformed structure via recrystallization and to continue the forming process on the ductile material with low pressing force in a second stage. For the flow curve, this entails a shift on the abscissa (Fig. 2.10). In principle, alternation between strain hardening and recrystallization can be repeated to an arbitrary extent.

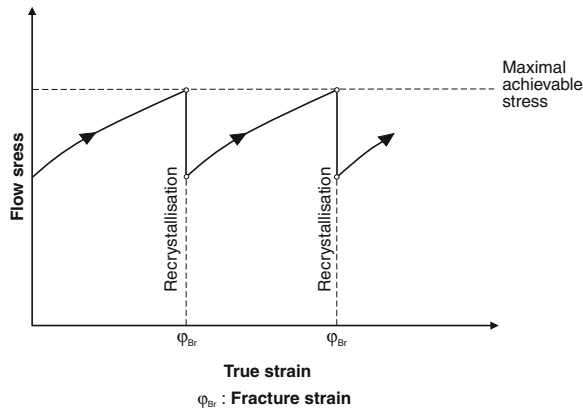


Fig. 2.10 Stress requirement in strain hardening with intermediary recrystallization annealing

Important in the heat treatment process however is precise control of the conditions. As one can see in the schematic representation in Fig. 2.9, the recrystallized microstructure is very coarse-grained in the case of “critical” combinations of temperature and deformation level, which has a negative effect on later component properties. The tendency to form coarse grains is also influenced by the carbon content and other alloying elements. With increasing amounts of C, the maximum grain size flattens quickly however, so that extreme coarse grain is no longer formed above a C-content of 0.3 % [EISE66].

2.2.4 Difference Between Cold and Hot Forming

One definition of cold and hot forming that is often used in practice is as follows:

In hot forming, the forming temperature is above the recrystallization temperature; in cold forming the forming temperature is lower than the recrystallization temperature. Since metals have very different recrystallization temperatures, this definition frequently leads to misunderstandings. For pure iron for example, Eq. 2.3 results in a recrystallization temperature of ca. 450 °C ($T_R \approx (1,536 \text{ K} + 273 \text{ K}) \cdot 0.4 = 723 \text{ K}$). Lead has a melting point of $T_S = 327 \text{ °C}$, so the recrystallization temperature of lead is about 3 °C. That means that forming lead at room temperature is already hot forming.

A more exact definition of hot forming takes the recrystallization rate and the forming rate into consideration. It states that in the case of hot forming the recrystallization rate is higher than the forming rate. Hereby, the structure is constantly reformed and no strain hardening occurs. In the case of low forming rates, the yield stress would then be independent of the true strain (Fig. 2.11 bottom). However, when very high forming rates above the recrystallization temperature occur, the time required for recrystallization can sometimes be

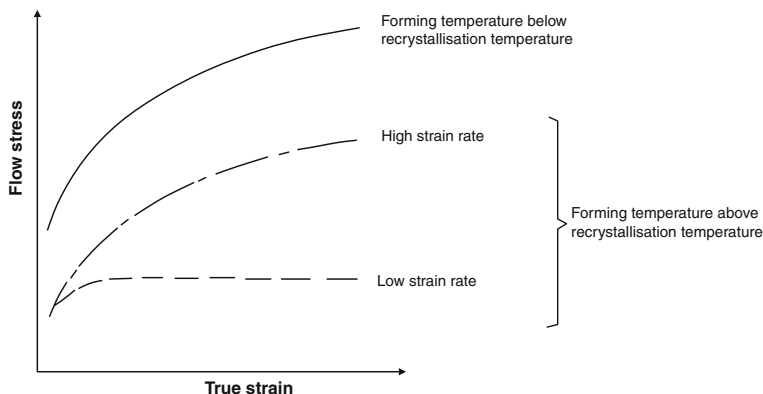


Fig. 2.11 The influence of forming temperature and rate on the flow curve

insufficient to reverse the strain hardening processes caused by forming. In this case, the yield stress exceeds the true strain, although forming takes place above T_R (Fig. 2.11 centre). This behaviour can become important if the working temperature is near T_R at high forming rates (accelerations) which can occur in certain forging processes in warm forming (also see Sect. 3.2).

Another important material property which can be exploited technically is when forming above the recrystallization temperature but with a very low forming rate. Due to the high thermal mobility, not only the atoms inside the crystal participate in restructuring processes, but the much weaker bonded atoms on the grain boundaries also participate in the reduction of lattice distortions. Grain boundary sliding can arise, which in the case of many metallic materials leads to a very high level of formability. This behaviour is called superplasticity. The prerequisites for this are a fine-grained microstructure, suitable temperature control and low forming rates (also see Sects. 3.4.3 and 4.6.2).

In the case of superplastic materials, true strain can be several times higher at low formation rates. One essential prerequisite is that the initial grain size of the material can be very small and also does not become coarse during forming. For this reason, a second phase must be present in the material in order to maintain superplasticity. Eutectic or eutectoid alloys are favourable in this context.

In practice, cold forming is preferred over hot forming in many cases. Advantages include:

- no energy cost for heating,
- low tool material costs,
- little influence on forming speed,
- no material losses and finishing treatment due to scale formation,
- no dimensional faults due to shrinkage,
- superior surface quality and
- increased component strength.

The disadvantages, such as the

- higher force and work requirement and
- limited formability

make clear, why usually hot forming is only applied when excessive forces in cold forming threaten tool fracture or machine overload, or when the strength of the material does not permit the required deformation. In this context, it has to be also examined, whether a gradual cold forming with respective recrystallization annealing is more economical.

2.3 Plastomechanical Foundations

2.3.1 *Comparison of Crystal Physics and Continuum Mechanics*

Large forces or pressures are usually required for the plastic forming of metallic workpiece materials. For this reason, it should be always proved by means of suitable calculation methods whether the target process is realisable with the given machines and tools and whether the workpiece material permits the planned deformation. Moreover, it has to be known in many cases how the mechanical properties of the material are altered by the forming process. One possibility would be to model the physical crystal processes on the atomic level to make them the basis of calculation models. This is the approach of molecular dynamic calculation approaches [RAPA04]. While the latter are not sufficiently developed for engineering practice in manufacturing, they are used in research. For practical application, the workpiece material is assumed to be a homogeneous continuum such that the physical values are described by space and time coordinates and their functions are constant and differentiable. The errors arising from these marginal conditions are by and large tolerable. Without going more deeply into the mathematical minutiae of plastomechanical solution methods, in the following we will show the physical relations that are required to understand forming engineering processes.

2.3.2 *State of Stress*

The force exerted by the forming tool on the workpiece creates a state of stress in the interior of the workpiece. As opposed to the vectorial force (first-order tensor), this is a two-directional quantity, i.e. a second-order tensor. For a general description of the stress tensor, six of its component must be known, the normal stresses

$$\sigma_x, \sigma_y, \sigma_z$$

and the shear stresses

$$\tau_{xy} = \tau_{yx}, \tau_{xz} = \tau_{zx}, \tau_{yz} = \tau_{zy}$$

While the components of the stress tensor change when the coordinate system is rotated, the sum of the normal stresses remains constant:

$$\sigma_x + \sigma_y + \sigma_z = \text{const.} \quad (2.4)$$

The sum of the normal stresses is an invariant and corresponds to three times the average principal normal stress σ_m , resulting in:

$$3\sigma_m = \sigma_x + \sigma_y + \sigma_z. \quad (2.5)$$

Often, σ_m is also described by the hydrostatic pressure p_m

$$\sigma_m = -p_m \quad (2.6)$$

Therefore, considering Eq. 2.5, the hydrostatic pressure is also invariant if the coordinate system is rotated. It exerts an equal stress in all directions of the continuum.

In every body subjected to external forces, three perpendicular planes resting upon each other can be defined, in which the shear stress components of the stress tensor become zero and in which only the normal stresses σ_1 , σ_2 , and σ_3 have an effect. These stresses are called principal normal stresses, while the planes are called principal stress planes. According to this definition, the principal normal stresses are described as follows:

$$\sigma_1 \geq \sigma_2 \geq \sigma_3.$$

In many cases, the position of the principal stress planes can be estimated from the type of external stress on the body.

In the top of Fig. 2.12, we can assume for the sake of simplification in the absence of friction that, in all planes of the square bar that lie parallel to the pressure pads, the principal stress σ_3 caused by force F_3 is in effect. The stress state is uniaxial. If the square bar is also stressed laterally by a second punch pair with pressure F_2 , the state of stress is biaxial, for besides σ_3 there is now a second principal normal stress σ_2 being exerted in all planes lying perpendicular to F_2 . Finally, a triaxial state of stress is created if a third punch pair exerts a force F_1 on the still free sides of the square bar, and principal normal stress σ_1 is generated. The planes in which σ_1 exerts an effect, stand both perpendicularly on the active planes of σ_2 as well as on those of σ_3 .

The right side of Fig. 2.12 contains the Mohr's circle belonging to the states of stress. With them, the components of the stress tensor can be determined for any arbitrary Cartesian coordinate system.

The hydrostatic state of stress is a special case of the general state of stress. In this case, the three principal normal stresses are equally large so that the Mohr's circles overlap at one point.

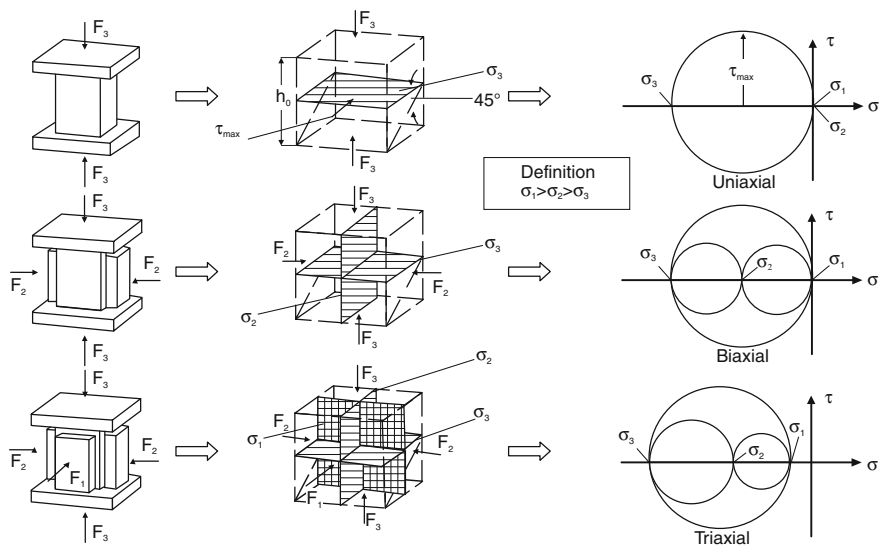


Fig. 2.12 States of stress with respective Mohr's stress circles

Every state of stress can be broken down into a deviatoric and a hydrostatic portion.

	Deviatoric portion		Hydrostatic portion
$\sigma_1 =$	σ_1	+	σ_m
$\sigma_2 =$	σ_2	+	σ_m
$\sigma_3 =$	σ_3	+	σ_m

The deviatoric part is relevant for forming. The maximum shear stresses and the position of the shear stresses can be derived directly from the Mohr's stress circles. The hydrostatic part determines the position of the Mohr's circles on the normal stress axis. In the case of the conditions selected in Fig. 2.12, only the states of pressure stress are taken into consideration. If there are tensile stresses, the circles are shifted to the right.

2.3.3
Yield Criterion

The yield criterion answers the question of how a state of stress must be constituted such that plastic flow occurs. The yield criterion establishes a functional relation between the yield stress k_f and the state of stress. In the following, an idealized thought experiment will be carried out on this subject.

Figure 2.13 again shows a square bar, which can be pressure-loaded on all sides by three punch pairs. The principal stresses inside the test bar should build up

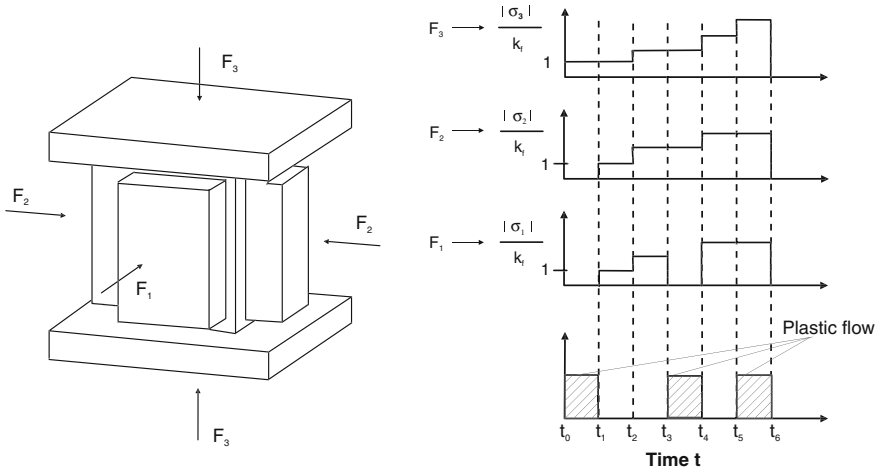


Fig. 2.13 Start of flow

independently of each other, so that F_3 produces σ_3 , F_2 σ_2 and F_1 σ_1 . The start of flow is indicated by a lasting deformation of the workpiece.

First, F_3 is applied and increased until plastic flow is initiated (t_0 to t_1). The state of stress is uniaxial and the only principal normal stress σ_3 corresponds to the yield stress

$$\sigma_3 = -k_f \quad (2.7)$$

Now, the lateral punch forces F_2 and F_1 produce stresses $\sigma_2 = -k_f$ and $\sigma_1 = -k_f$, and one observes that the flow is interrupted (t_1 to t_2). Even if all punch forces are simultaneously doubled during time t_2 to t_3 , flow is not reintroduced. On the other hand, if we remove one punch force between t_3 and t_4 , say F_2 , flow begins again provided the remaining punch forces remain constant between t_3 and t_4 . Renewed flow would also not result if all forces were to be simultaneously increased between t_4 and t_5 . Only if one of the forces were alone increased between t_5 and t_6 would flow start again. The experiment would proceed quite similarly with respect to the start of flow if the punches were to pull on the sides of the square bar, thus creating tensile stresses. In summary, the experiment described here suggests the following conclusions (Fig. 2.13):

- The start of flow is a function of a principal normal stresses σ_1 , σ_2 and σ_3 ;
- It is *no* function of the average principal normal stress σ_m ,

$$\sigma_m = \frac{1}{3}(\sigma_1 + \sigma_2 + \sigma_3)$$

and therefore

- it must be a function of the deviatoric portion of the stress tensor and thus a function of the absolute amounts of the differences of the principal normal stress:

$$g(|\sigma_1 - \sigma_2|, |\sigma_1 - \sigma_3|, |\sigma_2 - \sigma_3|) = 0 \quad (2.8)$$

The formulaic relations for g generally used were provided with a different physical and mathematical background by Tresca (1864) [TRES64] and later by von Mises (1913) [MISE13].

According to the shear stress theory of Tresca, plastic flow is only dependent on the shear stresses and begins when the largest shear stress reaches a value of $\tau_{\max} = k$ (Fig. 2.14).

The largest shear stress can be taken from the Mohr's circle. It corresponds to the radius of the largest stress circle or half the largest principal stress difference. One can therefore also formulate Tresca's yield criterion in this way:

$$\max\{|\sigma_i - \sigma_j|\} = k_f = 2k \quad (2.9)$$

(i and j extend from 1 to 3, $i \neq j$)

The following is valid for the case shown in Fig. 2.14:

$$k_f = |\sigma_1 - \sigma_3| = 2\tau_{\max}.$$

Von Mises's yield criterion is based on energy. Before plastic flow is initiated in a volume element of the workpiece, mechanical energy w must be applied to it. The energy w is divided into w_m , which only changes the volume, and w_{pl} , which deforms the shape of the body at constant volume. Since metallic materials, barring lattice transformations and precipitations, do not change their volume lastingly, i.e. plastically, w_m can only be elastically stored and cannot contribute to

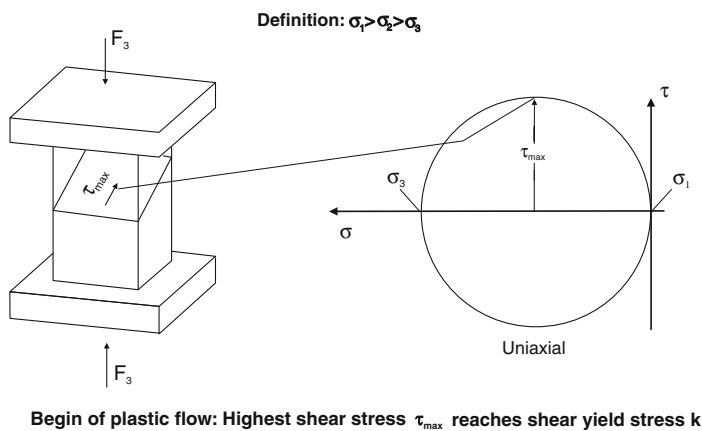


Fig. 2.14 Tresca's yield condition

plastic flow. If we separate w_m from w , only w_{pl} remains, which strives to deform the volume element and to cause plastic flow (Fig. 2.15).

With the help of Hooke's law, we can formulate w_{pl} as a function of the principal stresses σ_1 , σ_2 and σ_3 as well as the shear modulus G :

$$w_{pl} = \frac{1}{12G} \left\{ (\sigma_1 - \sigma_2)^2 + (\sigma_2 - \sigma_3)^2 + (\sigma_3 - \sigma_1)^2 \right\} \quad (2.10)$$

The yield criterion can now be stated in the following way: plastic flow is initiated in one volume element of the workpiece if w_{pl} has reached a critical value. Since this critical value is independent of the type of state of stress, it can, for example, be determined in the tension test ($\sigma_1 = k_f$, $\sigma_2 = \sigma_3 = 0$) or in the compression test ($\sigma_3 = -k_f$, $\sigma_2 = \sigma_1 = 0$).

If we assume

$$(w_{pl})_{tension/compression\ test} = (w_{pl})_{general}$$

then Eq. 2.10 results in

$$\frac{1}{12G} \cdot 2 \cdot k_f^2 = \frac{1}{12G} \left\{ (\sigma_1 - \sigma_2)^2 + (\sigma_2 - \sigma_3)^2 + (\sigma_3 - \sigma_1)^2 \right\} \quad (2.11)$$

the yield criterion according to von Mises:

$$(\sigma_1 - \sigma_2)^2 + (\sigma_2 - \sigma_3)^2 + (\sigma_3 - \sigma_1)^2 = 2k_f^2 \quad (2.12)$$

or

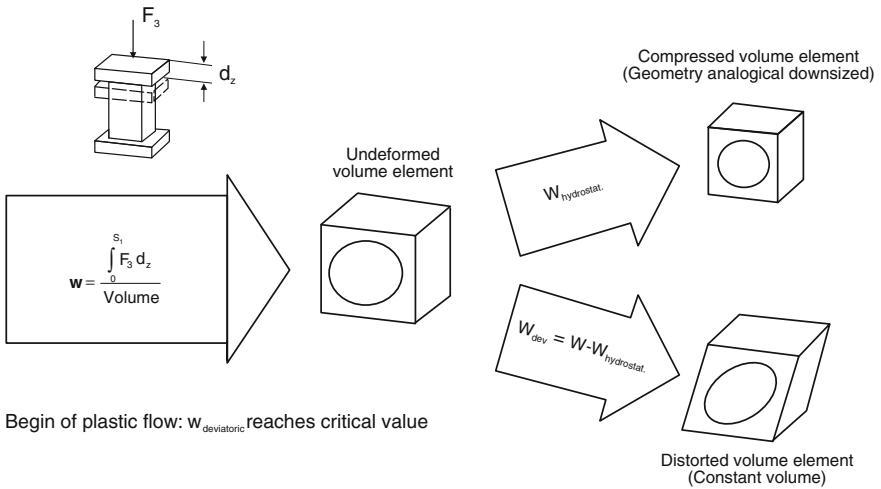


Fig. 2.15 Von Mises's yield criterion

$$(\sigma_1 - \sigma_m)^2 + (\sigma_2 - \sigma_m)^2 + (\sigma_3 - \sigma_m)^2 = \frac{2}{3} k_f^2. \quad (2.13)$$

The yield criteria of Tresca and von Mises only deviate from each other to a small extent depending on the state of stress. In the case of a pure tensile or compressive state of stress, they provide the same results; in the case of pure torsion, the maximum difference is 15 %. Trials have shown that the flow behaviour of technical workpiece materials are better described by the yield criterion of von Mises than that of Tresca [LANG90a].

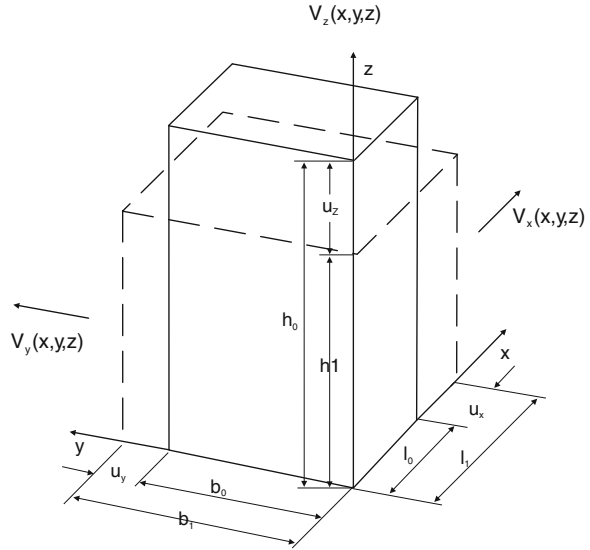
In the calculations of forming engineering, usually arithmetic reasons decide which yield criterion will be used. For example, Tresca's yield criterion can be advantageous because it contains the principal stresses only as linear terms; however, it must be determined prior to the calculation which principal stress difference is maximal. This disadvantage is not encountered in the case of von Mises's yield criterion—it is a constantly differentiable function of all principal stresses. The quadratic principal stress terms can be detrimental.

2.3.4 Kinematics of the Continuum

If the state of stress fulfils the yield criterion and therefore plastic flow occurs inside the workpiece, the question arises how the geometry of the workpiece is changed during plastic flow. In classic flow curves, in which important strength and ductility characteristic values are recorded in the uniaxial tension test, the elongations and stresses are generally referred to the output variables (see also p. 119). Stress σ is equal to the ratio F/A_0 and elongation ε corresponds to the ratio $\Delta l/l_0$. The reference variables are the cross-sectional area A_0 and the output length l_0 . These characteristic values are generally sufficient for strength calculations during design because the components are designed with respect to strength in the elastic range. In this case, both elongation and change in cross-section are minimal. The behaviour of materials above the yield point are interesting in the case insofar as information can be derived from it about whether the material tends to be brittle or ductile outside of the elastic range.

On the other hand, the plasticity of materials is in the foreground in forming technology. For this reason, true stress and true elongation characteristic values are used. In the case of true stress, the forming force is related to the actual (true) surface. The true stress is usually designated as strain strength or yield stress k_f . Elongations are also related to the actual reference value changing with deformation (the true value). In the German literature, true elongation is designated with the letter φ . For the reference elongation, usually the letter ε is used. In the English literature, this distinction is not made. ε designates both the reference elongation (nominal elongation) and for true elongation (true strain). Which variable is meant can often only be determined by context.

Fig. 2.16 Kinematics of an idealized upsetting process



The following example shows why nominal elongations are not suitable for describing plastic deformations. Let us first assume that the punch displacement u_z in Fig. 2.16 is small compared to the height h_0 of the square bar. Then the following is valid for the principal elongation ε_3 :

$$\varepsilon_3 = \frac{h_1 - h_0}{h_0} = -\frac{u_z}{h_0}. \quad (2.14)$$

If a 50 % height reduction was to be achieved by means of upsetting, then

$$\varepsilon_3 = \frac{0.5h_0 - h_0}{h_0} = -0.5.$$

In case of a further 50 % height reduction, the workpiece material is elongated again by $\varepsilon_3 = -0.5$. But if the elongation is calculated with the output height h_0 , the result is

$$\varepsilon_3 = \frac{0.25h_0 - 0.5h_0}{h_0} = -0.25.$$

This consideration makes clear that, in the case of large elongations such as are found in forming engineering, a fixed reference variable cannot be used to calculate elongation.

On the other hand, true elongation is a suitable variable, for which the Greek letter φ has been introduced. Its reference variable is the actual geometrical configuration of the continuum. For a small punch displacement du_z in Fig. 2.16, the increase in elongation amounts to

$$d\varphi_3 = \frac{du_z}{h}. \quad (2.15)$$

If the square bar is compressed from height h_0 to height h_1 , then:

$$\varphi_3 = \int_{h_0}^{h_1} \frac{du_z}{h} = \int_{h_0}^{h_1} \frac{dh}{h} = \ln \frac{h_1}{h_0}. \quad (2.16)$$

This parameter is called true strain, logarithmic elongation or true elongation. The true strain is positive if a section is elongated and negative if a section is compressed. As in the z direction, two further true strains can be introduced for the x and y directions:

$$\varphi_1 = \int_{l_0}^{l_1} \frac{dl}{l} = \ln \frac{l_1}{l_0}$$

and

$$\varphi_2 = \int_{b_0}^{b_1} \frac{db}{b} = \ln \frac{b_1}{b_0}. \quad (2.17)$$

Referring to the example in Fig. 2.16, the first height reduction from h_0 to h_1 using the true strain to describe the illustrated upsetting process amounts to:

$$\varphi_3 = \ln \frac{h_1}{h_0} = \ln \frac{0.5h_0}{h_0} = \ln 0.5 \approx -0.69.$$

The second height reduction from h_1 to h_2 follows as:

$$\varphi_3 = \ln \frac{h_2}{h_1} = \ln \frac{0.25h_0}{0.5h_0} = \ln 0.5 \approx -0.69.$$

In contrast to the nominal elongations, the true strains are the same for both height reductions.

In many forming problems, the situation is not as simple as in the idealized upsetting process described in Fig. 2.16, in which a homogeneous (i.e. equally distributed in all points of the continuum) forming process is assumed. Depending on the problem, determining the true strain can be very difficult, and it can be advantageous to calculate with forming rates. Forming rates are obtained via differentiation of the velocity field $v_x(x, y, z)$, $v_y(x, y, z)$, $v_z(x, y, z)$:

$$\begin{aligned}
\dot{\phi}_1 &= \frac{\partial v_x}{\partial x}, \\
\dot{\phi}_2 &= \frac{\partial v_y}{\partial y} \text{ and} \\
\dot{\phi}_3 &= \frac{\partial v_z}{\partial z}.
\end{aligned} \tag{2.18}$$

Elongation and elongation rates are 2nd-order tensors. While for the special case in Fig. 2.16 the true strains defined via Eqs. 2.16 and 2.17 correspond to the principal elongations, the forming rates defined in Eq. 2.18 are the principal elongation rates.

In the case of a general position of the coordinate system, the coordinates of the elongation tensor are

$$\begin{aligned}
&\varphi_x, \varphi_y, \varphi_z \\
&\varphi_{xy} = \varphi_{yx}, \varphi_{yz} = \varphi_{zy}, \varphi_{zx} = \varphi_{xz}
\end{aligned} \tag{2.19}$$

and those of the tensor of the elongation rates are

$$\begin{aligned}
\dot{\phi}_1 &= \frac{\partial v_x}{\partial x}, \dot{\phi}_2 = \frac{\partial v_y}{\partial y}, \dot{\phi}_3 = \frac{\partial v_z}{\partial z}, \\
\dot{\phi}_{xy} &= \dot{\phi}_{yx} = \frac{1}{2} \left\{ \frac{\partial v_x}{\partial y} + \frac{\partial v_y}{\partial x} \right\}, \\
\dot{\phi}_{yz} &= \dot{\phi}_{zy} = \frac{1}{2} \left\{ \frac{\partial v_y}{\partial z} + \frac{\partial v_z}{\partial y} \right\} \text{ and} \\
\dot{\phi}_{xz} &= \dot{\phi}_{zx} = \frac{1}{2} \left\{ \frac{\partial v_x}{\partial z} + \frac{\partial v_z}{\partial x} \right\}.
\end{aligned} \tag{2.20}$$

The result of Eqs. 2.19 and 2.20 is that the elongation tensor and the tensor of elongation rates are similar to the stress tensor. Above all, both can be broken up into deviatoric and hydrostatic parts. The deviatoric part is a measure of the deformation (elongation tensor) or the deformation rate of the continuum (elongation rate tensor). The hydrostatic part corresponds to the volume change or volume change rate of the continuum.

2.3.5 Volume Constancy

In plastic flow processes, the volume of the continuum remains as good as unchanged. For this reason, the elongations and elongation rates described by the hydrostatic stress become equal to zero. As proof, Fig. 2.17 shows the square bar again with the edge lengths h_0, b_0, l_0 before upsetting and h_1, b_1, l_1 after upsetting. Volume constancy then requires that

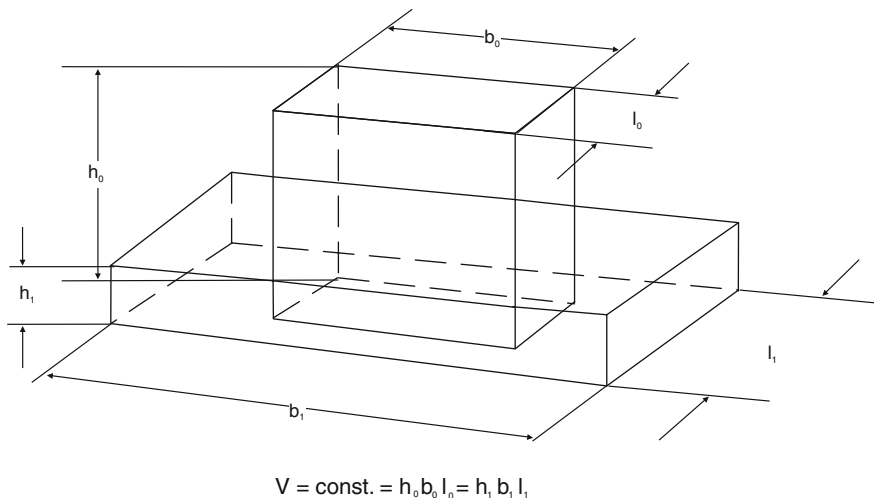


Fig. 2.17 Volume constancy in forming processes [LANG90a]

$$h_1 \cdot b_1 \cdot l_1 = h_0 \cdot b_0 \cdot l_0.$$

If we divide the left side of the equation just given by the right side and logarithmize, we obtain

$$\ln\left(\frac{h_1}{h_0} \cdot \frac{b_1}{b_0} \cdot \frac{l_1}{l_0}\right) = \ln 1 = 0$$

and thus

$$\ln \frac{h_1}{h_0} + \ln \frac{b_1}{b_0} + \ln \frac{l_1}{l_0} = \varphi_1 + \varphi_2 + \varphi_3 = 0. \quad (2.21)$$

Since similar considerations are also applicable for the forming rates, the following is also true

$$\dot{\varphi}_1 + \dot{\varphi}_2 + \dot{\varphi}_3 = 0. \quad (2.22)$$

2.3.6 Flow Rule

While stresses and deformations were previously treated separately, it is necessary for plastomechanical calculations to obtain a mathematical description of the relation between stresses and elongations.

To this end, we will again consider the example of upsetting a square bar. As the compressive force is applied, first elastic elongations arise, which are proportional to the stresses in accordance with Hooke's law. After the yield point is

reached, the stress $\sigma_3 = -k_f$ remains approximately constant, while with further upsetting the amounts of the elongations $\varphi_1, \varphi_2, \varphi_3$ increase monotonously. Therefore, a similarly simple relation such as Hooke's law cannot be given in the plastic range. Moreover, it has to be also assumed for real forming processes that the principal axes of the stress tensor change their directions, so that both the stress and elongation tensors no longer have the same principal directions.

To overcome this difficulty, the forming process is subdivided into small steps considering the tensor of elongation increase. It has the principal values

$$d\varphi_1, d\varphi_2, d\varphi_3.$$

Since the principal axes of this tensor now coincide with the principal axes of the stress tensor at every forming interval, proportionality can be applied between both tensors. However, it must be considered that the trace of the tensor of elongation increase must disappear due to Eq. 2.21 so that only the deviatoric part of the stress tensor comes into consideration for the proportionality:

$$\begin{aligned} d\varphi_1 &= d\lambda(\sigma_1 - \sigma_m), \\ d\varphi_2 &= d\lambda(\sigma_2 - \sigma_m) \text{ and} \\ d\varphi_3 &= d\lambda(\sigma_3 - \sigma_m). \end{aligned} \quad (2.23)$$

By division with dt , Eq. 2.23 can also be put into the form

$$\begin{aligned} \dot{\varphi}_1 &= \dot{\lambda}(\sigma_1 - \sigma_m), \\ \dot{\varphi}_2 &= \dot{\lambda}(\sigma_2 - \sigma_m) \text{ and} \\ \dot{\varphi}_3 &= \dot{\lambda}(\sigma_3 - \sigma_m). \end{aligned} \quad (2.24)$$

With a general position of the coordinate system, Eq. 2.24 becomes

$$\begin{aligned} \dot{\varphi}_x &= \frac{dv_x}{\partial x} = \dot{\lambda}\{\sigma_x - \sigma_m\}, \\ \dot{\varphi}_y &= \frac{dv_y}{\partial y} = \dot{\lambda}\{\sigma_y - \sigma_m\}, \\ \dot{\varphi}_z &= \frac{dv_z}{\partial z} = \dot{\lambda}\{\sigma_z - \sigma_m\}, \\ \dot{\varphi}_{xy} &= \frac{1}{2} \left\{ \frac{\partial v_x}{\partial y} + \frac{\partial v_y}{\partial x} \right\} = \dot{\lambda}\tau_{xy}, \\ \dot{\varphi}_{yz} &= \frac{1}{2} \left\{ \frac{\partial v_y}{\partial z} + \frac{\partial v_z}{\partial y} \right\} = \dot{\lambda}\tau_{yz} \text{ and} \\ \dot{\varphi}_{zx} &= \frac{1}{2} \left\{ \frac{\partial v_z}{\partial x} + \frac{\partial v_x}{\partial z} \right\} = \dot{\lambda}\tau_{zx}. \end{aligned} \quad (2.25)$$

Equations 2.23–2.25 are called the flow law or flow rule. The flow rule, together with the yield criterion, describes the behaviour of the workpiece material in the state of plastic flow. $d\lambda$ and $\dot{\lambda}$ are scalar parameters, but no constants. Otherwise, doubling the elongation rate, for example, would also lead to a doubling of stress.

To derive a functional relation for $\dot{\lambda}$, Eq. 2.24 is squared line for line and then added up:

$$\dot{\varphi}_1^2 + \dot{\varphi}_2^2 + \dot{\varphi}_3^2 = \dot{\lambda}^2 \left\{ (\sigma_1 - \sigma_m)^2 + (\sigma_2 - \sigma_m)^2 + (\sigma_3 - \sigma_m)^2 \right\}. \quad (2.26)$$

The state of stress must constantly fulfil the yield criterion during plastic flow as well. Thus, the right side of Eq. 2.26 can be substituted with von Mises's yield criterion with Eq. 2.13,

$$\dot{\varphi}_1^2 + \dot{\varphi}_2^2 + \dot{\varphi}_3^2 = \dot{\lambda}^2 \frac{2}{3} k_f^2 \quad (2.27)$$

so that for $\dot{\lambda}$

$$\dot{\lambda} = \frac{\sqrt{\frac{3}{2} (\dot{\varphi}_1^2 + \dot{\varphi}_2^2 + \dot{\varphi}_3^2)}}{k_f} \quad (2.28)$$

or with elongations increments for $d\lambda$:

$$d\lambda = \frac{\sqrt{\frac{3}{2} (d\varphi_1^2 + d\varphi_2^2 + d\varphi_3^2)}}{k_f}. \quad (2.29)$$

If the yield stress k_f is constant in Eqs. 2.28 and 2.29, then it is a case of ideally plastic material behaviour. The flow curve in Fig. 2.18 then has a horizontal gradient. In order to take real workpiece material behaviour into consideration, k_f is determined as function of natural strain, forming speed and also temperature. For this, flow curves are experimentally determined. This is done using uniaxial tests (see p. 118). We must therefore make a connection between the general state of strain of the given forming process and the particular uniaxial forming process with which the flow curve was determined.

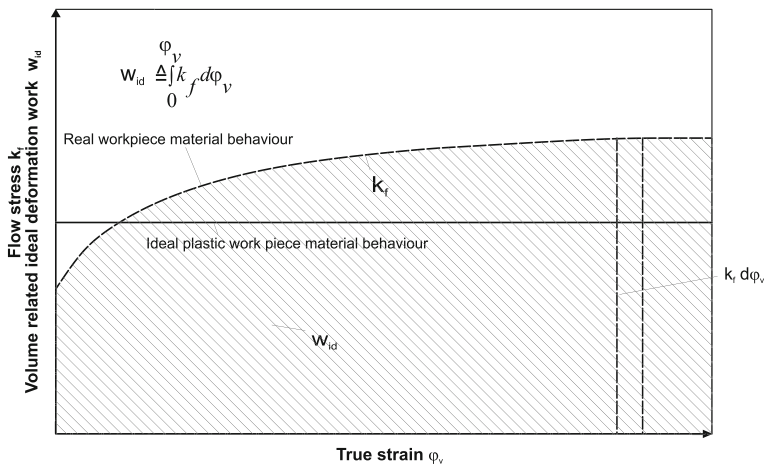


Fig. 2.18 Schematic representation of a flow curve

To this end, it is assumed that the flow curve of a workpiece material has been subjected to the idealized compression test described above.

The only principal stress that is not zero during the upsetting process is $\sigma_3 = -k_f$. With Eqs. 2.23 and 2.29, we can write for the increase in elongation $d\varphi_3$ in the direction of compression:

$$\begin{aligned} d\varphi_3 &= -\frac{\sqrt{\frac{3}{2}(d\varphi_1^2 + d\varphi_2^2 + d\varphi_3^2)}}{k_f} \left(k_f - \frac{1}{3}k_f \right) \\ d\varphi_3 &= -\sqrt{\frac{2}{3}(d\varphi_1^2 + d\varphi_2^2 + d\varphi_3^2)}. \end{aligned} \quad (2.30)$$

Following conclusions can be derived from Eq. 2.30: If a volume element is formed in time dt by a general forming process by $d\varphi_1$, $d\varphi_2$, $d\varphi_3$, this elongation, given the same workpiece material behaviour, corresponds to the increase in elongation $d\varphi_3$ in the tensile or compressive direction of a uniaxial tension or compression test.

Using integration the parameter is obtained

$$\varphi_v = \sqrt{\frac{2}{3}(\varphi_1^2 + \varphi_2^2 + \varphi_3^2)}, \quad (2.31)$$

which is called effective elongation or effective strain.

Quite similarly, the effective elongation rate/effective forming speed can be introduced with Eqs. 2.24 and 2.28:

$$\dot{\varphi}_v = \sqrt{\frac{2}{3}(\dot{\varphi}_1^2 + \dot{\varphi}_2^2 + \dot{\varphi}_3^2)}. \quad (2.32)$$

With Eqs. 2.31 and 2.32, the information in a flow curve can be applied to general forming processes. Both equations thus form an important foundation for calculating forming engineering problems.

2.3.7 Limits of Plastic Formation

In the literature, formability and the forming limit are utilized to describe the limits of plastic forming. Formability is a parameter specific to the material that restricts the forming process while the forming limit is a process-specific parameter. Both of these characteristic values will be described in more detail in the following.

2.3.7.1 Formability

Formability is a general expression for the property of a metallic material to sustain lasting deformations without damage (crack formation or fracture) [VDI76]. The fracture strain φ_{vB} is often used as a measure for the formability of a material. However, the fracture strain depends not only on the material but much more decisively on the temperature of the workpiece and the state of stress arising during the forming process [KOPP99]. Workpiece failure, described by formability, depends on the following parameters:

- workpiece material,
- workpiece temperature,
- forming rate and
- the type of stress in the workpiece.

Workpiece Material. The condition of the material is a result of the chemical composition (e.g. alloying elements), the material's microstructure (e.g. grain size), heat treatment (e.g. spheroidizing, sub-critical annealing, tempering, hardening and tempering) and the process steps in the course of component manufacture (e.g. casting, forging, rolling) [GRÄF93]. The condition of the material thus has a large influence on the formability of the material. For further details, the reader is referred to [Sect. 2.7.1.2](#).

Workpiece Temperature. As a rule, the formability of a material increases with the workpiece temperature. This is due to the recovery and recrystallization processes that take place during forming (see [Sects. 2.2.3](#) and [2.2.4](#)). In the case of carbon steels, the blue brittleness range between 200 and 400 °C shows an exception to this behaviour (see [Sect. 3.2](#), p. 222). The effect of temperature on a material can be represented with the help of a Charpy test in the impact work-temperature curve ($A_V - T - \text{diagram}$). The steel's properties are all the more favourable the higher the impact work is at low temperatures.

Forming Rate. The forming rate also has a considerable influence on the limit of a material's formability. For example, formability generally decreases with higher forming rates [LANG90a]. In many cases, this is accompanied by an increased tendency to brittle fracture. However, it must be taken into consideration that increasing rates of load lead to more intense heating of the workpiece since the forming heat cannot be removed quickly enough. This effect is superimposed over the embrittlement of the material, leading to a higher level of material formability at significantly higher forming rates since the forming heat generated has a stronger effect on material behaviour [ELMA01].

Type of Stress in the Workpiece. Formability is strongly dependant on the state of elongation and stress in the workpiece. The latter can be broken down into a deviatoric and a hydrostatic part. While deviator stresses are decisive for plastic flow, the hydrostatic part has little effect on flow itself. It does however have a major effect on the formability of the material. Hydrostatic stress σ_m , with reference to the yield stress k_f , can be utilized as a measure for the effect of the state of

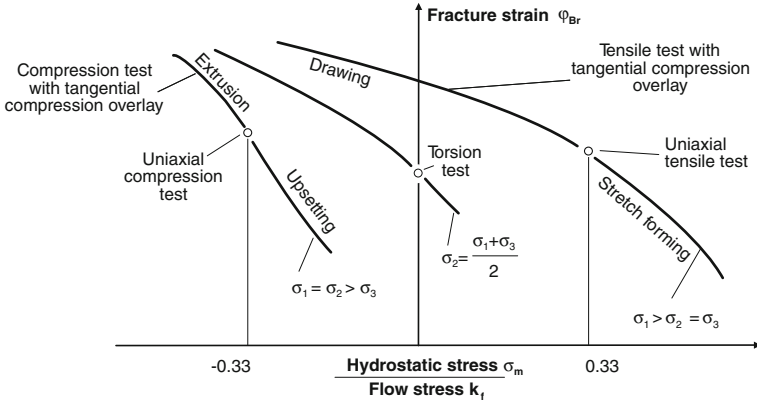


Fig. 2.19 The effect of the state of stress on formability according to Stenger [STEN65]

stress (see Fig. 2.19). For example, a value of 0.33 is obtained in a uniaxial tension test for σ_m/k_f , of 0 in a torsion test and of -0.33 in a uniaxial compression test. The smaller this value is, the larger the fracture strain φ_B , assuming that the second principal normal stress σ_2 is constant. If σ_2 shifts to the smallest principal normal stress σ_3 , the formability of the material is increased assuming that the reference stress average σ_m/k_f is constant. In summary, we must bear in mind that both σ_m and σ_2 are functions of position and time depending on the forming process.

It has also been pointed out that formability depends on the stress history as well [PUGH70]. In a first test, Pugh upset a sample without external surrounding pressure until fracture. In a second test, he pre-upset a sample with surrounding external pressure and then upset the same sample without surrounding pressure until fracture. This experiment led him to the conclusion that formability was several times higher in the second test than in the first. This can be explained physically in the following way: During the forming process, microscopically small cracks in the workpiece material attempt to open and propagate through the entire workpiece. Compressive stresses on all sides strive to close these micro-cracks and to hinder their propagation. It immediately follows from this interpretation that only average compressive stresses, i.e. negative values of σ_m , can increase the maximum obtainable true strain. Average tensile stresses on the other hand are extremely unfavourable since they promote the opening and propagation of cracks.

Many technical forming processes are designed so that a hydrostatic pressure builds up in the workpiece. For example, in fine blanking (Sect. 5.2), hydromechanical deep drawing (Sect. 4.1.2) and roll bending with an additional press cylinder [MEIE01], a state of compressive stress is brought about in the forming zone by means of additional tool elements. This additional stress significantly increases the formability of the material. In this way, even high-strength and brittle materials can be plastically deformed.

2.3.7.2 Damage Criteria

As already described, the deformability of a material depends on different factors and is difficult to describe by means of a single material characteristic value. Thus, different fracture criteria have been developed that describe ductile material failure on the basis of the state of stress and deformation introduced and formulate this in the form of a characteristic value. If these characteristic values reach a level specific for that process, the appearance of a crack in the material is indicated. These fracture criteria can be subdivided into macromechanical and micromechanical fracture hypotheses. In the case of macromechanical criteria, these are further subdivided into elongation-independent and elongation-dependent hypotheses.

Time-independent Macromechanical Fracture Criteria. In the case of macromechanical, time-independent fracture criteria, the individual parameters of the stress and deformation state are determined as limit values. The forming history including crack development is not taken into consideration. In the simplest case for example, the critical effective stress of von Mises σ_V can be used as a limit value. More complex criteria calculate a limit value using a more comprehensive stress relation [GOSH76]. Among these criteria, the fracture true strain φ_B has a special position. The fracture true strain is an elongation-dependent variable, but it is assigned to this class as well because it is subject to the same restrictions as apply to the other macromechanical criteria. This class of fracture criteria is very important in sheet metal forming and is used as forming limit diagrams (see Sect. 2.7.3.5). In massive forming, these criteria have not been implemented since the dominated multiaxial states of stress lead to the extremely varied workpiece failure configurations, and these combinations can only be accounted for insufficiently with these criteria.

Time-dependent Macromechanical Fracture Criteria. As opposed to time-independent fracture criteria, macromechanical time-dependent fracture criteria are also called integral fracture criteria. They are based on the work introduced during forming, which is stored as plastic energy in the material on the one hand and converted as forming energy into elastic springback and heat on the other. This class of fracture criteria has the following structure:

$$D_{\text{makro}} = \int_0^{\varphi} f(\varphi, \sigma, a) d\varphi. \quad (2.33)$$

Here, elongations are taken into account with φ , stresses with σ and different material constants with a . The calculation thus sums up the incremental stress and deformation increases of a material element caused by forming. If the forming energy added to the workpiece reaches a critical damage value D_{crit} , then the deformability of the material has been exhausted in this area. The integral fracture criteria differ in the configuration of the energy terms. The best-known criteria are integrated in most FEM codes [FREU50, STEN65, COCK66, BROZ72, AYAD84].

Micromechanical Fracture Criteria. Micromechanical fracture criteria have also been developed parallel to the integral criteria [MCCL68, RICE69, GURS77,

OYAN80]. These attempt to calculate directly the material behaviour and thus the damage by proceeding from a pore volume f and adding up a pore increase df caused by new pore formation and pore growth.

$$D_{micro} = f + df_{newformation} + df_{growth} \quad (2.34)$$

The reduced strength of the damaged material area compared to the undamaged area is mostly considered in the form of a special flow function that represents the pore volume f . If the calculated pore volume f in combination with pore increase df reaches a critical amount, then the deformability of the material is exhausted and the workpiece experiences macroscopic material separation and cracking.

Summary. A number of micromechanical and macromechanical damage criteria are integrated in most FEM programs and are utilized to assess the deformability of a material. The forming areas heavily loaded during the forming process can be determined very effectively by these means. Difficulties arise in the determination of the maximum damage value for the individual damage criteria, materials and forming processes. For example, it is decisive in the determination of the material's formability for a particular forming process that a test method is selected, which exhibits a forming behaviour very close to the forming method so that its forming history at the location of the first crack formation agrees with or closely approximates the forming history at the critical location of the component.

Taking into account different forming histories to determine workpiece failure compensates for the disadvantage of macromechanical and micromechanical fracture criteria that a critical damage value can vary with the forming process. Zitz [ZITZ95] has shown that a subdivision can be made between a crack-free and crack-affected area by determining the largest reference principal normal stress as a function of the effective strain for different test piece geometries. To this end, deformability was determined in a compression test run with rotation-symmetrical test pieces of the most varied geometries. By means of an FE simulation, the forming history of the crack-endangered areas could be determined. The stress and deformation space was then subdivided into a crack-free area and a crack-affected area by means of a line connecting the end points. By representing the forming history of a crack-endangered area, a limiting strain for this process can be determined using the point of intersection of the limit curve and the profile of the forming history. The focus of further investigations is to consider not only one part of the stress and deformation state at the time of crack formation but to incorporate both the complete stress and deformation state as well as the variation of this state as a function of the forming process into the fracture prediction [KLOC03a, KLOC04a].

2.3.7.3 Forming Limit

In the case of the forming limit, it is not material failure that leads to process breakdown, but process-specific parameters such as:

- tool fracture,
- insufficient machine power,
- impermissible form and dimension deviations,
- impermissible surface quality.

According to VDI guideline 3,137 [VDI76], the maximum effective true strain reached in the component is designated as limiting strain φ_{vG} upon reaching the above process limits. It is thus an index for the forming limit. In general, the forming limit can be at most equal to the deformability of the material, but in most cases it is smaller. This is especially apparent in massive forming with high tool strains (e.g. cold extrusion, hot drop forging), whereby $\varphi_{vG} \leq \varphi_{vB}$, while in sheet forming failure mostly stems from the workpiece, and so $\varphi_{vG} = \varphi_{vB}$.

2.4 Possible Solutions to Forming Problems from the Field of Plasticity Theory

Building upon the foundations from Sect. 2.3, this chapter introduces different possibilities for analyzing problems in forming technology.

If the three components v_x , v_y and v_z of the velocity field, the proportionality factor $\dot{\lambda}$ and the six components of the stress tensor are understood as unknowns of a plastomechanical boundary value problem, then these seven quantities result, with the constitutive law, i.e. the yield criterion (Eq. 2.12) and the flow rule (Eq. 2.25), in seven equations. The three equations still lacking provide the equilibrium conditions

$$\begin{aligned}\frac{\partial \sigma_x}{\partial x} + \frac{\partial \tau_{xy}}{\partial y} + \frac{\partial \tau_{xz}}{\partial z} &= 0, \\ \frac{\partial \tau_{yx}}{\partial x} + \frac{\partial \sigma_y}{\partial y} + \frac{\partial \tau_{yz}}{\partial z} &= 0 \text{ and} \\ \frac{\partial \tau_{zx}}{\partial x} + \frac{\partial \tau_{zy}}{\partial y} + \frac{\partial \sigma_z}{\partial z} &= 0,\end{aligned}\tag{2.35}$$

because depending on whether elastic deformation or plastic flow is taking place, the state of stress must be constituted such that all areas of the workpiece are in a state of static equilibrium. Dynamic effects are generally negligible [PAWE76]. Although this basically proves the solvability of the plastomechanical boundary value problem, the number of partial differential equations suggests that a closed solution is only possible in rare cases.

For this reason, a variety of solution methods have been developed. A classification of these methods can be made in accordance with their approaches and procedures (see Fig. 2.20).

The solution methods of elementary plasticity theory assume geometrical, kinematic and material simplifications and convert the general equation system

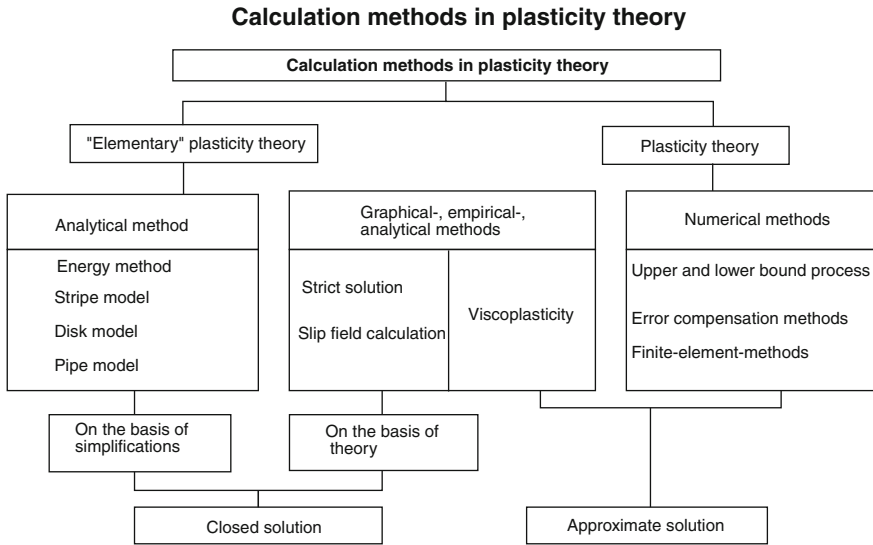


Fig. 2.20 Solution methods in forming engineering from plasticity theory (acc. to Roll)

into a system of analytically solvable equations. Today, high-performance computers enable the calculation of complex problems. The basics for such calculations are numerical calculation methods, which are used to solve the analytical approaches.

2.4.1 Solution Methods of Elementary Plasticity Theory

The basic assumption of elementary plasticity theory is that originally level sections do not experience any warping during the forming process. If the velocity in the normal direction is known for one section, then the speed at another location can be calculated by means of the condition of volume constancy, and thus information can be obtained about the forming rate at that location.

As a result of these assumptions concerning the kinematics of the forming process, simple equations are obtained for forming force and stresses. Moreover, the level state of motion implies a homogeneous deformation state in the entire section.

The following assumptions characterize the possibilities and limits of the elementary theory:

- the material behaves homogeneously and isotropically,
- a rigid/ideal-plastic material model is assumed,
- level deformation kinematics are assumed and

- material behaviour in the plastic state is described by the yield criterion and volume constancy.

These conditions reduce the problem of plastic deformation to a statically defined system.

2.4.2 Energy Method

The energy method requires the least amount of calculation. Using this method forming forces and performance can be approximated. It is applicable when the kinematics of plastic flow of a manufacturing process can be estimated. One disadvantage of the energy method is that the stress history can only be determined roughly.

We will consider upsetting a square bar as an example for this method [FINK74]. Let us assume the yield stress k_f as a function of the effective strain φ_v , i.e. the flow curve of the workpiece material. If the sample has a square cross-section, then the true strains φ_1 and φ_2 are the same during the upsetting process for reasons of symmetry. It then follows from Eqs. 2.21 and 2.31

$$\varphi_v = |\varphi_3|$$

During one forming step $|d\varphi_3| = d\varphi_v$, the compression paths perform the work

$$dW_{id} = F_{Sr}|dh| = A \cdot k_f|dh|. \quad (2.36)$$

After division with the volume of the compression sample, it is obtained

$$dw_{id} = \frac{A \cdot k_f|dh|}{Ah} = k_f \frac{|dh|}{h} = k_f|d\varphi_3| = k_f d\varphi_v. \quad (2.37)$$

By integrating Eq. 2.37, the ideal forming work relative to the volume w_{id} follows as:

$$w_{id} = \int_0^{\varphi_v} k_f(\varphi_v) d\varphi_v. \quad (2.38)$$

It has the dimension of a stress and corresponds to the surface beneath the flow curve (Fig. 2.18). Frequently, a diagram contains not only the yield point $k_f(\varphi_v)$ but also the curve progression $w_{id}(\varphi_v)$.

The reference forming work of a general forming process can be calculated by means of the effective strain, so the following steps are taken when determining forming work, forming force and workpiece strength:

1. Assumptions are made concerning material flow from tool movement during the forming process, the geometrical properties of the problem, the continuity equation and also from tests and the true strains φ_1 , φ_2 and φ_3 are estimated.

2. With Eq. 2.31 the effective strain φ_v is determined and with the help of the flow curve the yield stress $k_f(\varphi_v)$ and ideal forming work relative to volume $w_{id}(\varphi_v)$ are determined.

3. From

$$W_{id} = \int_V w_{id} dV \quad (2.39)$$

the ideal forming work to be applied to the forming process is obtained.

4. The forming force is calculated from tool displacement and forming work.

It is known from practice that an effective forming work W_{eff} is necessary for most forming processes, which is larger than the ideal forming work W_{id} .

$$\frac{W_{id}}{W_{eff}} = \eta_F$$

is designated as the efficiency of deformation.

The cause of the difference between ideal and effective forming work is essentially the previously ignored friction between the tool and the workpiece. Friction in forming processes is dealt with in Sect. 2.8.2, p. 138.

2.4.3 Calculation Method with the Strip, Disc and Pipe Model

Characteristic of this method are the strip, disc and pipe-shaped volume elements the calculation is based on (Fig. 2.21). The tool shape and forming process determine which model is used. The application of equilibrium conditions leads in all three models to a linear, inhomogeneous differential equation of the first order. It is analytically solvable at least in some sections. By joining the solutions of several sections, an overall solution is obtained.

Drawing wire or bars will be considered as an example [PAWE76]. In accordance with Fig. 2.22, the equilibrium condition in the drawing direction leads to

$$\sigma_z + A \frac{d\sigma_z}{dA} + p(1 + \mu \cot \alpha) = 0. \quad (2.40)$$

The yield criterion after Tresca reads

$$p + \sigma_z = k_f. \quad (2.41)$$

In this way, both p as compressive stress and σ_z as tensile stress are defined positively. The cross-sectional surface A is selected as an independent variable.

Eliminating p , a common 1st order differential equation is obtained:

Elementary models in plastomechanics

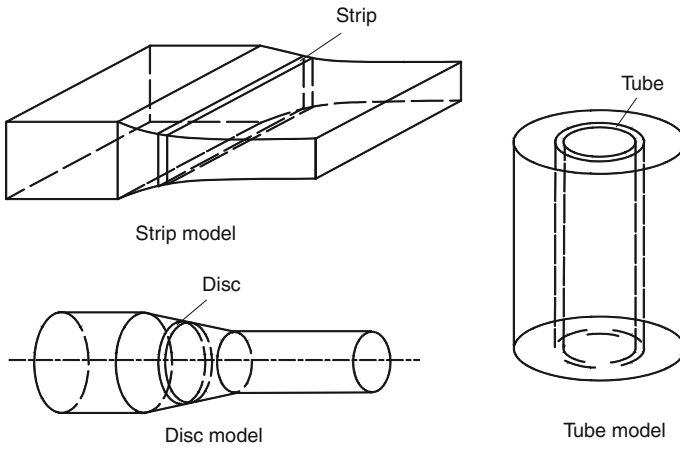


Fig. 2.21 Volume elements in elementary plastomechanics for different models (acc. to Pawelski)

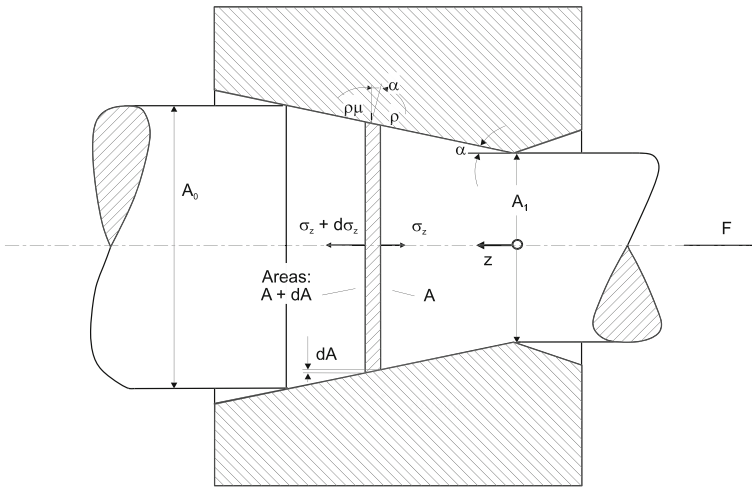


Fig. 2.22 Stresses on a disc-shaped volume element when drawing a wire or bar acc. to Pawelski [PAWE76]

$$\frac{d\sigma_z}{dA} - \frac{\mu \cot \alpha}{A} \sigma_z + \frac{k_f(1 + \cot \alpha)}{A} = 0. \quad (2.42)$$

It corresponds to the type of differential equation

$$\sigma'_z + f(x)\sigma_z + g(x) = 0, \quad (2.43)$$

as is always encountered in the foundation of elementary plasticity theory. The functions $f(x)$ describe the forming geometry and the influence of friction. Such differential equations can be solved sometimes analytically, but always numerically (e.g. using the Runge-Kutta method). For constant values of k_f and μ , the solution leads to the drawing force formula acc. to [SACH27]:

$$P_z = \sigma_z(A_1)A_1 = k_f \left(1 + \frac{1}{\mu \cot \alpha} \right) \left[1 - \left(\frac{A_1}{A_0} \right)^{\mu \cot \alpha} \right] \quad (2.44)$$

2.4.4 Strict Solution

“Strict solutions” can only be applied in the case of very simple, straightforward problems. A strict solution means that there are functions for stress distribution and the state of motion in the entire plastic area that fulfil the continuity equation, equilibrium conditions, the yield criterion as well as von Mises’s constitutive law. They must also comply with the marginal conditions. Usually we are dealing with tasks in which the geometry of the tools has partially determined the stress and deformation state. Examples of processes that can be solved in a strict way are provided in [PRAG54].

2.4.5 Slip Line Method

Slip lines are lines that have the direction of maximum shear stress at each of its points. The theory of the slip line method is based on the plane consideration of the forming process. The three unknown stresses σ_x , σ_z and τ_{zx} are subject to the equilibrium conditions in the x and z directions and the yield criterion. The task is thus statically determined. From these three static basic equations we obtain a system of partial differential equations of the first order. The latter represent two orthogonal curve sets corresponding to the slip lines. They are subdivided into α - and β - slip lines.

One disadvantage is that this theory is only valid for a planar formation and for an ideal-plastic material. Wall friction on the tool is also difficult to take into consideration.

If the slip line method is applied to axial symmetrical problems, formulations result that previously could only be solved with numerical iteration methods. We then refer to them as principal line methods. A detailed description of this method can be found in [HILL50, PRAG54, DIET86].

2.4.6 Visioplasticity and the Measuring Grid Method

Using the visioplasticity method, better approximations can be made of actual forming processes using plasticity theory than is possible with pure theory. The test piece to be formed is subdivided in a symmetry plane, and a line mesh is applied to the joint. In this way, the velocity field can be approximated by means of the mesh distortion arising during the forming process. With these input parameters, the stresses and forces can be calculated using the theory of plasticity. This will be explained in accordance with [LANG90a] in an abbreviated form using an axially symmetrical extrusion process (Fig. 2.23).

It will be assumed that the punch velocity and thus the velocity of the material in the undeformed shaft of the workpiece has the value v_{wz} . Then a line I-I in the shaft (Fig. 2.23) switches to line II-II in time

$$\Delta t = \frac{\Delta s_0}{\Delta v_{wz}} \quad (2.45)$$

In the same time, the intersection point A of the mesh migrates in the forming zone to A' . If the projection of the path AA' on the r -axis is designated with Δs_r and that on the z -axis with Δs_z , then with

$$\bar{v}_r = \frac{\Delta s_r}{\Delta t} \quad \text{and} \quad (2.46)$$

$$\bar{v}_z = \frac{\Delta s_z}{\Delta t}. \quad (2.47)$$

We obtain approximate values for the velocity components of point A . These are the more accurate the more tight the mesh selected.

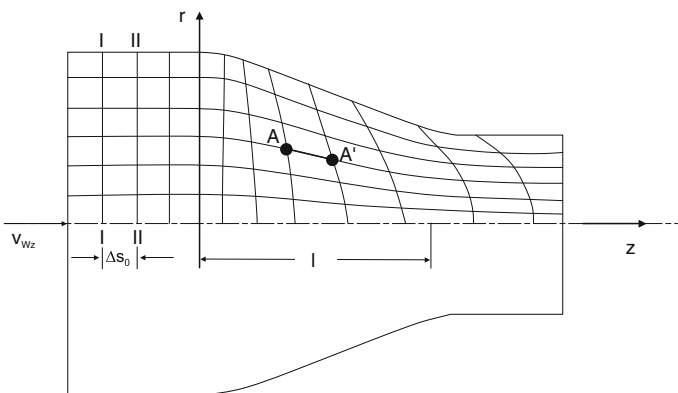


Fig. 2.23 Determining the velocity field from a distorted mesh for a stationary process, acc. to [LANG90a]

In the case of unstable processes, we obtain the velocities in a similar way if we determine the change in lattice distortion for two steps of the forming process that are in close sequence.

From the velocities v_i we can now determine the deformation rates graphically by plotting the calculated velocity components \bar{v}_r and \bar{v}_z over r and z and connecting them with a series of curves.

$$\bar{\dot{\epsilon}}_r = \frac{\partial \bar{v}_r}{\partial r} \quad \bar{\dot{\epsilon}}_r = \frac{\partial \bar{v}_r}{\partial r} \quad (2.48)$$

$$\bar{\dot{\epsilon}}_z = \frac{\partial \bar{v}_z}{\partial z} \quad \bar{\dot{\epsilon}}_{rz} = \frac{1}{2} \left(\frac{\partial \bar{v}_r}{\partial z} + \frac{\partial \bar{v}_z}{\partial r} \right) \quad (2.49)$$

The selected mesh must be fine enough to make an interpolation of \bar{v}_r and \bar{v}_z on lines $r = \text{const.}$ and $z = \text{const.}$ possible with sufficient precision. Now, the deformations can also be approximated from the deformation rates by integrating the deformation rates that a particle experiences on its way along a flow line. If the effective strain is also calculated, the yield stress can be obtained from the flow curve and thereby calculate the approximate values for the deviator components of the state of stress as functions of the spatial coordinates using the von Mises flow rule. In this method, a line mesh of a particular geometry, the “measuring grid”, is applied to the sheet surface to be formed and evaluated after forming. The grid nets commonly used in practice are almost exclusively composed of circles, but these can also be combined with square grids. Evaluation is significantly simpler in the case of circular grids, as the forming process distorts them into ellipses, the principal axes of which indicate both the size and direction of the principal deformations. On the other hand, square grids are usually distorted into undefined rhombi that are very difficult to evaluate [KÜBE80]. Circular grids have a diameter of about 3–10 mm depending on the size of the drawn part. Small dimensions make measurement more difficult, but they allow for a more differentiated evaluation of smaller areas. Great demands are made on methods for plotting measuring grids. In order to determine deformations accurately, the grid must survive the deformation of the sheet without damage. This requires good adhesive power, while at the same time the deformation behaviour of the sheet must be influenced as little as possible. Furthermore, the accuracy of the dimensions must be guaranteed to such an extent that measurement prior to deformation is superfluous [MÜSC69].

Mechanical application of measuring grids with the help of scribes or scribing compasses, formerly widely utilized, is the most inexpensive method with respect to device-related costs, but it is also very time-consuming and low in precision. Moreover, the notch effect brought about by the scribing process and the resulting influence on the material surface cannot be neglected, especially in the case of fine sheets.

The most precise and, with respect to grid quality, best results can be obtained by means of electrochemical and photochemical processes. However, the device-related costs are considerably higher. In the case of electrochemical application, the sheet is covered with a template and etched. In the photochemical method, the

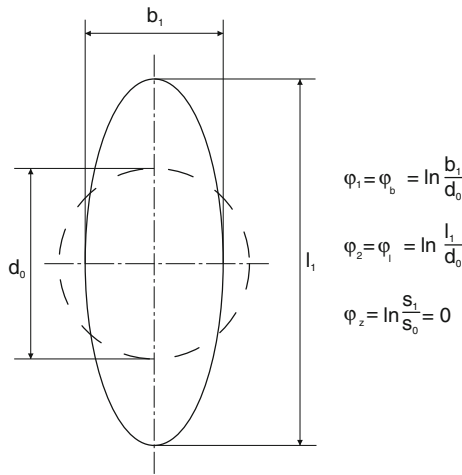


Fig. 2.24 Determining the true strain from a deformed measuring grid

grid is first applied to the sheet with a photosensitive lacquer by means of a grid negative. Then the surface not protected by lacquer is etched.

Other simple and economical ways to apply a line mesh include imprinting with rubber roll stamps, the screen printing method or the offset method. Due to the low abrasion resistance, these methods generally cannot be employed for deep drawing, but they can be for stretch drawing or tension test.

When evaluating a deformed circular grid, the length of both axes of the ellipse generated is measured and applied to the output diameter d_0 of the circle to determine the true strain in the longitudinal direction (φ_1) and the direction of width (φ_2). With the help of volume constancy, deformation in the direction of thickness (φ_3) or the local sheet thickness can be calculated from both true strains (Fig. 2.24).

In the case of curved surface areas, it has to be considered that deformations on the top and bottom sides of the sheet are approximately identical.

2.4.7 Upper Bound Method

In case the exact solution for forming performance cannot be determined for a forming process, often the upper and lower bound, between which lies the exact solution, are sufficient. Of primary interest in performing measurements on forming machines is the upper bound.

In the case of an exact solution, both the calculated stress field as well as the calculated velocity field fulfils the equilibrium conditions, the constitutive law, the condition of volume constancy and all marginal and starting conditions of the

problem. As a rule, there are several stress and velocity fields that fulfil part of these conditions independently of each other.

When calculating the lower bound for forming performance, only a statically permissible stress field is required; kinematics are not taken into consideration. Such a field needs only to satisfy the equilibrium conditions, the yield criterion and the marginal stress conditions. When calculating the upper bound, we start from a kinematically permissible velocity field which must fulfil the condition of volume constancy and the marginal velocity conditions [LANG90a].

2.4.8 Error Compensation Method

ECM originated in the direct treatment of variational calculus problems. It is basically restricted to planar and axially symmetrical forming processes.

In one section of a continuum, a function is sought (velocity field, stress field) that is determined by a differential equation and a marginal condition. For the unknown solution, a method of approximation is set up, e.g. in the form of a power series. If this approximate solution is inserted into the differential equation, it will not be satisfied exactly. The error depends on the form of the method and the choice of parameters. These parameters must be set so that the error distribution satisfies the target requirements. This can be done, for example, by using the method of least squares. In the first approach, usually viscous constitutive equations are applied. Then the plastic attributes of the material are taken into consideration. In the practical calculation, we alternately calculate a stress field from the constantly held velocity field and vice versa. This is repeated until the errors no longer exhibit diminutions or the velocity and stress fields no longer change.

With the error compensation method, we can calculate the local velocity distributions, deformation rate distributions, deformations/distortions, stress distributions as well as the yield stress, friction coefficient, forming force/performance and temperature fields. Areas that remain rigid during the forming process cannot be measured well using ECM. Errors arise with respect to satisfying the yield criterion that are also propagated in the plastic section. The consequence is an inexact calculation of the stress distribution. The use of this method is often limited by geometrical eventualities.

[LANG90a] includes an extensive description of the use of ECM in the upsetting of a cylindrical body. Further examples can inter alia be found in [ROLL81].

2.5 Finite Element Method

In the last 20 years, simulation has been established both in sheet and massive forming as an indispensable tool in research and industrial practice. The most frequently utilized method for simulating forming processes is the finite element

method (FEM). This is a numerical method for finding approximate solutions to continuous field problems. These are problems in which the behaviour of the continuum can be described by partial, time-dependant and location-dependent differential equations. Each state variable (e.g. stress, temperature) of a continuum possesses infinitely many values, since it is a function of every point of the continuum. The problem thus has an infinite number of unknowns. The basic principle of FEM consists in breaking down the continuum into a finite number of parts called finite elements. Thus, an initially complex, continuous problem is subdivided into a finite number of simple, mutually dependent problems. Applied to forming processes, FEM enables to make assertions about the size and distribution of various state variables in the material and tools during and after forming. It is thus a valuable aid in the interpretation and analysis of forming processes. FEM enables the investigation of such processes in forming engineering that, due to their complexity, can be handled with analytical methods only with great difficulty if at all.

Since the development of the basic concepts of FEM took place at the same time and with the same motivations in the spheres of mathematics, physics and engineering sciences, the exact time point of FEM's origination cannot be determined exactly. The designation "finite element method" was first used however in the year 1960 by Clough [CLOU60]. [HUEB82, KNOT92], among others, provide a history of FEM with reference to the three abovementioned areas of specialization.

In the following, the basic concepts of FEM will be introduced in addition to some application examples from forming technology. The goal is not to provide an introduction to the foundations of FEM, but rather to communicate the basic concepts as well as some of the technical terms. A good introduction into the foundations of FEM for engineers can be found, for example, in [KNOT92, BETT03, HUEB82]. In [ROLL93, KOB89], the method is explained with particular reference to forming technology. More advanced standard works on the topic include [BATH96, ZIEN00, REDD93].

2.5.1 Basic Concepts of the Finite Element Method

Even in the case of the use of forming-specific program packages, it is helpful to be acquainted with the basic concepts of FEM in order to avoid errors and to evaluate correctly the results of the calculation. The user should be conscious of the assumptions made by the software and their potential effects on the results. The process analysis by means of FEM is also called finite element analysis (FEA). The following steps are taken in every FEA [HUEB82, ZIEN00, REDD93, ROLL93]:

1. discretizing the continuum,
2. selecting interpolation functions,

3. determining the element properties,
4. assembling the element equations and
5. solving the system equations.

During continuum discretization, the solution domains (e.g. the workpiece) is subdivided into a finite number of subdomains, the finite elements. In the process, the type, number, size and distribution of the elements is set.

The selection of interpolation functions, which are often designated as shape or basis functions, takes place in practice at the same time that the element type is selected. The interpolation functions serve to approximate the progress of the state variables within an element. The element nodes function as support points for interpolation. In the case of “linear elements”, these are the vertices of an element. Higher-order elements have available a set number of additional nodes on the element edges or within the elements and, because of the larger number of nodes, supply a more exact solution. Due to their differentiability or integrability, polynomials are frequently used as interpolation functions. The order of the polynomials depends here on the number of element nodes, the number of unknowns of each node as well as on the continuity conditions at the nodes. Since the interpolation functions represent the behaviour of the state variables in the inside of the element, the values of the state variables at the nodes represent the unknowns of the discretized problem.

After selecting the element types and the associated interpolation functions, the element equations (element matrices) are determined. These equations describe the relations between the primary unknowns (e.g. velocity, dislocation, temperature) and the secondary unknown (e.g. stresses). To determine the element equations, several approaches are possible. The basic variation formulation for plastic problems is [ROLL93, KOBA89]:

$$\delta\pi = \int_V \sigma_V \delta\dot{\epsilon}_V dV + K \int_V \dot{\epsilon}_{ii} \delta\dot{\epsilon}_{ii} dV - \int_{S_F} F_i \delta u_i dS = 0 \quad (2.50)$$

with:

- π power generated by forming and friction
- $\delta\pi$ variation of power with the variation of the velocity field
- σ_V effective stress field
- $\dot{\epsilon}_V$ field of forming velocity
- V volume
- K penalty constant to limit volume change
- $\dot{\epsilon}_{ii}$ volumetric shape change
- S_F surface
- F_i surface forces
- u_i surface velocity field

With the help of numerical methods, the velocity field is sought that satisfies Eq. 2.50. This velocity field minimizes power consumption and thus the energy

cost. The “penalty term” ensures that volumetric deformation is kept low, and so the condition of volume constancy is nearly fulfilled. In addition, the velocity field sought must satisfy the marginal conditions.

One of the fundamental differences between FEM and other numerical approximation methods is that the solution is first formulated for every single element. In order to approximate the properties of the overall system built of these elements, the element matrices are assembled into the global matrix of the problem. Also, the marginal conditions (clampings, external forces, etc.) are introduced. Assembly of the element equations yields the system equations, which are then solved with the help of suitable methods. The numerical integration methods employed to integrate the element matrices require the evaluation of the integrals at certain points within an element, so-called integration points. In the process, the number of required integration points can be reduced without affecting accuracy by carefully selecting their positions. The Gaussian quadrature is a very common method used for numerical integration in FEM. The positions of the integration points within an element are exactly determined and represent the positions at which stresses and elongations are calculated [KOB89, ROLL93, ZIEN00]. Even if the basic procedure of all FEM-based calculations is the same, the programs used differ in a few fundamental aspects.

2.5.2 Lagrangian and Eulerian Representations of the Continuum

The continuum can be discretized using different approaches. The most common approaches in FEM are the Lagrangian and Eulerian [BATH96].

The Lagrangian method is the most dominant in forming engineering. In this case, the nodes of an element move along with the material. An observer travelling on a node would observe change in the state variables of a particular particle throughout the entire forming process. One disadvantage of the Lagrangian approach is the mesh distortion entailed by large-scale plastic deformations, which can sometimes require remeshing. The interpolations of the state variables from the distorted to the new mesh lead to an undesirable, more or less distinct smoothing of the state variables depending on the number of remeshing cycles.

The Eulerian approach proceeds from the movement of a continuum through a fixed mesh. An observer on a node of such a mesh would observe the changes of all particles that pass his fixed point of observation. The method is especially appropriate for investigating stationary processes and is frequently employed in flow simulation. The “arbitrary Lagrangian-Eulerian” (ALE) method is being increasingly used. This is a combination of the above methods permitting the mesh a motion independent of the material as long as the shape of the domains under considerations remains intact [KOB89, WU03].

2.5.3 *Explicit and Implicit Solution Methods*

Most programs employed in massive forming make use of so-called implicit methods, whereas in sheet forming and for highly dynamic applications (e.g. crash simulations) explicit time integration is widely used. Explicit methods consider the process under investigation as a dynamic problem subdivided into time increments. The target variables at time $t + \Delta t$ are determined only from the values available at time t . This is done usually by means of difference schemes. Yet this method is only stable if time increment Δt is smaller than the time required for an elastic wave to cover a distance corresponding to the shortest element edge. In this way, the possible size of the time increment is contingent on the sonic velocity c present in the material. The following is valid for solid bodies:

$$c = \sqrt{\frac{E}{\rho}}.$$

The maximum possible time increment thus depends on the density ρ and modulus of elasticity E of the material. Since the time increment can be in the range of microseconds, a very large amount of calculation steps is sometimes required. “Mass scaling”, the artificial increase of material density or artificial shortening of process time, represents an attempt to increase the possible size of the time increments. The mass effects caused by such interventions have to be compensated by suitable measures [ROLL93, CHUN98].

This limitation does not exist when using implicit methods. Implicit solvers seek the solution for every time $t + \Delta t$ under consideration of the values of the target variables both at time t and at time $t + \Delta t$ [HUEB82]. Due to the nonlinearities involved, this requires the solution of a non-linear equation system by means of an iteration process (e.g. Newton-Raphson) [ROLL93, ZIEN00]. To the advantage of the up to 1,000 times larger possible time increments compared to the explicit method is thus joined the disadvantage of the calculation time required for the iterative equation solution.

2.5.4 *Thermal Coupling*

When considering thermal processes, the mechanical and thermal calculations must be coupled. In the case of simultaneous coupling, this is achieved by setting up a completely coupled equation system. Non-simultaneous coupling proceeds from a purely mechanical formulation, in which the temperature serves only to determine temperature-dependent material characteristic values (e.g. the flow curve). The mechanical calculation calculates frictional heat, heat from plastic deformation and heat exchange with other objects or the environment. These data are then the input variables for the thermal calculation. This coupling can take

place at every iteration (iterative coupling) or at every time increment (incremental coupling) [KOPP99].

2.5.5 Element Types

Basically, three different categories of elements are used in forming engineering [ROLL93]:

- volume elements (continuum elements),
- membrane elements and
- shell elements.

In massive forming, mainly continuum elements are used. In this case, we distinguish between planar, axially symmetrical and three-dimensional elements, depending on the state of deformation. Continuum elements make it possible to capture all normal and shear stresses. The complete definition of an element type includes the element shape, number of nodes, type of node variables and the interpolation functions. In massive forming, so-called isoparametric elements without centre nodes have become established [ROLL93]. An element is isoparametric if it has the same interpolation function both for the state variables within the element and for the coordinate transformation from the global into the local coordinate system (element coordinate system) [ZIEN00, ROLL93]. Figure 2.25 shows

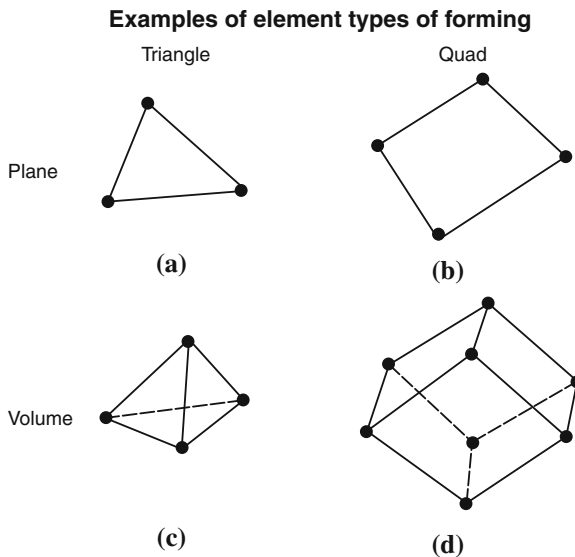


Fig. 2.25 Examples of element shapes used in forming engineering triangle (a), square (b), tetrahedron (c), and hexahedron (d)

some examples of element types that are used in forming engineering. Typical element shapes are triangular and quadratic elements with three or four nodes as well as tetrahedral and hexahedral elements with four or eight nodes [HUEB82]. In sheet forming, mainly membrane and shell elements are employed, in rare cases continuum elements as well. Membrane elements cannot convey bending moments, are not suitable for capturing wrinkle formation and are thus hardly used anymore. Shell elements on the other hand are capable of capturing bending moments and of taking wrinkle formation in shell forming into consideration. “Thin” shell elements (acc. to Kirchhoff) have a finite bending and shear stiffness [ROLL93]. Since triangular shell and membrane elements only differ in the freedom of their nodes, the representation in Fig. 2.25a is valid for both element types.

2.5.6 Non-Linearities

A linear analysis is the analysis of a problem that exhibits a linear relation between the loads applied and the answer of the system. Linear analysis represents a simplification, since every real physical system is non-linear. These non-linearities can however be neglected in many cases. If we speak of non-linearities in FEM, this indicates that these non-linearities must be taken into consideration.

Basically, we differentiate between three different kinds of non-linearities:

- material non-linearities,
- geometric non-linearities and
- non-linearities in the boundary conditions.

Material non-linearities result, for example, from a non-linear relation between stress and displacement which occurs in metallic materials after leaving Hooke’s range. Further causes for material non-linearities include material behaviour that is dependent on the forming rate and/or temperature as well as material failure.

Geometric non-linearities are caused by an alteration of geometry during the calculation. As soon as the displacements arising are large, thus influencing the behaviour of the system, it is considered a non-linearity.

Non-linearities in the marginal conditions are caused, for example, by a change in the external loads or by new contact or loss of contact between two objects (e.g. tool—workpiece). As a rule, we encounter all three types of non-linearity in a typical forming process simulation.

2.5.7 Constitutive Laws

The constitutive laws implemented in the simulation of forming processes for the representation of metallic materials can be subdivided into two main groups: those

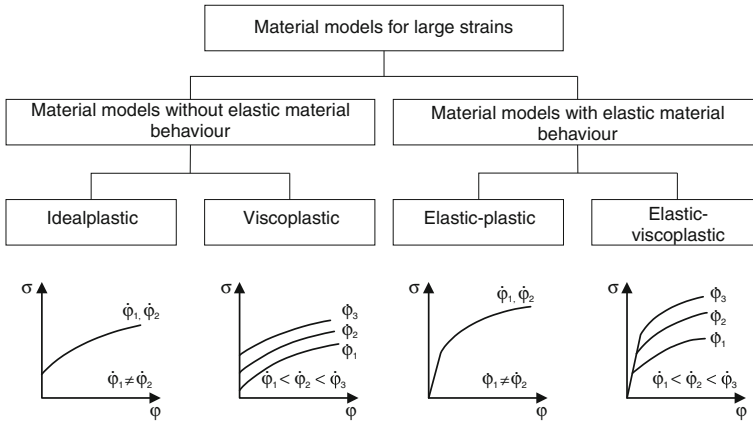


Fig. 2.26 Classification of material models for large plastic deformations [ROLL93]

that take elastic material properties into consideration by regarding the material first elastically and upon further deformation plastically, and those that consider the material as rigid until the plastic limit is reached (Fig. 2.26). The use of a rigid-plastic constitutive law accelerates the calculation and provides satisfactory simulation results for many applications in massive forming, since the amount of plastic deformation compared to elastic deformation is significantly larger [ROLL93]. Elastic-plastic material models are important when elastic effects (such as spring-back and residual stresses remaining in the component) are no longer negligible. The velocity-dependence of the material's properties, such as the "viscous" constitutive laws take into account, plays a role for steel materials mainly in hot and warm forming. Most programs permit the inclusion of temperature-dependence of material behaviour. The consideration of textures and the associated geometrical anisotropic material behaviour is especially significant in sheet forming, but it is growing in importance in massive forming as well with the increasing demands on component quality. Observation of anisotropism in the stress space (Bauschinger effect) is becoming increasingly important as well, especially in massive forming.

2.5.8 Software

Both commercially available FEM packages as well as packages specially tailored for forming processes have become established for process simulation in forming engineering. An overview of such packages can be found in [ADLO04]. These programs offer user interfaces that are adjusted to the needs of forming engineering and make the design and execution of simulations easier for the user. The simplified operability of such specialized program systems usually entails a restriction

on the possibilities of the model's control. So-called "general purpose" systems on the other hand are indeed flexible and can be used for diverse applications outside the field of forming technology, but the modelling process often requires a large amount of experience and a larger expenditure of time. Depending on the application spectrum, the use of different FEM programs by one company is quite common.

Among programs specialized for forming engineering, a distinction is drawn between programs for sheet forming and programs for massive forming. This distinction is the result of various demands that manufacturing processes make on the simulation as well as the possible ways to describe material behaviour.

The decision of whether a problem should be investigated in two dimensions or spatially depends on the problem definition and the dominant state of deformation. Many problems exhibit axis or rotation symmetry, i.e. we can assume a level state of elongation or stress [ROLL93]. By exploiting existing symmetries, the calculation time required can be significantly reduced in comparison to the three-dimensional of an entire component.

2.5.9 Hardware

With the rapid development of the computer industry, processors are becoming continuously more powerful. While a few years ago cost-intensive computer systems were required to carry out calculations with FEM, these days many personal computers (PCs) used as workstations are equipped with the necessary requirements with respect to working memory and processing power for calculating simple calculations. Personal computers for calculating larger problems are already available at moderate prices. To handle very demanding problems with a large number of elements, such hardware can also be used for operation in "clusters". In this case, several computers are networked in such a way that a substantial problem can be calculated on several computers simultaneously. The precondition for this is the support of this functionality with FE software. The computation time for a problem does not become reduced in a linear way with the number of nodes (here: computers) in the cluster. The effective increase in speed depends rather on the hardware and software employed. The behaviour of a specific software as a function of the available processing power is called scalability. A software scales well if the calculation time required for a task is approximately halved when the available processing power is doubled.

2.5.10 Phases of a Finite Element Analysis

From the user's point of view, a typical finite element analysis (FEA) takes place in three phases:

- data preparation with a pre-processor,
- calculation and
- evaluation of the results with the postprocessor.

With the help of the preprocessor, the user provides the software with all information necessary for the modelling of the problem. The problem must be rendered abstract enough for it to be represented with the help of the software. The simplifications made and the quality of the data the user provides to the system have a decisive effect on the quality of the simulation results. As a rule, pre-processing contains the following steps:

- geometry definition,
- networking,
- material data input and
- defining the marginal conditions.

Modern programs are equipped with import filters for common CAD formats. The geometries of the objects involved in the simulation can thus often be taken from the 2D or 3D CAD data sets present in the design in electronic form.

Meshing of the objects (discretization) takes place after the object geometries are defined. For mesh creation, most software manufacturers provide tools that permit a rapid meshing of geometries. If these tools reach their limits, separately available commercial meshers can be used. If several element types are available, then the user can select one. Specialized software packages frequently provide a specific element type. The size and distribution of the elements are determined by the user. The element type and element density of a mesh have a significant effect on the quality of the simulation result. Basically, using a larger amount of elements leads to more precise results. To save calculation time, often adaptive meshes with a locally varying density are used in order better to resolve local gradients in the state variables. Some programs offer the possibility of automatic adaptive remeshing, in which the element density is automatically adjusted to existing gradients.

After discretization, the mechanical and thermophysical material data are inputted. This step requires that the corresponding data is available under the conditions of the simulation. Then the boundary conditions are indicated such as external loads, contact conditions, friction between different objects and velocities.

After calculation, the results are evaluated in the postprocessor. Depending on the software, a number of possibilities are available for representing the results graphically and for further processing. Evaluation of the results also includes the critical judgement of the user. A comparison of the results with experience, roughly estimated calculations or experimental results is essential.

Possible sources of error of FE analysis include:

- discretization errors from the interpolation of the geometry during meshing and interpolation of the state variables,
- faulty input data (e.g. material data, process data, friction conditions),
- numerical errors (e.g. from numerical integration) and

- rounding errors due to the limited accuracy of the floating-point representation in the computer.

2.5.11 The Use of FEM in Forming Engineering

Due to the varying process kinematics and differing focal points in the consideration of the process, many FEM programs are tailored to special processes of massive and sheet forming. Only a few programs are suited to both areas. Due to the geometry of the components and the arising states of deformation, in most cases volume elements are used in massive forming and shell elements are applied in sheet forming. The focus of the evaluation of the results is also significantly different. While in massive forming the material flow and with it the mould filling behaviour, deformability and tool load are investigated, the foci of investigation in sheet forming engineering are deformability (thinning and crack probability), wrinkle formation and spring-back of the component.

2.5.11.1 Massive Forming

In the 1990s, finer and more detailed models have led—hand in hand with increasing processing power—to drastic improvements in massive forming simulation. Commercial FEM systems allow for the calculation of the 3D material flow of a forming level with high precision in a few hours. In the simulation of massive forming processes, the focus on the workpiece side is generally on material flow, mould filling, subsequent grain flow, material hardening, grain structure formation and the deformability of the material. With respect to the tool, the mechanical, thermal and tribological tool stresses and tool flexibility are determined. Several applicable programs for massive forming have thus been established for industrial use in recent years [ADLO04]. The uses of FE simulation and its savings potential can, according to [FELD01], no longer be ignored.

Tool Design

Mechanical Tool Stresses. To calculate tool stresses, the elastic properties of the material must be known. Figure 2.27 shows the die stresses that arise as a result of a lateral extrusion operation for manufacturing a helical gearing. Observation of the stresses induced in the die shows that the maximum principal normal stresses σ_1 can be significantly reduced by prestressing the die. Thus, the maximum tensile stresses are encountered in the non-prestressed die in the area of the tooth base. The tooth base acts as a chamfer on the die and can, in combination with the high tensile stresses, lead to crack formation in this area of the die. After a short period of use, a non-prestressed die exhibits hair cracks in almost every tooth base that

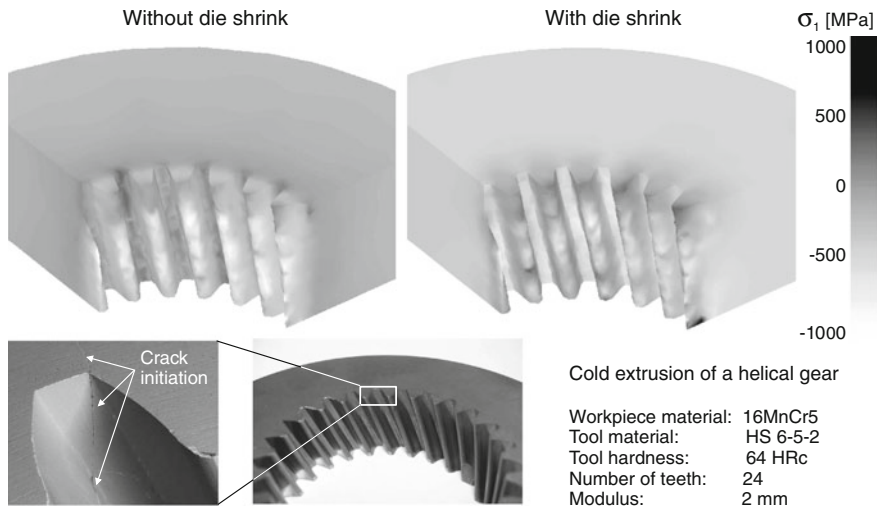


Fig. 2.27 3D simulation of the stresses of a tool die for lateral extrusion of a helical gearing

grow radially and outwardly. Crack formation can be prevented with the help of die prestressing. In that case, the first principal normal stresses in the tooth base of the die may not lie in the positive range (the tensile stress range) when under maximum load by the forming process.

Tribological and Thermal Tool Stresses. The following will show, using the example of fine blanking, how FE simulation can be used to determine tribological conditions like contact stress distribution, the relative velocities of the contact partners and temperature distribution. Analytical considerations can only deliver rough reference values about the order of magnitude of the contact normal stresses to be expected. Thermal processes are very transient, so elementary considerations are not accurate enough to be consulted for correlation with wear processes. Furthermore, the temperatures encountered in fine blanking can only be captured metrologically with great effort, whereby the measurement results are generally unsatisfactory on the whole. The area of interest, in which the danger of adhesion formation is the greatest, is the area directly over the punch edge. It is almost impossible to reach this area with thermoelements. Also, the area affected by high temperature is very small, so there is a large drop in temperature already after tool opening, making a pyrometrical (optical) measurement meaningless at that point. For these reasons, FE simulation makes sense for this process as well. For the example shown in Fig. 2.28, the temperature field has been calculated once with and once without friction. A free friction law was utilized for the friction model, which characterizes dry contact between the friction partners and will be described in more detail in Sect. 2.8.2.3. For the parameters given in Fig. 2.28, the calculated maximum temperatures are equally high for both cases. At the start of the partial cutting process, the contact zone temperatures are not significantly different. At the end, much higher temperatures were calculated for the case with friction. From

2D-Simulation of temperature & distribution during fineblanking

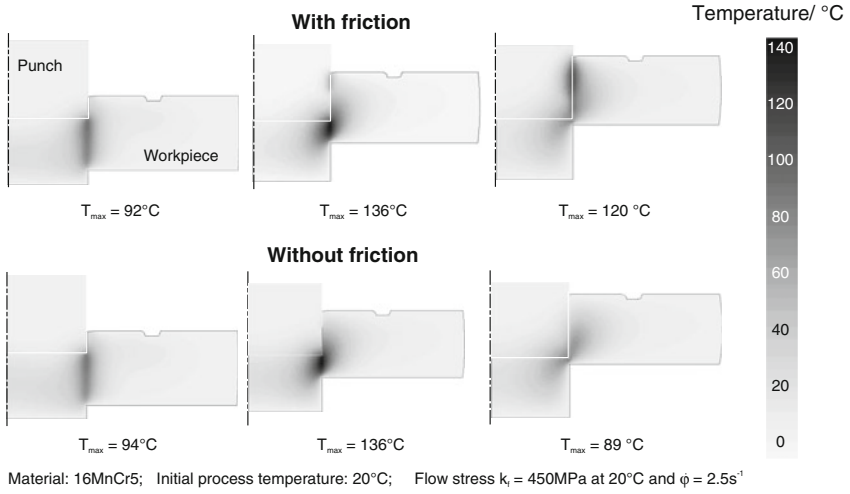


Fig. 2.28 2D simulation of the temperature field during the fine blanking process [RAED02]

these results, we can also derive for the case at hand that the amount of heat created by the forming process is much larger than that caused by friction. This is however not generally the case, but is valid only for the conditions shown in Fig. 2.28.

Workpiece Design

Determining Workpiece Geometries. Fine blanking is a sheet cutting manufacturing process. However, the forming processes taking place in the shape forming zone correspond to those of massive forming. For this reason, fine blanking processes are generally evaluated with the methods of massive forming. Up to the point of final separation of the material, fine blanking is a pure material forming process that is characterized by strong shearing. The heavily localized shearing and surface regeneration result in special marginal conditions of the simulation: The elements on the surfaces and in the peripheral zone near the surface in particular can become considerably distorted very quickly. In order to nonetheless proceed stably with the simulation, meshes must be regenerated frequently, whereby the calculated new information must be transferred to the new mesh. This is generally done automatically.

A special problem is encountered in case of fine blanking of fine contours (e.g. gears). Here, the material is especially strongly drawn in the cutting direction at the edges at the beginning of the fine blanking process. This phenomenon is called edge draw-in. Edge draw-in is not desirable because it reduces the useful functional surface. It is thus of particular importance in designing the active elements

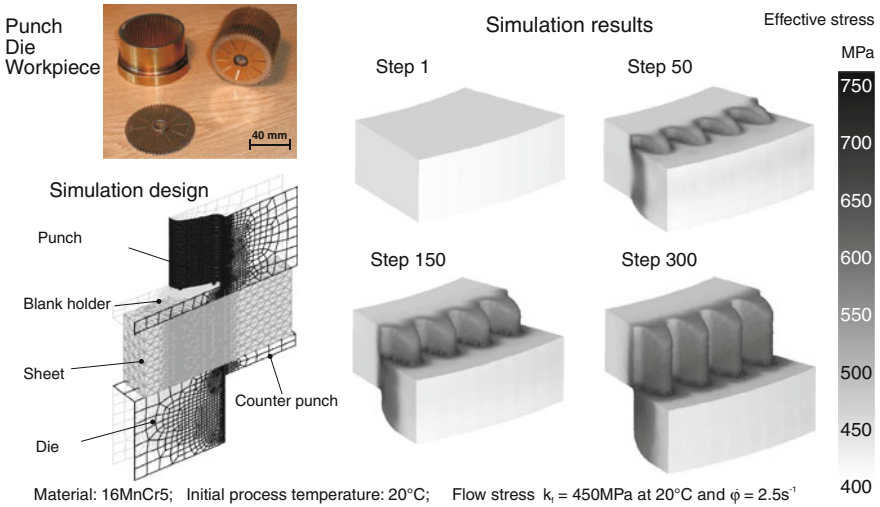


Fig. 2.29 3D simulation of a fine blanking process with respect to the formation of draw-in on the sheet surface [KLOC02a]

of a fine blanking tool [i.e. the punch and pressure pad as well as the die and knife-edged ring (holding-down device)] that the expected edge draw-in be determined beforehand in order to introduce countermeasures via tool design and process design, if required. Figure 2.29 shows the structure of a 3D simulation for the gear fine blanking and the formation of draw-in on the sheet surface. By exploiting the level symmetry of the gear, it is sufficient to model only half of a gear width. The four tool elements concerned have been represented as rigid, while elastic/plastic material properties (constitutive law) were assumed for the workpiece. The numerical results show that the edge draw-in is very distinct on the tip, since the stresses are not sufficient for plastic flow as the cutting process is introduced on the sheet surface. The material is curved near the gear tip due to the relative motion between the punch and the die so that plastic deformation of the gear tip takes place in the direction of the tooth width. In summary, it can be concluded that the simulation of fine blanking is comparable to the simulation of a cold forming process.

Let us consider orbital forging of a wheel hub made of C55E as an example of hot forming. Figure 2.30 shows the simulation of the orbital forging process with the help of FEM. This is an incrementally working forming process in which the contact surface between the upper die and the workpiece is small in comparison to the overall surface and rotates around the workpiece axis with progressive forming. Incremental forming can significantly reduce the forming force in contrast to massive forming. Figure 2.30 shows the stationary lower die and an upper die which carries out a linear feed motion superimposed with a gyrating feed motion. Due to the complex process kinematics, the calculation must be 3-dimensional even if the component being manufactured is rotation-symmetrical.

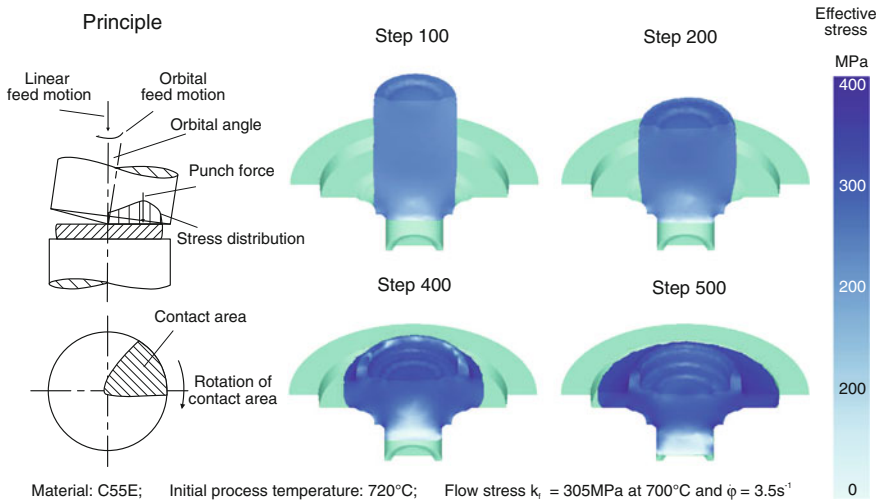


Fig. 2.30 3D simulation of orbital forging

The cut through the main component shows that the effective stresses in the area of the lower pin hardly exceeds the yield stress k_f of the material. This is not the case near the flange, which is well-moulded. Because of such complete mould filling, material flow ceases in the flange area. Despite increased punch forces, the yield criterion cannot be maintained in the area of the pin. Complete mould filling of the pin is not possible with the indicated parameters.

Determining the Sequence of Stages. With the stage sequence the most important working steps in the forming process chain are determined until the final shape is obtained. As an example the forging of an eccentric shaft for a fully variable valve control will be considered here. Figure 2.31 shows the material flow simulation of this complex forging part. Figure 3.55 shows the actual component and the individual intermediate stages. The cylindrical output blank (section) is heated to the process starting temperature of 1,250 °C by means of induction. Since the tooth segment in the centre of the eccentric shaft required a highly inhomogeneous material distribution across the length of the forging part, in the first forming stage a material agglomeration is applied to this area by pre-upsetting. A preforming stage follows and then the finishing stage. In the finishing stage, the final contour of the eccentric shaft is obtained with the forging measurements to a large extent. Since almost complete mould filling is already realized in the pre-stage, the finishing stage serves primarily again to reduce the tolerance width and to compensate for any dimensional deviations resulting from tool wear in the pre-stage. Comparison of the simulation results with the real component in Fig. 3.55 shows that the simulation represents the process well, which also manifests itself in the reduced flash formation. In this way, simulation can help realize a sequence of stages with an optimal use of material.

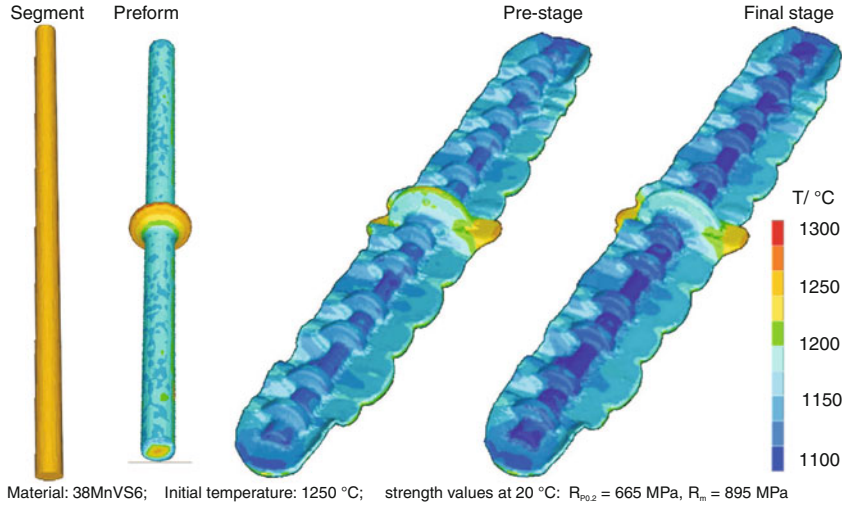


Fig. 2.31 3D FEM material flow simulation for the forging of an eccentric shaft in three stages (Source Hirschvogel Umformtechnik GmbH)

FE simulation can also be used to help calculate the obtainable component quality of a laterally extruded spur-toothed gear, in which case both procedural principles of radial lateral extrusion and “divided flow” are employed. The top row of images in Fig. 2.32 shows the first forming stage, in which a ring-shaped punch introduces divided flow in both axial and radial directions.

Friction in metal forming

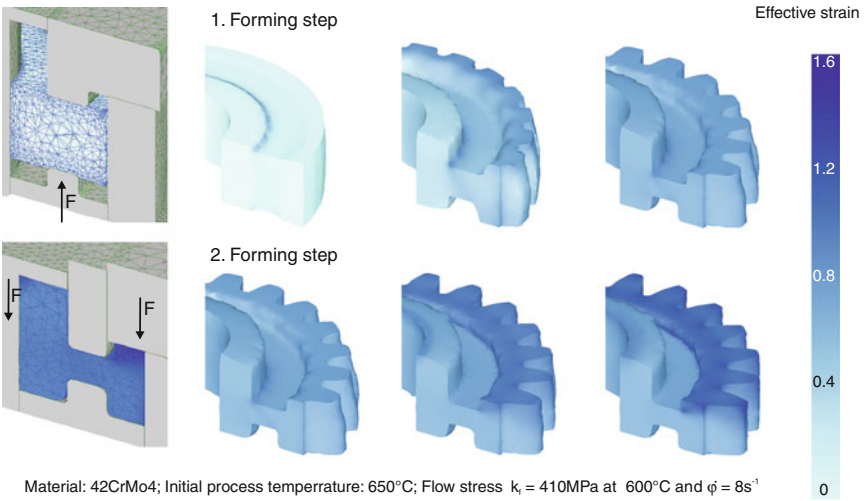


Fig. 2.32 3D simulation of the lateral extrusion of helical spur gears in two stages with the procedural principle of “divided flow”

In the internal component area, there is a flow of material in the axial direction, and in the external component area, the flow is in the outward direction. In the first forming stage, radial material flow is not sufficient enough to provide a complete material filling of the teeth. Thus, in the second forming stage the material is pressed radially outwards in the axial direction into the tooth mould and radially inwards by upsetting the external gear area. In this way, the tooth shape is formed along the entire width of the tooth.

Both examples show that FE simulation is an important aid in designing individual forming stages in massive forming. If the designer recognizes problems in the simulation calculation, many ways to intervene are opened up. On the one hand, the final result can be affected positively by varying the feeding positing into the cavity. On the other hand, it may be necessary to change the tool geometry of the corresponding forming stage. Changing the previous forming stage would be much more difficult and is not at all desirable. Attempts are thus being made to determine the individual stages of forming proceeding from the geometry of the finished part via reverse simulation. A definite prediction of material flow is absolutely necessary here, since it would be otherwise impossible to determine the individual forming stages [BEHR04a].

Modelling Heat Treatment Processes. During heat treatment, many mutually influential thermal, transformation-related and mechanical processes take place simultaneously. This affects the input data required for the simulation of heat treatment. Besides temperature-dependent elastic and plastic material behaviour, one must also possess information on structural transformation (e.g. TTT and TTS diagrams), diffusion coefficients, carbon distribution as well as carburizing and diffusion times. Many of these variables are difficult to determine or are highly imprecise. This is especially true when the mutual dependence of the processes on each other has to be taken into consideration. For this reason, the determination of these material data is usually very difficult and costly, and such calculations are usually undertaken only for especially sophisticated components. Figure 2.33 left shows martensite formation on the tooth flanks of a bevel gear made of carbon-manganese steel, which forms when cooling from an austenitizing temperature of 850 °C to room temperature. Oil is used as a cooling medium.

The right side of Fig. 2.33 shows a grain size distribution adjusted to the recrystallization behaviour of the material when hammer forging a low-pressure compressor disc made of Inconel 718. Grain size plays an important role in components subjected to high thermal and mechanical loads, whereby an opposing tendency can be recognized. With a diminishing grain size, the strength of the material increases, but the creep strength is reduced [GOTT98]. In turbine components, the attempt is made to use different grain sizes for different component areas. This can be done by means of a focused thermomechanical design of the forming process that is inhomogeneous along the cross-section of the component.

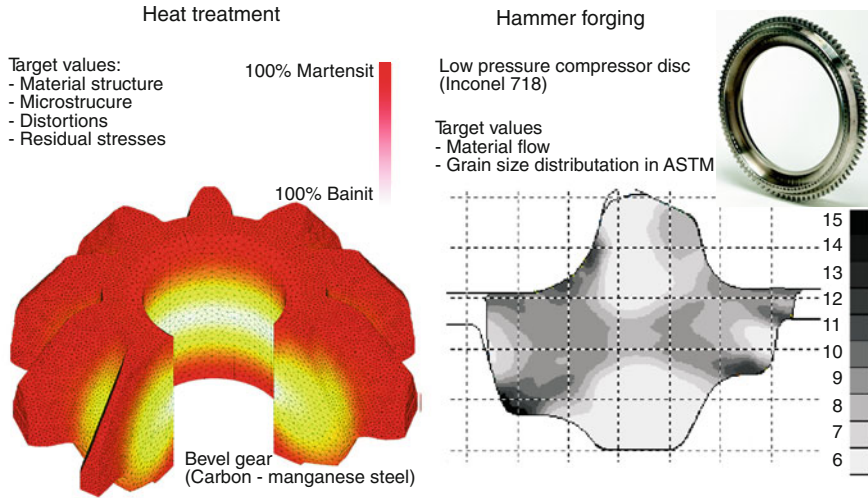


Fig. 2.33 Modelling heat treatment processes—*left* calculation of martensite formation on a bevel gear caused by heat treatment (*Source* SFTC); *right* calculation of the grain size distribution for the hammer forging of a low-pressure compressor disc (*Source* MTU Aero Engines und Thyssen Umformtechnik GmbH)

2.5.11.2 Sheet Forming

The focus of FEM development in the area of sheet formation has been in feasibility studies of particular forming operations. In addition, the crash behaviour of automobiles has been the subject of analysis since the end of the 1980s. In the latter case, the centre of attention is on the deformation of body parts, which are almost exclusively sheet forming parts. Figure 2.34 shows an example of such a FEM crash simulation.

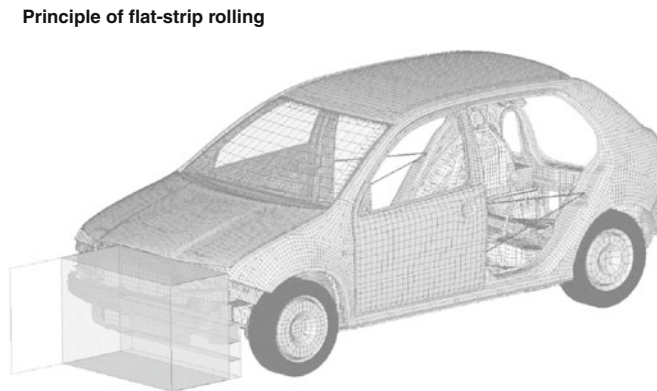


Fig. 2.34 Structure of a crash simulation with the program Pam-Crash by ESI GmbH

Due to the development of the automobile industry, the largest user of FEM simulation in the area of sheet forming, specifications have also been adjusted to modern simulation technology. With the help of FEM, concepts can be tested for their feasibility in the production process already at an early development stage. This leads to shorter product cycles with correspondingly short development times overall.

At the same time, growing environmental consciousness has led the automobile industry to develop fuel-efficient vehicles based on lightweight designs. Motor vehicles should be both light and safe. With an eye to this goal, new materials have been developed not only for components and body parts but for interior equipment as well. The industry is now using aluminium alloys and new steel types such as DP, CP and TRIP steel, the capability of which lies far above the range of earlier steel types (see Sect. 2.7.1.1). Components made of these materials can only be implemented in forming simulation with a high degree of precision.

The uses of present-day FEM simulation in the area of sheet forming are concentrated on deformation prediction. With the help of common software tools, usually feasibility analyses of different sheet metal geometries are undertaken. Of particular importance is recognizing and predicting material thinning. Such effects during the deep drawing process lead to weak points in the component, increasing the danger of failure. Besides thinning, material agglomeration along the component geometry also occurs frequently. With the right process design, the areas in which thinning occurs can subsequently be supplied with sufficient material, while the material can be used more effectively in those areas in which agglomeration takes place [FRIE02]. Figure 2.35 shows an example of the simulation of sheet thickness alteration in the mudguard of a passenger car.

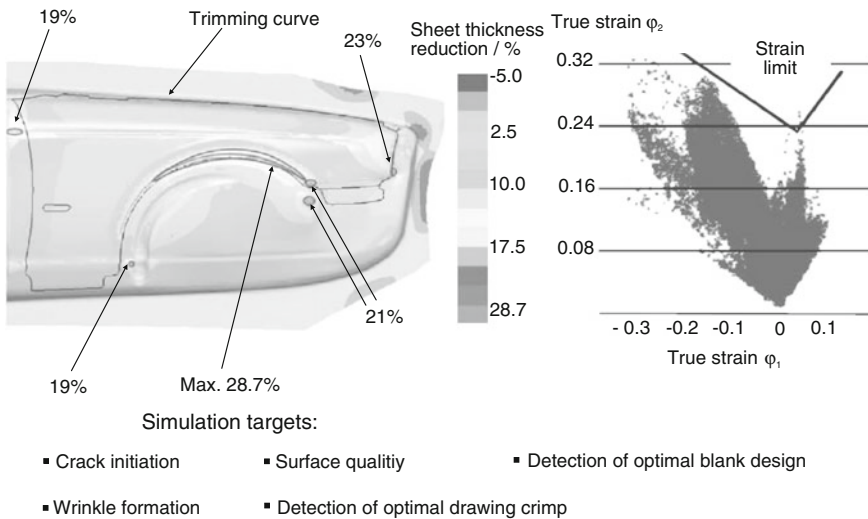


Fig. 2.35 Simulation of a mudguard with calculation of sheet thickness change and local true strain with respect to cracking (Source Thyssen Nothelfer GmbH)

Material flow is predominantly controlled in sheet forming with the help of drawbeads (Sect. 4.1.2.1). These can be designed and constructively adjusted for the load case at hand with the help of FEM. In this way, the sheet forming process can be optimized already, without taking geometrical component changes into consideration.

Wrinkle formation during the process is an important influencing parameter in sheet forming operations. It is especially important in the outer skin of body parts that no wrinkling occurs, as it remains visible even after finishing. Moreover, wrinkling can also produce weak areas in the component leading to failure under strain. For these reasons, wrinkles must be avoided—see Sect. 2.7.1.1 for more on this subject.

In most cases, shell elements are used in sheet forming simulations. Variation in material thickness during the process is calculated using shell elements by means of special algorithms. If volume elements are used, the actual change in sheet thickness can be calculated more accurately. However, a volume element has more degrees of freedom than a shell element, leading to an increase in calculation time. In the last several years, further development in the computer industry has made it possible to increase the element numbers or element information used without slowing down the simulation. For this reason, the use of volume elements is on the rise [WU00]. In sheet forming, the use of shell elements is sufficient in most cases however, since sheet thickness change is desired in only a few processes [KUBL95].

One of the greatest problems is calculating the springback that occurs after a forming process. It is essentially caused by free bending and is difficult to calculate beforehand. This problem is currently still under investigation.

Besides complete calculation approaches, partial approaches are also used in sheet forming in order to answer specific questions:

1. Cross-Section Simulation

In cross-section simulation, the complete component is not considered, but only the cross-section presumed to be in danger. The durations of the simulation is drastically reduced by considering only a part of the entire workpiece.

A further advantage of investigating only a single cross-section is that it enables the reduction the required input data. Only the data required in the cross-section being considered and not the exact definition of the entire component are necessary to obtain an executable simulation.

The disadvantage is that the cross-section to be investigated must be selected such that it also illustrates the effects that are to be analyzed. The correct selection of the cross-section is not trivial, and there is also the danger that the effects to be analyzed do not arise in the selected cross-section. Also, investigating only a small cross-section of the entire forming problem involves a large amount of simplification. This simplification allows mostly for qualitative and only rarely quantitative predictions using the obtained results.

2. One-Step Simulation

One-step simulation is used for inspecting geometry. With the help of this simulation, feasibility analyses can be carried out quickly and efficiently without

the necessity of long calculation times. The only crucial factor for the calculation is the change in geometry from the blank to the component. With the reverse method, the sheet cut required for the forming operation can be determined. In the forwards direction, the amount of true strain can be estimated from the change in geometry. Stress on the workpiece beyond its deformability limit can thereby be determined and prevented at an early development stage.

By calculating the phenomenon to be investigated in only one simulation step, calculation time is significantly reduced. In this case too, the specifications of the input data are normally not as high as in full simulations. In this way, it is possible to obtain valuable results quickly. Example of the use of this procedure include the initial feasibility estimations in product creation. A detailed consideration of the overall process is not possible with this method however.

2.6 Metallography and Analysis

2.6.1 Introduction

Metallography is the investigation of grain structure for the sake of qualitative and quantitative description. Structural investigation permits inferences regarding physical, chemical and mechanical properties of a material. The required microscopic analytical methods are applied to forming tools and unformed components during development and current quality control in the manufacture of forming parts as well as in the clarification of damage cases.

Grain structure is characterized by size, shape, distribution and volumetric content of the phases. Qualitative or quantitative evaluation of structure provides information regarding phase boundaries, precipitations, segregations, grain size distribution, lattice defects, deformation structures and their regeneration and recrystallization. Information regarding cracks, pores and other irregularities can also be obtained.

The most important methods and devices in metallography will be briefly described in this chapter from the standpoint of the manufacturing engineer. Using practical examples, the possibilities of metallography in manufacturing technology will be shown both in general and in the field of forming engineering specifically. The relevant literature will be referred to at corresponding locations for more in-depth study. An extensive treatment of the topic with ample reference to praxis can be found in [SCHU04b].

2.6.2 Optical Microscopy

For metallographic investigations, visible light with a wavelength between 350 and 780 nm is the most relevant. Here, the wavelength represents the limiting factor for the maximum resolution in light microscopes. The obtainable depth of sharpness is less than one in the case of a magnification of 1,000 depending on the aperture of the lens system [DOMK86, SCHU04a].

Only reflected-light microscopes are used for metallurgical optical microscopy. As opposed to the transmission electron microscope (medicine), only the reflected light beams enters the tube and can be captured by the human eye or by cameras or optic sensors (digital cameras). Figure 2.36 shows examples of micrographs taken with a reflected-light microscope at relatively low magnifications.

The contrast between different metallographic constituents arises from the varying reflecting power of individual constituents (light absorption, index of refraction, roughness/reflexion angle [DOMK86, SCHU04a]). Since the refraction/reflexion power of metals is very similar, in most cases different measures must be applied to increase the contrast such as etching, multiple reflection through vapour deposit coatings etc. [DOMK86, PETZ94, SCHU04a]. The individual methods are treated in Sect. 2.6.5 in more detail.

Methods of quantitative structural analysis are used for a more exact characterization of metallic materials [EXNE86, SCHU04b]. These yield structural characteristic values that describe things like the volumetric percentage, size, distance and orientation of individual phases and metallographic constituents. To this end, diverse arithmetic and metrological processes can be used, including comparative methods with rating charts.

2.6.3 Microhardness Testing

Besides the traditional hardness testing methods of Rockwell, Brinell, Knoop and Vickers, which are carried out using relatively large test loads, testing methods with extremely small test loads are practical for conducting tests on metallographic specimens. The Vickers test according to DIN EN ISO 6507-1 thus distinguishes between the Vickers hardness test, Vickers small load hardness test and the Vickers microhardness test [ISO04a]. The latter is suitable for use in metallography [SCHU04b]. The test loads in this case are between 0.09807 and 1.961 N (0.001–0.2 kp). The designation of the determined value depends on the test load (e.g. HV 0.2 corresponds to a test load of 1.961 N). Should the application require an especially low indenter penetration depth, often a Knoop pyramid is used instead of the Vickers pyramid [SCHU04b].

With the help of microhardness measurements, high-resolution hardness profiles can be obtained along the cross-section of metallic samples in addition to measurements of finely structured surfaces or thin layers. Depending on the grain

size of the metallic sample to be investigated, hardness differences between individual grains can also be determined. In the case of coatings, this is also the only method with which hardness and the modulus of elasticity can be established (see Sect. 2.8.5.3).

In many applications, microhardness testing is used to investigate the hardness gradients in the peripheral zone of components. Figure 2.36 shows two typical examples. On the left is the etched cross-section through the area near the surface of a forged and induction-hardened component made of 100Cr6. After exposure of the etched specimen, on which the effective hardening depth can be clearly recognized (change in colour), the sample was repolished and numerous microhardness impressions with a test load of 1,000 mN were made (corresponding to HV 0.1). In this way, the hardness of the peripheral layer can be quantified for quality control purposes (see Fig. 2.36 left).

The second example shows the loss of hardness in the peripheral zone of a sample from the intersection between the impression and die land of an overheated and plastically deformed die (see the SEM image, Fig. 2.36 top right). Here, the hardness measurement was utilized for damage analysis. The die is a forging die made of plasma-nitrided hot-working steel X 38 CrMoV 5-1. The hardness of the nitrided layer, which is completely worn out after damaging, can be seen clearly in the diagram in Fig. 2.36 right (in the microgram in Fig. 2.36 no longer recognizable).

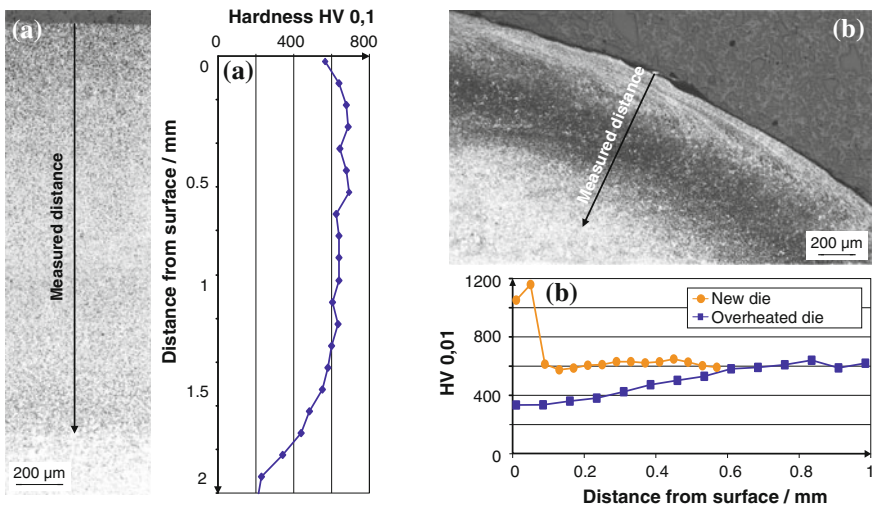


Fig. 2.36 Examples of optical micrographs of etched metallographic specimens and associated depth profiles of microhardness acc. to Vickers. **a** Sample taken from the surface of a forged induction-hardened and ground component made of 100Cr6, magnified 100x. **b** Sample from the intersection between the impression and die land of a significantly overheated, plastically deformed forging die made of plasma-nitrided hot-working steel X 38 CrMoV 5-1, magnified 50x

2.6.4 Electron Microscopy

As opposed to optical microscopy, which works with visible light, in electron microscopy electrons are sent in high vacuum ($<10^{-3}$ mbar) through/on the preparation, where they are diverted in different directions. Detectors capture the electrons generated through various interactions and convert them into electric voltage. Amplified and modulated, a visible light spot is created on a screen. In this way, the electron beam gradually scans the surface area to be displayed.

The object under investigation must be subjected to a suitable preparation technology and be completely free of water. Depending on whether the electrons scan the surface of a preparation or penetrate it, it is distinguished between scanning electron microscopy (SEM) and transmission electron microscopy (TEM) (Fig. 2.37).

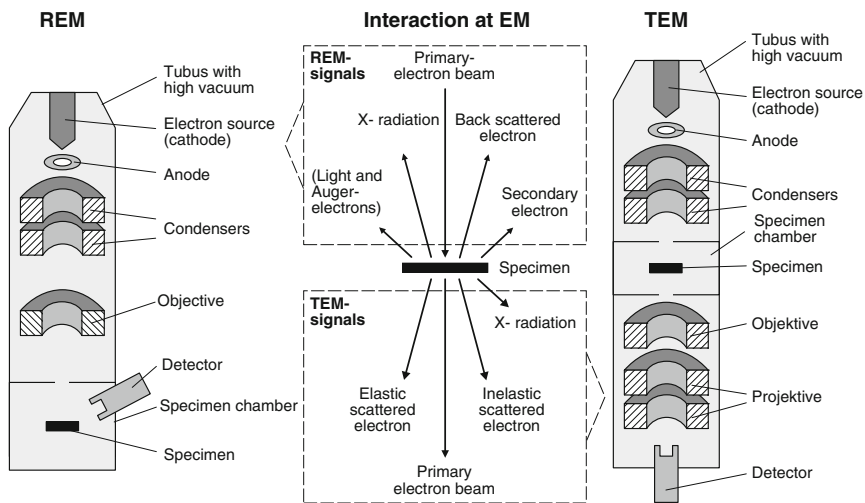


Fig. 2.37 Simplified diagram of SEM and TEM as well as the interactions between the electron beam and the sample

To create the image, signals are used that arise in the interaction between the electron beam and the preparation. Figure 2.37 right shows these signals, whereby the illustration above the sample represents signals significant for SEM. Under the sample are those signals that are used for TEM.

2.6.4.1 Scanning Electron Microscopy

Introduction. With the scanning electron microscope, it is possible to scan a surface by means of a highly focused beam of electrons. As opposed to the magnification of an optical microscope (maximum ca. 1,000 times), a very large

range of magnification is possible with the scanning electron microscope, between 10 and 150,000. The resolution amounts to a few nm, which corresponds to the size of large molecules. Since lenses are superfluous, associated deficiencies (highly limited depth of sharpness range, distortion) are avoided. One can thus obtain very plastic images of the geometrical surface configuration of the sample, which permits both the representation of coarse, gorge-like structures and the recording of very fine details in a nanometer range. Figure 2.38 shows an example of an image of a cemented carbide structure in the cross section through the surface of a forming tool. Here, we can observe a washing out of the cobalt binder phase, which can subsequently lead to chipping.

SEM is suitable for depicting surface configurations from the millimeter to the nanometer range, for looking for structural anomalies and damage to component surfaces and cross sections, such as corrosion islands, wear etc. Furthermore, it serves as an ideal search monitor for EDX analyses (see Sect. 2.6.4.3 and Fig. 2.38 right).

Structure. The scanning electron microscope has the following structure (Fig. 2.37 left) [SCHM94]:

- Electron generation system, consisting of a tungsten thermionic cathode from which electrons are emitted, a control cylinder (Wehnelt cylinder) and an anode. The electrons are accelerated by the electrical voltage between the cathode and the anode.
- XY deflexion system for producing a line raster.
- Electromagnetic lens system, consisting of two condenser lenses and a final lens (objective lens), which sharply focuses the primary electron beam, as well as several spray blinds.

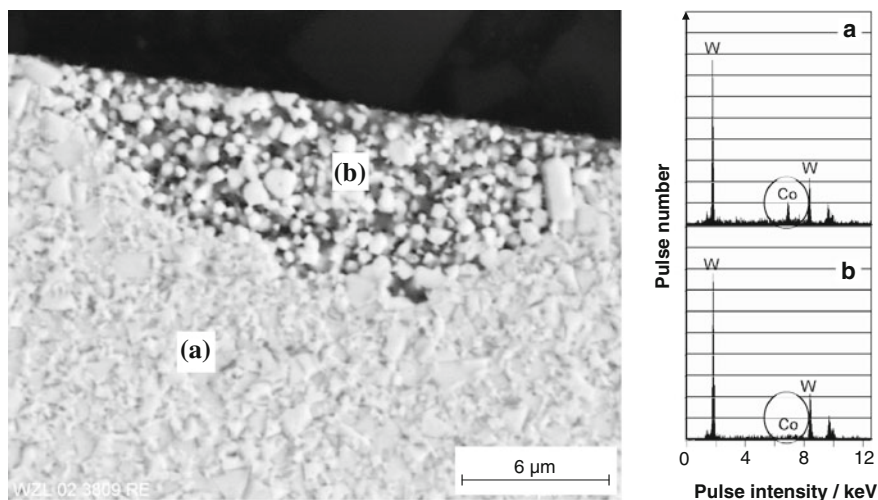


Fig. 2.38 Scanning electron microscopic image and EDX analysis of a metallographic specimen perpendicular to the surface of a damaged cemented carbide forming tool **a** undamaged matrix, and **b** structure of the damaged spot (cobalt washout)

- Secondary electron detector, which registers the secondary electrons accelerated away from the sample upon impact of the electron beam. There are also other detectors: RE detectors register backscatter electrons, EDX detectors register X-rays (Sect. 2.6.4.3). Different detectors are used depending on the method of application.
- One or more monitor screen to display the observation area.
- Electronic signal processing, which controls the brightness of the corresponding light point on the monitor.
- Raster generator, which synchronizes the XY deflexion system of the SEM tube and the monitor.
- Sample chamber, into which the preparation can be housed.
- Vacuum pumps, which create a high vacuum ($<10^{-3}$ – 10^{-8} mbar) in the EM tube.

The electron microscope tube and the monitor work analogously and in correspondence, but they are two separate units.

Functionality. As a rule, the entire process of microscoping takes place in high vacuum, in order to prevent interactions with atoms and molecules in the air. The electrons are generated with a tungsten hot cathode in the Wehnelt cylinder and are concentrated to a saturated electron cloud.

By applying high voltage (1–30 kV) between the cathode and the anode, the electrons are formed out of the electron cloud into a beam. The electron beam thus generated is then deflected and focused with the help of magnetic coils. These magnetic coils serve as lenses (two condenser lenses, 1 objective lens), i.e. they focus the electron beam. The final lens of the multi-stage condenser lens system, consisting of a stigmator and a multi-stage deflexion coil system, is frequently referred to as an “objective”. In addition to beam focusing, XY deflexion also occurs here with the help of deflexion coils, with the help of which the object is scanned. Deflexion is controlled by a raster generator and takes place synchronously both in the EM tube and on the monitor.

If the electron beam strikes the sample surface, the electrons are then decelerated. They release kinetic energy to the sample. In this way, secondary electrons are detached from the sample surface (Fig. 2.37). By analyzing this, especially the topography of the surface becomes visible (topography contrast). Furthermore, backscatter electrons can be analyzed, which are diverted by attraction to the positive atomic nuclei and accelerated back. This gives them an energy that is characteristic of the material of the atomic nucleus, which is why the corresponding image presents different materials at varying brightness levels (material contrast). While light materials appear dark, heavy materials are bright. Further signals include x-rays, light impulses and “Auger electrons” (Sect. 2.6.4.3).

2.6.4.2 Transmission Electron Microscopy

In contrast to the much more frequently used SEM, which structurally resembles a reflected-light microscope, transmission electron microscopes (TEM) can radiate electrons through solid bodies [SCHU04b]. This method is especially practical for showing crystal defects and the finest structures in the nanometer range. It is used in particular to investigate precipitation and recrystallization processes in steel. Magnification can extend to up to 800,000 times the normal size. Details of a few tenths of a nanometer can be resolved. Figure 2.39 shows examples of images from TEM.

The structure of TEM is very similar to SEM, whereby additional projective lenses and an objective lens below the sample are required in addition (Fig. 2.37). Furthermore, TEM is generally equipped with a much stronger radiation source than SEM. This is why the acceleration energy of the generated electron beams amounts to several hundred keV.

Even when most of the electrons pass unaffected through the sample, numerous interactions between the primary beam electrons and the sample atoms occur, which contribute to the generation of the TEM image (Fig. 2.37 right). Elastically scattered electrons are electrons that interact with the atomic nuclei of the sample. These electrons are scattered at a large angle and do not lose any energy. Inelastically scattered electrons interact with the electrons of the sample atoms and so exhibit energy loss, but they are scattered at small angles.

TEM generates a transmitted light electron image of a very thin sample. Ultrathin cross-sections with thicknesses of <100 nm are required. For this, a very costly, high-precision technology is necessary (Sect. 2.6.5.1). In the case of a standard bright field image, as many electrons of the electron beam as possible have to be able to penetrate the sample. The quality of the image depends not only on the microscopy process used and the quality of the beam, but also on the quality on the sample preparation in particular. Image capture is currently almost exclusively digital.

In every transmission electron microscope, one can produce—in addition to structural images—so-called diffraction images. These contain information about the lattice structure and lattice constants of the sample material. If electrons strike a crystal, Bragg diffraction occurs [SCHU04b]. From the diffraction images, we can draw conclusions about the crystal structures at hand. If it is a polycrystalline substance, the electron beam that makes contact with the preparation is diffracted into different directions according to the structure and orientation of the individual crystals. “Debye-Scherrer rings” are formed. If we limit the diameter of the primary beam with a blind on a small section of the sample, then the electrons are only diffracted on a few monocrystals. As a result, the points of the diffraction rings are reduced in correspondence to the different crystal orientations (Fig. 2.39 bottom left). In the case of a monocrystal, we can then only recognize single, sharply differentiated points, as is shown in Fig. 2.39 (bottom right) using the example of a clearly monocrystal carbide [RAED02].

In summary, TEM is particularly suited to the following problems:

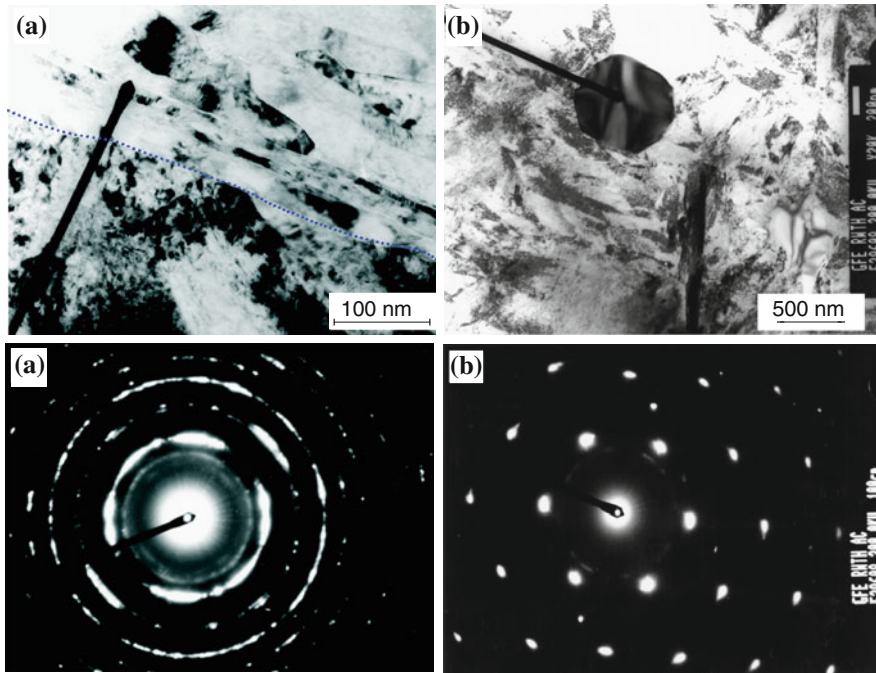


Fig. 2.39 Examples of transmission electron microscopic (TEM) images and associated TEM diffraction images **a** smeared workpiece material 16MnCr5 on a forming tool made of powder-metallurgical HS-PM 6-5-3, and **b** visibly monocrystalline carbide in the matrix of HS-PM 6-5-3 [RAED02]

- detection, illustration and analysis of precipitations (>5 nm), Fig. 2.39 top right,
- illustration and analysis of crystal faults such as displacements, stacking faults and boundary layers in general, Fig. 2.39 top left,
- chemical composition of precipitations and phases (>5 nm) with the help of EDX analysis (Sect. 2.6.4.3) and/or electron area diffraction, Fig. 2.39 bottom.

2.6.4.3 X-Ray Microanalysis

In the case of chemical analysis with x-ray microanalysis, the sample is fired with a very finely focused beam of high-energy electrons such as are used to create images in SEM or TEM devices [HANT94]. These electrons sometimes penetrate deep into the sample and can interact with the shell electrons of the sample's atoms, which can initiate many different processes.

Among other things, the electrons release x-rays (Fig. 2.37). A distinction is drawn here between x-ray braking radiation and characteristic x-rays. In the latter case, the energy of the ray is characteristic of the atom from which the x-ray quantum was emitted. The characteristic ray can be detected with a semiconductor

detector in both SEM and TEM. The term used is “energy dispersive x-ray spectroscopy” or EDX [HANT94, SCHU04b]. Less common is the use of crystal lattice spectrometers that use a different kind of evaluation called wavelength dispersive x-ray spectroscopy (WDX).

In the case of EDX, the x-rays are subdivided with an energy spectrometer (multichannel analyzer) according to energies. The respective radiant energy thus becomes an index for the atom type, while the number of evaluated impulses per chemical element represents a measure for its concentration (Fig. 2.38). In the case of SEM analysis, one must bear in mind that the location of the measurement reaches from the surface into the inside of the sample and covers an area of 1–10 μm depending on the material. Moreover, it needs to be taken into consideration that the energetic resolution is relatively low in comparison to other methods. Thus, the signals of single elements intersect, which can lead to mistakes. Detection of light elements (carbon, oxygen) is difficult and quantitatively uncertain. In summary, from an EDX or WDX analysis we obtain:

- Qualitatively: type of elements and laterally resolved distribution in the sample. Depending on intent, point, line and area scans are possible. Clear-cut identification of elements is sometimes difficult.
- Quantitatively: concentration of elements (with a corresponding statistical evaluation of the energy impulses detected).

2.6.5 Preparation Methods

2.6.5.1 Sampling and Embedding

The removal and preparation of metallographic samples should be adjusted as much as possible to the purpose of the investigation [SCHU04b] (lateral/longitudinal cross-section etc.) and should also avoid any structural changes resulting from excessive heat or deformation [PETZ94, SCHU04b]. To separate a sample from a metallic component, in principle all separation methods are conceivable [PETZ94]. As a rule however, the sample is removed by means of special cutting devices that work according to the principle of plunge grinding. Here, the component is affixed and cut with a quickly rotating disc. The disc material depends on the material to be cut. Also, spark-erosive cutting, also called electrical discharge machining (EDM), is ideal for more precise cuts—see Volume 3 of this series, “Electrical Erosion and Hybrid Processes”.

To improve handling of the removed sample, they are either cramped or embedded hot or cold in plastic, depending on the size of the sample and the application case [PETZ94]. For cold embedding, two substances, an uncrosslinked polymer and a catalyst, are mixed to a liquid or paste and poured over the sample, which is lying in an embedding mould, where the embedding medium polymerizes and hardens. The advantage of cold embedding includes faster applicability and

low costs. In the case of hot pressing into special embedding presses, the sample is completely surrounded by plastic granules that fused under the influence of increased heat and high pressure. The advantage in this case is the improved bond between the sample and the embedding medium. In both cases, the result is a cylindrical, easily manageable sample that can be further prepared in the following step on the front face.

Sample removal for TEM studies represents a special case. Since the samples for TEM have to be extremely thin (<100 nm), special techniques are required that permit major thinning of the material. Recently, the FIB method (focused ion beam) has become established, in which the sample is cut with a heavily focused ion beam, resulting in thin lamellae [ENGE02, GIAN99].

2.6.5.2 Grinding and Polishing

To render the grain structure visible, an extremely smooth, generally polished surface is required. First, the depth of the faulty surface layer (e.g. thermally influenced or plastically deformed during sample removal) is reduced by gradual grinding until the actual structure is recognizable [DOMK86, PETZ94, SCHU04b].

The sample is ground with an aluminium oxide abrasive paper (Al_2O_3) on rotating discs. The sequence of abrasive papers is customarily 180, 240, 320, 400, 600, 800, 1,000. The size of the number stands for the finesse of the grain, not the grain size. It is defined by the number of meshes per square inch screening surface when screening the abrasive material.

After every grinding process, the sample is cleaned, rotated 90° and ground further in the same direction. In this way, grinding grooves from the previously used paper are removed. In modern, metallographic grinding devices, the samples are not manually pressed against the paper, but are clamped in special devices that also take over the function of rotating the sample. Sometimes even fully or semi-automatic grinding machines are used that can take over all grinding, polishing and cleaning steps autonomously.

Polishing removes the grinding grooves remaining from the grinding process. Diamond paste or diamond suspension (with a grain size of 15, 6, 3, 1 μm) applied on velvet or wool cloths serve as the polishing agents [DOMK86, PETZ94]. Formerly, de-mudded aluminium oxide (Al_2O_3), green rouge (chromium oxide) (Cr_2O_3) and other abrasive substances were utilized.

2.6.5.3 Contrasting

In the polished state, pores, cracks, cavities and other such things can be recognized under the microscope. One can also easily recognize many non-metallic inclusions since these generally have a different reflectivity than metals—e.g. graphite in cast iron or precipitations in Al-Si alloys [SCHU04b]. However, in order to render differences in the microstructure visible, contrasting methods are

still required that are adjusted to the application case. Therefore, a variety of preparation and etching formulae are available for metallic and ceramic materials as well as for plastics [PETZ94].

A distinction is drawn between contrasting without changing the polished surface (optical contrasting methods) and contrasting with a change of the polished surface (chemical and physical contrasting methods) [PETZ94, SCHU04b]. Optical methods make use of the interaction of the incident light and the ground metallic surface. This requires a specially equipped reflected-light microscope. In the case of electrochemical and physical methods, the polished surface is treated further. The term etching is also used in this context. What both methods have in common is that they amplify the difference in reflectivity of various structural components. This is done either by creating a variously strong oxide formation and/or by setting back individual structural components (relief formation) so that they become visible under the microscope.

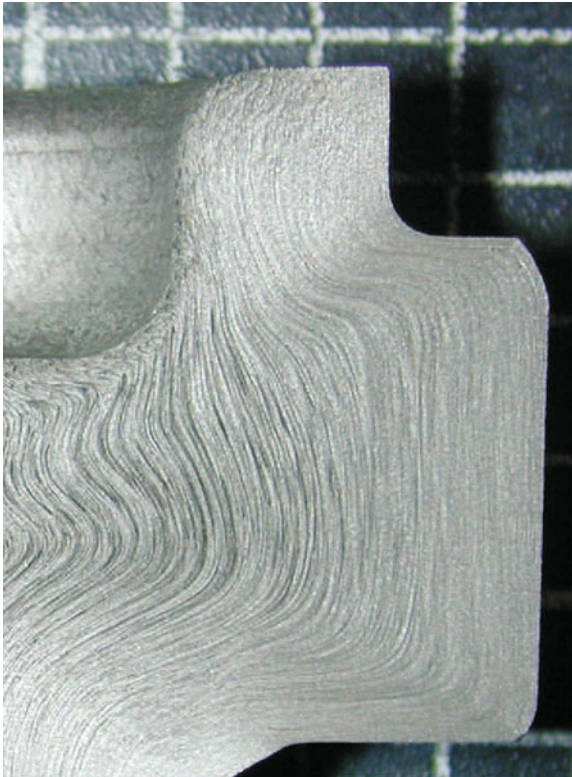


Fig. 2.40 Cross-section through part of a cold-formed gear shaft made of case hardening steel 16MnCr5, etching agent: lukewarm to boiling hydrochloric acid (Source Hirschvogel Umformtechnik GmbH)

The “classic” etching process is dip etching. It makes use of etching agents that act purely chemically and act upon different structural components with various levels of intensity.

We distinguish between macroetching and microetching. Macroetching is meant to provide a complete overview of segregations and primary structure (Fig. 2.40). The magnifications involved in such evaluations are in the area of 1:1–30:1. In the investigation of microetched surfaces, magnifications of 50:1–1,000:1 are used. The purpose of microetching is the development of the microstructure. In the following, several details concerning macroetching will be described since these are typically used in forming technology. The best-known macroetching process is “Oberhofer etching”, in which the sample is held at room temperature in an etching agent composed of distilled water, ethanol (96 %), hydrochloric acid (32 %), copper(II) chloride, iron(III) chloride and tin(II) chloride [PETZ94].

In this etching method, segregation-free areas appear dark, while segregation areas are unaffected. In this way, the “fibre structure” of a component becomes quite visible, which makes it interesting to forming engineers. Formed components (such as crankshafts, screws, etc.) exhibit a continuous fibre flow and are thus more prone to stress than components that were manufactured by machining (interrupted fibre structure). Figure 2.40 shows an example of a microetched cross-section through part of a cold-formed gear shaft made of case-hardening steel 16MnCr 5. The fibre structure of the sample is rendered visible in this case by cleaning it with lukewarm to boiling hydrochloric acid.

2.6.5.4 Coating

Since scanning electron microscopy can only be used on conductive surfaces, non-conductive samples (e.g. ceramics, sometimes also ceramic coatings) must be specially prepared [GÖCK94]. By vapour-depositing a metal film (e.g. gold), the surfaces of the objects can be rendered conductive. One must bear in mind that the coating is not deposited too thickly, or else the fine structures of the object would be covered. Since scanning with the electron beam takes place in a vacuum, the objects must also be prepared prior to vapour-depositing so that they are absolutely anhydrous.

2.7 Materials in Forming Technology

2.7.1 Workpiece Materials

2.7.1.1 Sheet Metal

Modern sheet metal materials as used in sheet metal processing are following the demand for increasingly lightweight design. Based originally on classic soft deep

drawing grades, a development in the last several years in direction of higher and higher strength steels can be observed.

As before, there is still no exact definition of soft steel as opposed to a high-strength material. In accordance with the current state of materials development, the following classification is suitable:

- soft steel: tensile strength <300 Mpa
- higher-strength steel: tensile strength >300 MPa
- high-strength steel: tensile strength >500 MPa
- highest-strength steel: tensile strength >950 Mpa.

Which nomenclature is finally used is not really decisive. Comparative forms such as “ultra high-strength” or even “mega high-strength” are already in use. In general, the obtainable tensile strength should be used for a clear distinction of sheet metal qualities. Figure 2.41 shows the development of sheet materials with varying quality and strength properties. In the following, we will pursue individual steel materials and their active mechanisms in more detail.

The development of steel materials had already been advanced to high-strength sheet materials in the 1970s. First, microalloyed and phosphorus-alloyed steels were developed. In the case of microalloyed steels (alloy contents up to about 0.1 %), finely distributed carbides and carbon nitrides are formed in the grain structure which both refine the grain and have a hardening effect. The cause of the grain refining effect is that finely precipitated particles hinder grain growth during hot forming are available as germs in the transformation of austenite into ferrite.

Typical representatives of microalloys steels are the IF steels (interstitial free). An IF steel is a steel without interstitially incorporated alloying elements, i.e. no iron atoms are substituted by carbon or nitrogen atoms in the metal lattice. In this steel type, the C and N atoms are bound by titanium or niobium, which must be present in hyperstoichiometric amounts. In this way, IF steels obtain a ferritic microstructure without perlite or cementite. That guarantees favourable cold-formability and good deep drawing properties in particular. Because they lack interstitial atoms, these steel types are free of aging symptoms.

In the case of phosphorus-alloyed steels, the element phosphorus is added. This element helps to solidify the mixed crystal phase.

“Dual phase” steels (DP) were developed in the 1980s. As with the microalloyed steels, solidification is brought about by the second phase. In the case of DP steels, we make use of the fact that the martensitic components become hardened by the unavoidable solution of carbon in its crystal structures. How high the obtainable increase in strength is, depends on the amount, hardness and distribution of the martensite and bainite islands in the softer ferritic matrix. The microstructural development can be controlled by the conditions of the manufacturing process.

What makes “bake-hardening” steels special is that they have both good cold formability and attain a large increase in strength during subsequent heat treatment

(e.g. baking the body paint). This is achieved by diffusion of interstitial carbon and nitrogen to displacements within the crystal structure.

IF steels can be further developed and their strength increased to a higher-strength steel quality by alloying with elements that solidify mixed crystals. The latter are normally not as strong as carbon or nitrogen, but they occupy different positions in the crystal structure. Thus, these foreign atoms, in analogy to microalloyed steels, represent obstacles to dislocations without introducing irregularity to the stress/elongation values.

Without attempting to achieve a significant increase in strength, isotropic steel sheets were developed in the 1990s. Since anisotropy has a decisive influence on the required size of the sheet section and on the quality of the target component, engineers attempted to create anisotropic steel by adding suitable alloying elements. It was discovered that isotropy could be affected by alloying with titanium and its precipitations. We can now avoid anisotropy-caused earing and flow lines to a much larger extent.

Since the turn of the century, sheet metals have been further developed with the aim of increasing strength values. The focus has largely been on further developing DP steels. Other multiphase steels such as complex phase steels (CP) and TRIP steels (“transformation induced plasticity”) also belong to this development. In the case of TRIP steels, which fall into the category of residual austenite steels (RA), there is an elongation-induced transformation of the metastable residual austenite into martensite, substantially increasing strength. In future, lightweight design will also be advanced further, and with it the development towards higher-strength materials. L-IP steels (“lightweight steels with induced plasticity”) are a further development of TRIP steels. In this case, by adding further alloying elements, density is reduced while the strength remains the same in comparison to TRIP steels.

In Fig. 2.41, the stainless steel family is not explicitly indicated. This group of materials lies above the materials developments shown. What is special about this group is its high resistance against corrosion. This is a result of the high amounts

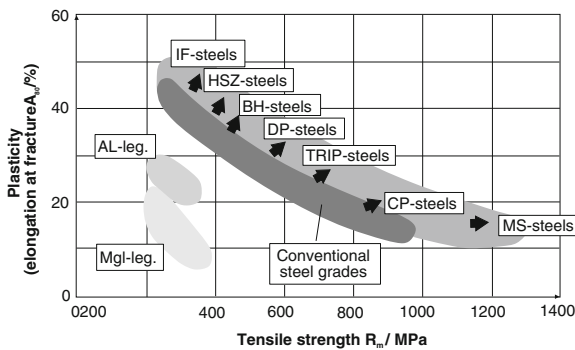


Fig. 2.41 The development of sheet materials of varying quality and strength [NN01a]

of the alloying constituents chrome (>12 %) and nickel, for which reason they are also known as chrome-nickel steels. This advantage is always exploited whenever components without additional protection (e.g. lacquering, zinc and eloxal) against corrosion are to be used. Stainless steels have a relatively high amount of residual austenite. For this reason, they are highly adhesive in production. In addition, deformation martensite can be formed when austenite is transformed to martensite during deformation.

The Anisotropy Coefficient r . In many sheet forming processes, it must be taken into consideration that a material does not have the same properties in all directions, but is anisotropic. The anisotropy of a polycrystalline material is characterized by the fact that the atomic lattices of the grains are not oriented in a statistically random way, but tend to prefer certain levels and directions. Such a preferential orientation, also called texture, can arise both during manufacture (e.g. casting) as well as during subsequent processing (rolling, forming, heat treatment). Consequently, the plastic deformations required for sheet manufacture lead to orientation changes as a result of sliding in the grains and thus to the formation of typical rolling textures [MACH81]. Due to this, tensile strength and plastic properties are to some extent direction-dependent, among other things.

To measure the anisotropy of the plastic properties of sheets, the perpendicular anisotropy is determined in the tension test—the so-called r coefficient. This is defined as the ratio of true strain in the width and thickness directions of a tensile specimen (Fig. 2.42).

$$r = \frac{\varphi_2}{\varphi_3} = \frac{\varphi_b}{\varphi_s}. \quad (2.51)$$

If $r = 1$, the material behaves isotropically and the same deformations take place in the width and thickness directions. In case of values of $r > 1$, the sheet is more resistant to changes in thickness under tensile stress and is deformed more in width. If $r < 1$, deformation occurs more in the thickness direction.

The r coefficient is generally not constant in the sheet plane, but rather has varying values depending on the position of the sample relative to the rolling

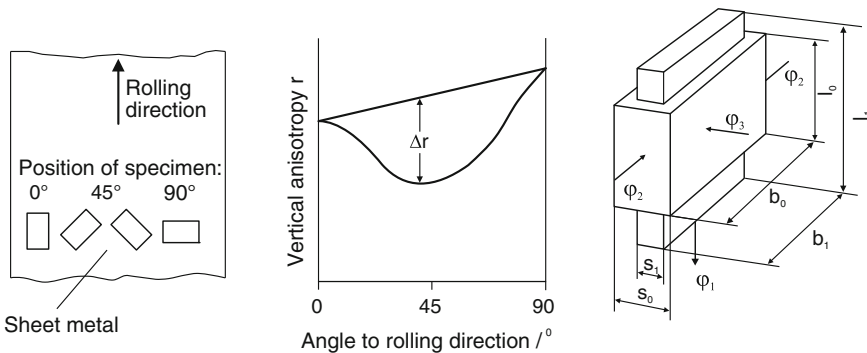


Fig. 2.42 Definition of the anisotropy coefficient

direction. We thus define the average for this reason, which is measured at certain angles (0° , 45° , 90°) to the rolling direction:

$$\bar{r} = \frac{r_{0^\circ} + 2 \cdot r_{45^\circ} + r_{90^\circ}}{4}. \quad (2.52)$$

The variation of the r coefficient with direction is called plane anisotropy and is defined:

$$\Delta r = \frac{r_{0^\circ} + r_{90^\circ}}{2} - r_{45^\circ}. \quad (2.53)$$

The experimental determination of anisotropy coefficients is standardized in DIN EN 10130 [EN04]. Accordingly, perpendicular anisotropy is determined after executing a tension test up to a deformation of 20 % from the change in length and width of the sample. It is recommended that one record length variation (L , L_0) instead of thickness variation. Then perpendicular anisotropy can be determined with the law of volume constancy using the following formula:

$$r = \frac{\ln \frac{b_0}{b}}{\ln \frac{L \cdot b}{L_0 \cdot b_0}}. \quad (2.54)$$

The Effect of Anisotropy in Deep Drawing. A cup produced by deep drawing often exhibits a wall of varying height and thickness despite symmetrical stress. This phenomenon is called “earing” and is due to the distinct plane anisotropy of the sheet material (Fig. 2.43).

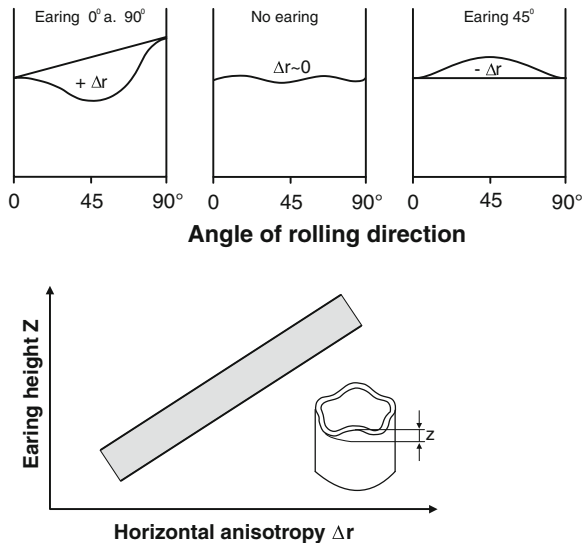


Fig. 2.43 Dependence of earing on plane anisotropy

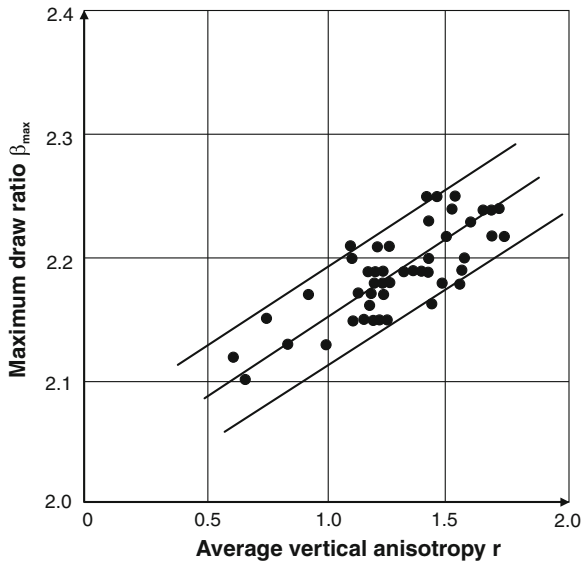


Fig. 2.44 Limiting draw ratio as a function of the average perpendicular anisotropy (acc. to Whiteley)

Given higher coefficients of perpendicular anisotropy, the sheet material tends to be constricted in width/the circumferential direction. The sheet is highly resistant to thickness changes. The material flows from neighbouring areas. As a result, both earing as well as larger wall thicknesses (relative to the circumference) arise here. At locations of minimal r coefficients on the other hand, valleys appear. The height of the tip is all the higher the higher the coefficient of plane anisotropy Δr is. In the case of a positive coefficient, the tips are under 0° and 90° —in the case of a negative coefficient, under 45° to the rolling direction. Since usually a smooth edge is usually required for technical and optical reasons, the cups require post-processing, which is associated with additional costs and a reduction of the useful cup height.

Large coefficients of perpendicular anisotropy can sometimes have a positive effect. For example, the limiting draw ratio rises with increasing r coefficients (Fig. 2.44). This can be explained with the help of Hill's yield locus curves for various r coefficients [HILL50] (Fig. 2.45). Yield locus curves describe the geometrical location for the start of flow in the stress area. These curves are applicable under the assumption of a level state of stress for materials that exhibit only a perpendicular anisotropy but no plane anisotropy [PÖHL84].

The yield locus curve is closed [Fig. 2.45 only shows the range between ideal stretch forming (tension-tension) and ideal deep drawing (tension-compression)], convex and generally cannot be described by an analytical function. In order to determine the represented yield locus curves experimentally, it is necessary to determine the start of flow for two-axis states of stress [PÖHL84].

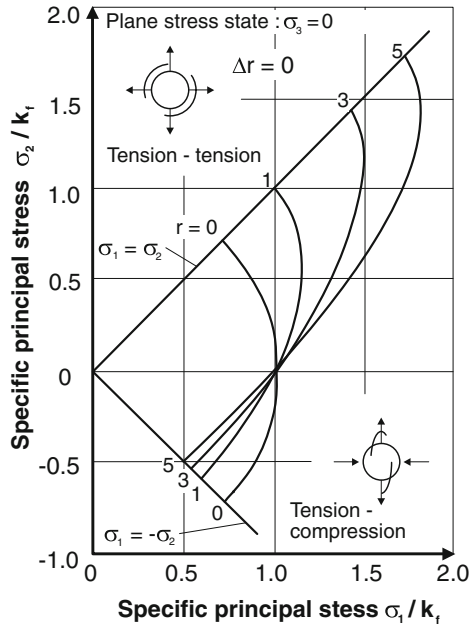


Fig. 2.45 Yield locus curves of sheet materials as a function of the r coefficient (acc. to Hill/Pankin)

We can determine the yield locus curve experimentally, for example, with the help of tension or crush tests. In this case, the individual samples must have a different orientation to the rolling direction. The tests are carried out in analogy to the test procedure used for isotropic material. From the measurements, information about the yield locus curve is derived [PÖHL84].

We can see that in the case of two-axis tensile stress, which is predominant in the wall of a cup during deep drawing, the state of stress required for plastic flow rises with increasing r coefficients. On the other hand, in the case of a tension-compression state of stress, which is found in the flange, there is a reduction of the stresses required for flow. Applied to the conditions of cup-drawing, the conclusion is that the forming force drops in the flange area with increasing coefficients of perpendicular anisotropy, while the force transferable in the wall rises. Thus, larger limiting draw ratios can be obtained.

2.7.1.2 Cold Massive Forming

The following criteria are desirable for all workpiece materials that come into consideration for the manufacture of extrusion parts:

- minimal flow stress k_f ,
- low tendency to strain-hardening,

- homogeneous grain structure along the entire initial cross-section and
- high formability.

To initiate flow, a quite distinct stress is required for each material. This can be used as a feature for classifying extrusion materials. With increasing flow stress, we obtain the following ranking:

- lead and lead alloys,
- tin and tin alloys,
- aluminium and aluminium alloys,
- zinc and zinc alloys,
- copper and copper alloys,
- unalloyed and alloyed steels up to about 0.45 % C in an annealed state,
- corrosion-resistant ferritic and martensitic Cr steels,
- austenitic CrNi steels,
- nickel and nickel alloys in a solution-annealed state and
- titanium and titanium alloys.

Of the non-ferrous metals indicated, lead and tin alloys are of relatively little importance although they are the easiest to form. These alloys are used especially for thin-walled parts such as cups, sheaths and tubes.

Aluminium and Aluminium Alloys. Aluminium materials are much more important. They can be roughly subdivided into

- ultra-pure and pure aluminium,
- non-age hardenable alloys and
- age-hardenable alloys.

Ultra-pure aluminium contains more than 99.98 % aluminium. The aluminium content of pure aluminium is between 99 and 99.9 %. The main alloying element is magnesium, of which up to 0.5 % is permissible. Ultra-pure and pure aluminium types have low strength (Table 2.1). They can be cold-formed already at low pressures. In this case, from large to very large deformations are possible. This is universally applicable however only for the soft state. In a semi-hard or hard state, strength is higher and the required pressure as well. Formability is accordingly reduced. Ultra-pure or pure aluminium is always in a semi-hard or hard state after cold-forming. This can be removed again by means of recrystallization annealing.

Alloyed aluminium materials contain mainly copper, magnesium, manganese, zinc and silicon as alloying elements. They are subdivided into non-age hardenable and age-hardenable alloys.

Among the non-age hardenable alloys are mainly the groups AlMg, AlMn and some variations of these. They obtain their higher strength compared to ultra-pure and pure aluminium from the effect of the alloying elements and from cold-forming. For this reason, they are often referred to as wrought alloys. Their strain-hardening tendency limits the formability of these materials.

Table 2.1 Non-ferrous metals for cold-forming

Material denomination/ number	Elastic limit R_p MPa	Tensile strength R_m MPa	Elongation at fracture A %	Hardness HB	Notes
Al9,5 EN	20	70	23	20	Electrical parts, ferrules, pipes
AlMg5 EN AW5019	110	240	17	55	AW1050A Self-hardening, container and vehicle construction
AlCuMg1 EN	260	400	10–15	100	Age hardening, vehicle and engineering parts AW2017A
Zn99,95 2.2035	–	120–140	52–62	32–34	
ZnAl4 2.2140	200–230	250–300	3–6	70–90	Pressed parts, profiles, armatures
ZnAl4Cu1 2.2141	220–250	280–350	2–5	85–105	
E Cu57 Cu-ETP	120	200–290	38	45–70	Semifinished goods for electrical engineering
CuSn2 –	150	260–280	35–50	60	Pipes, springs, screws
CuZn37 CW508L	180–250	300–380	45–50	70–75	Main alloy for cold forming, universally applicable
CuZn33 CW506L	150–180	270–370	46–50	65–70	Well cold formable, screws, rivets, formed parts
CuZn28 CW504L	(150)	280	44	70	Very well cold formable, versatile applications
Ti99,7 3.7035	250–350	400–550	22	150	Aircraft industry, jet engine parts, chemical apparatus and reactor construction
Ti6Al4V 3.7165	820–940	880–1,130	8	260–310	Aircraft and jet engine industry

Examples of age-hardenable alloys include those of the groups AlMgSi, Al-ZnMg, AlCuMg and AlZnMgCu. In this case, phases that increase strength are eliminated by natural or artificial aging. Cold forming increases this strength again. Forming age-hardened alloys is more difficult than other alloy types. Table 2.2 [BILL73] provides a qualitative overview of the cold-formability of aluminium materials.

Zinc and Zinc Alloys. Zinc and zinc alloys are used only to a very limited extent for cold forming parts. The main reason for this is that zinc already starts to creep under low amounts of stress. This disadvantage can indeed be compensated to some extent by adding aluminium and copper, but the consequence is a very distinct reduction of elongation at fracture (Table 2.1).

The variety of workpieces composed of zinc materials comprises rivets and bolt-shaped parts, moulds, fittings and pressed parts.

Table 2.2 Classification of some aluminium materials in accordance with their cold formability [BILL73]

Good formability	Medium formability	Low formability
Ultra-pure aluminium	AlMgSi soft	AlMgSi warm age-hardened
Pure aluminium soft	AlMg3 soft	AlMgMn semi hard
AlMn soft	AlCuMg soft	AlMg5 semi hard
	AlMgSi cold age-hardened	
Pure aluminium semi hard	AlMg5 soft	AlCuMg age-hardened
AlMn semi hard	AlMgMn soft	AlMg7 semi hard
		AlCuMg age-hardened
	Pure aluminium hard	AlMn hard
	AlMg3 semi hard	AlMgMn hard
	AlMg7 soft	AlZnMg1
	AlCuMg soft	AlZnMgCu1.5

Copper and Copper Alloys. Copper and copper alloys have become very important as materials for cold-forming parts. This is due to the diverse potential applications of this material group and, with a corresponding alloy composition, their high deformability in the cold state.

The highest deformability can be obtained with pure copper types. Here, the copper content is between 99.50 and 99.90 %. They have trace amounts of residue from deoxidation agents (e.g. phosphorus or arsenic). Certain types (electrolytic copper) contain up to 0.04 % oxygen. Figure 2.46 illustrates the change in the mechanical properties R_m , R_p and A of electrolytic copper during cold forming.

The cold forming of pure copper materials is primarily applied to the manufacture of semi-finished products like solid and hollow profiles of the most varied cross-sections. These are made further use of predominantly in the electronics

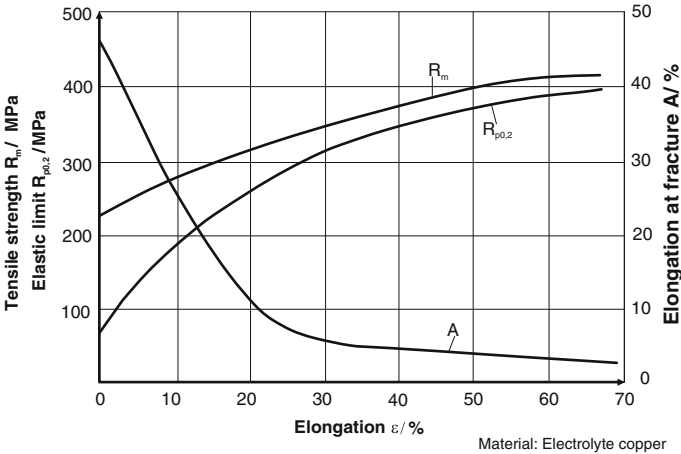


Fig. 2.46 Effect of cold forming on the mechanical properties of electrolytic copper [NN86, NN01b]

industry. Pure copper in the form of sheets and tubes functions as a workpiece material when there are high requirements concerning thermal or electrical conductivity [NN01b, NN86].

Most important of the alloyed copper materials are the copper-zinc alloys—commonly known as brass—with a production share of about 70 % of all copper alloys [NN03]. Their properties, including their formability in the cold state, depend on their zinc content. If the latter is under 37.5 %, then the alloy consists in solid state completely of α -mixed crystals (α -brass). Among others, these include the alloys CuZn20, CuZn28 and CuZn37. Alloys that contain only α -mixed crystals are very easy to form (Fig. 2.47). They exhibit high elongation at fracture, making forming operations with high degrees of deformation possible.

In the case of zinc contents of over 37.5 %, a second phase is formed in addition to the α -mixed crystal, the β -mixed crystal. Both crystal types are encountered side by side when the zinc content is up to 46 %. ($\alpha + \beta$) alloys are especially interesting because the phase boundaries shift according to temperature. Thus, the properties of these materials can be influenced by heat treatment. The ($\alpha + \beta$) alloys group includes CuZn40 and CuZn40Pb2 among others. In the case of CuZn40Pb2, the amount of β is in the area of 30–50 % [NN88]. The appearance of the second phase is of considerable influence on cold formability, which is poorer in materials than in pure α -alloys. Increasing zinc contents lead to a larger amount of β in the grain structure and thus in ever poorer formability in the cold state. On the other hand, these alloys are very well suited to hot forming.

If copper-zinc alloys contain still other elements, then they are called special brass. These materials consist of 56–79 % copper. What remains is composed of zinc and one or more other elements. As a whole, the content of such additional elements is usually 4 % at most [NN88]. These are aluminium, iron, magnesium,

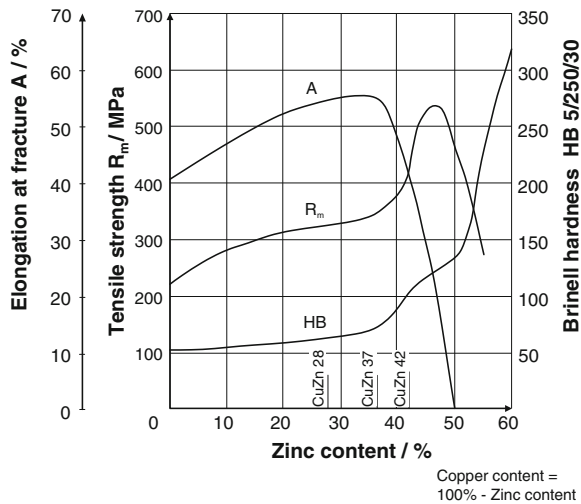


Fig. 2.47 Mechanical properties of copper-zinc alloys as a function of their zinc content [NN88]

Table 2.3 Relative cold formability of copper-zinc wrought alloys [NN88]

Good formability	Medium formability	Low formability
CuZn20	CuZn20Al2	–
CuZn28	CuZn28Sn1	–
CuZn31Si1	–	–
CuZn35	CuZn35Ni2	–
–	CuZn39Pb0,5	CuZn39Pb2
–	CuZn40Mn2	CuZn40Mn1Pb

manganese, nickel, silicon or tin. Their effect on the alloy's mechanical properties varies. With respect to the properties of special brass types in cold forming, they can be considered from the standpoint of the shifting of phase boundaries. For example, nickel like copper causes an increase of the amount of α . The other additional elements function like zinc, i.e. the amount of β in the microstructure is increased. As a result, formability in the cold state generally becomes more difficult. Table 2.3 shows some frequently used special brass types along with a classification with reference to cold formability.

Other binary and multinary alloys based on copper are of minor importance as materials for cold-forming parts in comparison to copper-zinc alloys. All wrought alloys can indeed be formed into construction parts as well, but their main area of application is in the manufacture of semi-finished products like sheets, belts, rods, pipes and moulds of all kinds.

A further area of alloyed copper materials includes copper-tin alloys, commonly called bronze. In Germany, they have a production share of about 14 % of all copper alloys [NN03]. Copper-tin alloys are easily formable using processes such as rolling, drawing, bending, cornering and deep drawing. The high strain hardening of these materials is the reason for their wide-spread use as a material for resilient contact elements in the electronics industry [NN04].

High Temperature Non-Ferrous Metals. High temperature and chemically resilient non-ferrous metals such as nickel and titanium as well as certain alloys are also processed into construction elements using cold forming, if only in special cases.

Of nickel materials, the technical pure nickel types are the easiest to cold form. They contain 99.5 % or more nickel as well as some carbon, manganese, iron, silicon and copper. High degrees of deformation are obtainable with these materials (Fig. 2.5), so intermediate annealing is required to restore formability only in case of extreme deformations. Cold forming increases strength and hardness. Elongation at fracture on the other hand is reduced already with small amounts of true strain. Pure nickels have attributes similar to steel within a range of comparable degrees of deformation with 0.2–0.25 % carbon [NN75] (Fig. 2.48).

Nickel wrought alloys have much higher mechanical characteristic values as pure nickel types depending on their composition. With respect to deformability in the cold state, they have similar properties concerning potential true strain and the tendency to strain hardening. Their higher strength in the undeformed state is

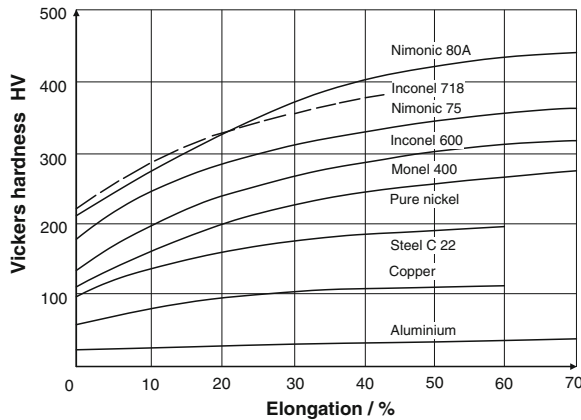


Fig. 2.48 Increase in hardness via cold forming [NN75]

further increased with higher degrees of deformation (Fig. 2.48). This also increases the demands made on machines and tools.

For reasons of material savings, the cold forming of nickel alloys is of great economical interest. They are also interesting because they can be machined only with difficulty [BILL73, LANG90a].

Titanium and Titanium Alloys. Metallic titanium and titanium alloys are, due to their favourable relation of density ($\rho \approx 4.5 \text{ g/cm}^3$) to strength, of interest as construction materials when a combination of minimal component weight and high strength are essential. Since these materials also have good resistance to many chemicals, they are often used in the construction of chemical apparatus and plants. Titanium is a very expensive metal that is difficult to machine. For these reasons, the possibility of cold forming is highly interesting. The high strength of titanium is, however, an obstacle. Large forming forces then become necessary. The true strain obtainable with pure titanium are roughly comparable to ultrahard steels. Technical pure titanium types have tensile strengths in the range of $R_m = 300\text{--}700 \text{ MPa}$ elastic limits of $R_{p0.2} = 200\text{--}600 \text{ MPa}$ and elongations at fracture of $A_5 = 20\text{ to }35\%$. These variables change considerably with the degree of cold forming, as the example of cold rolling pure titanium makes clear (Fig. 2.49).

Titanium alloys become increasingly difficult to cold form with increasing amount of alloying elements. The cause is not the content of additional elements alone however, but rather their effects with respect to the phases that they form. Technical titanium materials are subdivided into α -, β - and $(\alpha + \beta)$ alloys. The α -phase has a hexagonal lattice, the β -phase has a body-centred cubic crystal structure. β -alloys stand behind pure titanium with respect to their deformability in the cold state, but before the α - and $(\alpha + \beta)$ alloys. They contain vanadium, chrome, molybdenum, niobium, tantalum or manganese as their main alloying elements. Among others, this group includes the technical alloys TiV13Cr11Al3, TiV8Fe5Al1 and TiV16Al2,5.

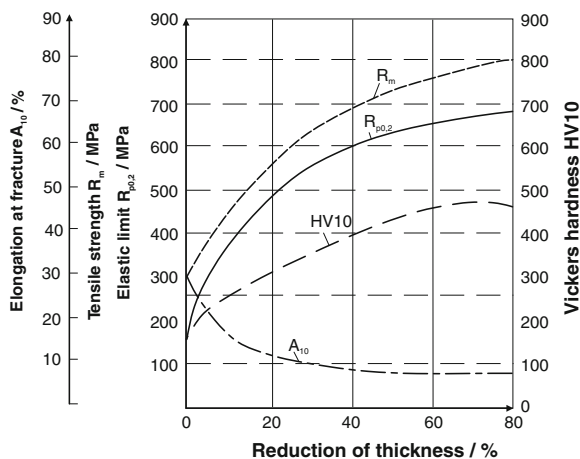


Fig. 2.49 Effect of height reduction in the rolling of titanium [ZWIC74]

The main alloying elements of α - alloys are aluminium, tin or zircon. The materials of this group are much more difficult to cold form than the β -alloys. Mentionable examples of technical α - alloys are TiAl5, TiAl5Sn2,5 and TiAl8-Mo1V1. One of the most well-known titanium materials is the $(\alpha + \beta)$ alloy TiAl6V4, which is considered poorly formable (Table 2.1).

Should titanium alloys be cold-processed into moulded parts, this generally is done for special cases in chemical apparatus manufacture, in reactor construction as well as in the aerospace industry.

Steel and Steel Alloys. Presently, steel is the most commonly utilized material for cold forming parts. Due to its high strength compared to most non-ferrous metals, steel must fulfil special requirements with respect to homogeneity, microstructure and mechanical properties in order for cold forming to be economical. This is especially true for ultra-high strength alloyed steels, the field of application of which is being continually expanded.

The formability of ferrous materials essentially depends on the type and content of the alloying elements. The formability of unalloyed carbon steels improves as the carbon content decreases, i.e. with increasing proportion of proeutectoid ferrite within the microstructure. Ferrite (α -iron) is a low-carbon iron mixed crystal that is highly cold-formable. With increasing carbon content, another microstructural component is formed, pearlite. This is a lamellar-structured mixture of ferrite and iron carbide (Fe_3C , cementite). Carbides are exceedingly hard ($>1,000$ HV), brittle and almost undeformable. An increase in carbon content leads to a larger pearlite proportion in the microstructure and thus to a higher strength and a diminished formability, which in return requires an even higher expenditure of energy. These characteristics of carbon steels can within limits be influenced by a suitable heat treatment. The goal of this is to transform the carbides in the pearlite from a lamellar to a globular structure. In this form, the carbides hinder yielding

during forming to a lesser degree. Material behaviour becomes more homogeneous as a whole and the ductility is increased. Globular shaping of the carbides is achieved by annealing to spherical cementite (GKZ). Soft-annealing often suffices as well. But since the long annealing times are frequently not realizable for economic reasons, blanks to be formed often have mixed microstructures still containing some amounts of perlite with lamellar carbides.

As for the homogeneity and the yielding the effect of hard and brittle non-metallic inclusions can be evaluated in the same way as that of cementite. However, the essential difference is that the shape of such inclusions cannot be influenced by heat treatment. Consequentially, especially high demands must be placed on the purity level of extrusion steels.

Unalloyed steels specially produced for extrusion contain the capital letter “C” in their designation as an attachment to the carbon content. C15C and C45C are examples of steels from this group. In such materials, the accompanying elements phosphorus and sulphur are undesirable because they cause inhomogeneities in the microstructure already during steel production, therefore reducing the deformability of the steels. In special cases however, steels containing higher amounts of sulphur are also cold-processed. These cases comprise simple forming processes with small strains where no special demands are made in terms of the final strength of the workpieces and where difficult finish-machining operations are to be performed on the workpieces.

Especially due to cost reasons, extrusion is also noteworthy as a manufacturing process for higher-loaded construction and machine parts. This is why alloyed case hardening steels and quenched and tempered steels are being increasingly processed. They are still relatively easy to cold form in the soft-annealed state. The strengthening associated with cold forming is frequently utilized purposefully (Table 2.4) and is already taken into consideration along with the dimensioning of workpieces.

Stainless steels are being increasingly subjected to cold forming as well. Because of the higher prices of these steels, the cost savings due to lower usage of materials is more significant than in the case of construction steels. Moreover, machining these materials is often difficult to execute because of increased tool wear and unfavourable chip shapes.

Stainless steels are generally classified as follows:

- austenitic CrNi and CrNiMo steels
- ferritic Cr steels
- martensitic Cr steels.

Depending on the respective content of alloying elements and the crystalline structure the characteristics of steels from different groups differ widely when being cold formed. Figure 2.50 illustrates this aspect with a juxtaposition of the yielding behaviour of three steels (including a stainless austenitic steel).

Table 2.4 Steels for cold forming [LANG90c]

Material denotation	Before/after forming	Elastic limit R_p MPa	Tensile strength R_m MPa	Elongation at fracture A %	Examples of use
C15	Before	280	400–450	20	Screws, nuts, trusses, levers,
	after	500	600–700	8	
C15C	Before	280	400–450	20	Pressure pads, shafts,
	after	500	600–700	8	
C35E	Before	320	420–500	18	Small machine parts
	after	600	700–800	6	
C45C	Before	340	500–600	16	
	after	650	750–850	6	
16MnCr5	Before	340	420–500	18	Gear wheels
	after	500	650–750	8	
41Cr4	Before	400	600–750	18	Gear wheels, screws
	after	650	750–850	8	
42CrMo4	Before	500	650–750	14	Steering arm
	after	750	900–1,000	8	
100Cr6	Before	450	600–750	12	Wear part
	after	650	800–900	6	
X10Cr13	Before	450	600	18	Corrosion-resistant parts
	after	600	750	10	
X5CrNi18-9	Before	220	550–700	50	Acid-resistant parts
	after	600	800–900	6	

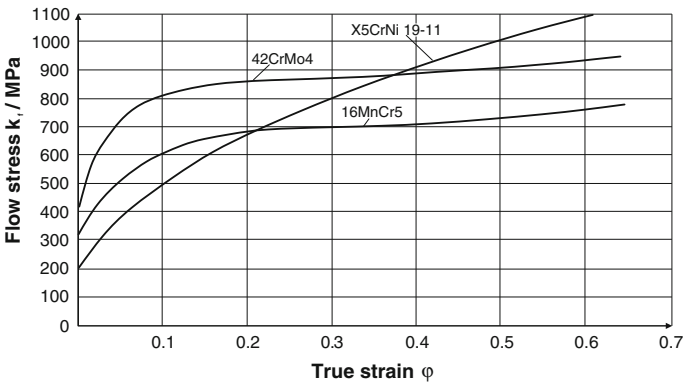


Fig. 2.50 Profile of yield stress for various steels

The difference in the strain hardening exponent n is very clear in the case of ferritic and austenitic steels. The major tendency of austenitic stainless steels to strain hardening makes it necessary to carefully adjust the blanks with respect to the deformations arising in the course of the forming process.

2.7.1.3 Hot Massive Forming

Hot forming is always utilized when the yield stresses are to be reduced and the formability of the material has to be increased. In general, all formable metals are suitable for this. Above all, unalloyed and alloyed steels are of technical importance today, moreover magnesium, aluminium, titanium, copper, nickel and their alloys as well. Also used, though to a much more limited extent, are highly heat resisting materials like niobium, tantalum, molybdenum, tungsten and their alloys.

The most important material for hot forming is steel, which can be adjusted within broad limits by means of alloy additives and heat treatment to different specifications concerning hardness, yield strength, tensile strength, failure strain, toughness, fatigue strength, high temperature strength, machinability and corrosion resistance.

Tables 2.5, 2.6 and 2.7 provide an overview of the types of steel used in forging.

Precipitation-hardening ferritic-perlitic steels were developed specially for hot forming and documented in DIN EN 10267. They are generally referred to as AFP steels. They obtain a ferritic-perlitic matrix by means of targeted cooling from the forming temperature. Due to simultaneously transpiring precipitation processes, dispersion hardening occurs in the ferrite, resulting in high strength. The obtainable strength parameters are comparable with those of heat-treated steels. The cost advantages of these steels are caused by their low price as well as by the omission of hardening, annealing and flattening costs.

The forming behaviour of metallic materials depends on the temperature, the forming speed and the formability [BARG83]. In hot forming the upper temperature limit is determined by the solidus temperature, phase transformations or chemical reactions (oxidation processes) and grain growth. Since areas with eutectic composition can arise in heavily segregated alloys, the highest temperature must be lower than the eutectic temperature in such cases. The lower temperature limit is theoretically the temperature limit of recrystallization, below which—due to the advent of strain hardening—the deformability is reduced respectively the resistance to forming is increased.

The strain rate as well should be regarded along with the recrystallization. At the respective temperature, the strain rate must not exceed the recrystallization rate in order to avoid strain hardening.

In addition to the minimum temperature set by recrystallization, a forming temperature must be selected for which homogeneous mixed crystals are to be expected corresponding to the phase diagram. Varying deformation properties among several structural constituents can thereby be avoided, and, in particular, secondary phases at the grain boundaries can be re-dissolved. If phases of differing lattice types exist, the more formable lattice type at hand is preferred for plastic deformation (e.g. face-centred cubic).

Since the deformability of the material must be maintained during the forming process, yet cooling is unavoidable due to the temperature difference between the

Table 2.5 Steels for hot forming I

Denomination (DIN/steel-iron- mat.data sheet)	Application characteristics	Examples of use	Tensile strength ^a (MPa)	Forming temperature ^a (°C)
General construction steels (DIN EN 10025)	Application in forged state	Flanges, bosses, levers, bushes, bodies, rings	300–800	850–1,150
Quenched and tempered steels (DIN EN 10083)	Through heat treatment (quenching and tempering) broadest influencing of mechanical characteristics: high toughness along with defined strength	Drive and gear parts: waved parts for force and torque transmission (e.g. crank shafts); gear wheel; wheel bosses, stub axles, piston rods etc.	500–1,500	850–1,100
Case-hardened steels (DIN EN 10084)	High hardness of case- hardened surface layer along with high core toughness → wear parts	Cam shafts, control shafts, gear wheels, measuring devices, bosses, levers, gear and steering shafts	500–1,500	850–1,150
Nitriding steels (DIN EN 10085)	High surface hardness, good wear resistance, good fatigue resistance, rust inertance	Wear parts of high surface hardness: heavy machine parts of large dimensions	800–1,600	850–1,100
Steels for flame and induction hardening (DIN 17212)	Hardenability of the surface layer without influencing the core characteristics	Drive shafts, gear wheels, bevels, crank shafts, cam shafts, gudgeon pins	500–1,300	850–1,100
Heat-resisting steels (DIN EN 10269) (DIN EN 10273)	Load temperature up to 540 °C	Forgings for turbine engineering, steam boiler engineering, former apparatus construction: flanges, screws, nuts, high pressure pipes	450–1,000	850–1,100
AFP-steels (DIN EN 10267)	Hardening through targeted cooling from forming heat	Dynamically highly loaded parts such as piston rods, stub axles, suspension arms	700–900	900–1,100

^a according to: Stahlschlüssel

workpiece and the tool, the forming process is initiated with the highest permissible temperature.

In case of larger cross-sections and in case of materials with lower heat conductivity along with elevated high temperature strength an even temperature

Table 2.6 Steels for hot forming II

Denomination (DIN/steel– iron-mat.data sheet)	Application characteristics	Examples of use	Tensile strength ^a (MPa)	Forming temperature ^a (°C)
Highly heat resisting steels (W 670-69)	Load temperature up to 800 °C; additional demand of toughness, fatigue strength and corrosion resistance	Parts for container and apparatus construction for thermal power plants and reactors: armatures, valves, pipes, pressure containers, turbine blades etc.	500–1,250	850–1,250
Corrosion and acid- resistant steels	High corrosion resistance	Construction and apparatus engineering parts for chemical industry, food industry (armatures, shafts, screws, bolts, bushes)	450–900	750–1,150
Bearing steels (W 350- 53)	High surface hardness, high strength martensitic-carbide microstructure (→high tension- compression cyclic stress and wear)	Rolling bearing rings through partial forging (preform)	(only	hardness data) 60–66 HRC
800–1,100 <i>Tool steels</i>				
Non-Alloyed tool steels (W 150- 63)	Surface hardening (low hardening depth)	Hand tools, simple shearing tools	58–65 HRC	800–1,100
Cold work steel ^a (W 200-69)	Up to 200 °C surface temperature	Shearing and cold forming tools	55–67 HRC	800–1,100
Hot work steel ^a (W 250-63)	Permanent temperature above 200 °C; high heat resistance, high hot wear resistance	Forming tools (hot forming) plastics molding tools	900–2,000	800–1,150
High speed steel ^a (W 320-69)	High tempering resistance and hot hardness up to app. 600 °C, hot wear resistance	Big tools of chipless forming	64–67 HRC	900–1,150

^a according to: Stahlschlüssel

Table 2.7 Non-ferrous metals and hard alloys for hot forming

Denomination	Application characteristics	Examples of use	Tensile strength (MPa)	Forming temperature (°C)
Pure aluminium and AL-alloys	Low part weight along with high continuous load; high corrosion resistance	Forgings for aircraft industry, vehicle manufacturing and shipbuilding; pressure vessels, electrical engineering	Up to 400	350–550
Magnesium alloys	Lowest density of metallic materials along with medium strength properties; good machinability; high hot resistance (Mg-Zr-alloys) problem: high chemical reactivity	Die forgings: mechanical parts of medium to high mechanical and thermal load (Zr-alloys); housing in turbine manufacturing	Up to 260	370–400
Titanium alloys	High strength along with low density and excellent corrosion resistance	Aircraft and jet engine manufacturing (compressors, turbine blades), armatures, chemical apparatus	300–750	700–1,000
Copper alloys	High electric and heat conductivity, good strength properties; corrosion resistant	Electrical engineering, vehicle manufacturing, fine mechanics. Apparatus construction (armatures)	Up to 600	700–900
Hard alloys with nickel, cobalt and tungsten basis	Very high heat resistance	Turbo jet engine parts: turbine blades and disks		1,050–1,250

distribution across the workpiece cross-section can only be realized through a long warm-up phase. As for large open-die forging pieces, uniform heating down to the core can last several days. Uneven heating with temperature gradients from the surface to the core can lead to thermal stresses and thus to damage.

The criterion for judging the level of forging difficulty is the so called “forgeability” of a material, a qualitative indicator of the formability respectively deformability.

According to Lange [LANG90b], the following qualitative ordering of material groups can be made with respect to hot forming:

1. aluminium alloys
2. magnesium alloys

3. copper alloys
4. carbon steels, alloyed steels
5. martensite-hardening steels
6. austenitic stainless steels
7. nickel alloys
8. titanium alloys
9. iron-based superalloys
10. cobalt-based superalloys
11. molybdenum alloys
12. nickel-based superalloys
13. tungsten alloys
14. beryllium.

2.7.2 Tool Materials

2.7.2.1 Casting Materials

Cast Iron. Cast irons are iron alloys with a high carbon content of about 2.7–3.8 % and a silicon content of 0.8–3 % as well as further components like manganese, chrome or nickel. The carbon in cast iron is mostly in the form of graphite and immediately leads to cracking during forming processes. For this reason, the material is poured into moulds and subsequently processed into tools using machining or dissociative material removal. Along with the disadvantages of low deformability and toughness in comparison to steel, it has significant cost advantages, high machinability as well as favourable sliding properties resulting from the graphite content. For the construction of forming tools, cast iron with lamellar graphite and spheroidal graphite are of primary interest.

Cast Iron with Lamellar Graphite. In this type of cast iron, the carbon in graphite form is predominantly lamellar. As a result of its low mechanical strength, the graphite flakes do not take part in load transmission but rather act as hollow spaces that reduce the load-bearing section and produce concentrations of stress at its edges as a result of the notch effect. The deformability and impact strength of this cast iron type is thus especially low. The mechanical properties are essentially determined by the microstructure and the graphite form. Thus, the Young's modulus of ferritic cast iron is in the area of 90,000 MPa and increases with perlitic cast iron content to about 150,000 MPa [BEIT01]. Beyond that, this material has the peculiarity that the Young's modulus decreases as the stress increases. Thus, there is no linear relation between stress and strain, which must be taken into consideration in the context of tool design. The tools should be subjected to as little tensile stress as possible, since the tensile strength of the material is only a fourth of the compressive strength [MERK03]. Because the high internal notch effect, caused by the graphite flakes, dominates tool failure, an notch-reduced surface construction is

Table 2.8 Cast iron materials with lamellar graphite [MERK03, OEHL01]

Cast type	Tensile strength/ MPa	Hardness/ HB	Application purpose
EN-GJL-150	150–250	100–175	Lowly loaded drawing punches, bonnets, base plates for column mounts for light cutting and shearing tasks
EN-GJL-200	200–300	120–195	Drawing tools for large and flat parts, car body pressing, furthermore for cylindrical Bowden cables at high load and simple geometry
EN-GJL-250	250–350	140–215	
EN-GJL-300	300–400	165–235	Drawing and forming tools for high wear resistance, base plates and bonnets for high strength load
EN-GJL-350	350–450	185–255	

not required for reasons of strength. Furthermore, the strength of cast iron with lamellar graphite depends on the fineness of the graphite distribution, which is increased with rising cooling rates. Thus, higher strengths can be realized in thin-walled workpiece areas. This is exploited especially in the production of stiffening ribs [OEHL01].

Table 2.8 shows some frequently used cast iron materials with lamellar graphite as well as their mechanical characteristic values and examples of their applications.

Cast Iron with Spheroidal Graphite. It is possible to create a graphite shape that is not lamellar but spheroidal by providing a scarceness of sulphur in addition to certain carbon and silicon contents. This form has the advantage of reduced internal notch effects and therefore a considerably increased material strength. Furthermore, the Young’s modulus is increased to about 175,000 MPa [BEIT01].

By means of appropriate heat treatments, the properties of this type of cast iron can be improved to a greater extent than those of cast iron with lamellar graphite. To obtain the highest level of impact strength for example, heat treatments are undertaken that result in a ferritic microstructure. The machinability is good. For these reasons, this material represents an economical alternative for large tools exposed to higher loads.

Table 2.9 lists some frequently used cast iron materials with spheroidal graphite, their mechanical characteristic values and examples of their applications.

Steel Casting. Steel casting constitutes iron materials with carbon contents of up to 2 % that are poured into moulds. Here, the melting and alloying processes used

Table 2.9 Cast iron materials with spheroidal graphite [MERK03, OEHL01]

Cast type	Tensile strength/ MPa	Hardness/ HRC	Application purpose
EN-GJS-500	500	54	Drawing tools and molds for high wear resistance, base plates and bonnets for high strength load
EN-GJS-600	600	56	
EN-GJS-700	700	56	

Table 2.10 Cast steel materials [MERK03, OEHL01]

Cast type	Tensile strength/MPa	Hardness/ HRC	Application purpose
<i>Cold working steel casting</i>			
G45CrNiMo4-2	1,000 – 1,030	50 ± 2	Molds and embossing tools
GX100CrMoV5-1	800 – 900	60 ± 2	Embossing, cutting, drawing tools
G45CrNiMo4-2	800 – 900	60 ± 2	Molds and jigs
<i>Hot working steel casting</i>			
GX38CrMoV5-1		–	Dies; unsusceptible to hot cracking
GX40CrMoV5-1		–	Die inserts, parts for compression dies; very good tempering resistance
G37CrMoW5-1		–	Punches, dies, die inserts; very good tempering and hot wear resistance

correspond to those of rolled and forged steel. However, its strength properties are largely independent of direction since no distinct texture is created by subsequent forming processes. Compared to cast iron, it is of higher strength and sometimes higher toughness. For this reason, it is particularly suitable for large-format tools exposed to high mechanical loads [BEIT01]. Depending on the use, a distinction is made between hot and cold working cast steel. Table 2.10 lists some examples among the large number of possible alloys.

Zinc Alloy Casting. Zinc alloy casting can be poured simply. With them, dies and cutting tools are cast in order to produce corresponding tool pairs in a simple fashion. The good reproduction of the tool geometry permits a reduction of further treatment, keeping production costs to a minimum. The tools can withstand small loads such as those arising in the forming of soft light-metal sheets and spacious steel sheet parts with large radii and can be re-cast into other tool geometries after their use without a problem. The most common alloy for tool manufacture is ZnAl4Cu3 with a tensile strength of 335 MPa [MERK03].

2.7.2.2 Aluminium Bronze Alloys

Alloys composed of aluminium bronze, used in the manufacture of deep drawing tools, consist of about 80 % copper, 14 % aluminium, iron and sometimes nickel. They have a hardness of 300–400 Brinell and are characterized by their very low friction coefficient [MERK03]. Because of these properties, this material is employed for mounting or armouring highly stressed tool edges for the manufacture of drawing parts made of stainless steel sheets that are hard to form. With it, the surfaces of the drawing material are spared extremely well, and the formation of wrinkles, grooves and scratches is largely avoided.

2.7.2.3 Tool Steels

Tool steels are classified as unalloyed and alloyed cold working steels, hot working steels and high-speed steels. Cold working steels are suited to applications in which the operational surface temperature is generally under 200 °C. Hot working steels and high-speed steels on the other hand can be used in temperatures of up to 600 °C. Cold working and high-speed steels are used above all to produce tools for machining and forming. Hot working steels are used mainly to manufacture forming tools such as dies, die-cast moulds or tools for forging and extruding.

Unalloyed Cold Working Steels. Unalloyed cold working steels, also called carbon steels, obtain their hardness with a corresponding heat treatment by the formation of a martensitic microstructure. Besides the carbon content of up to 1.25 % C required for this, they also contain up to 1.5 % Cr, 1.2 % W, 0.5 % Mo and 1.2 % V. Wear resistance is increased with hardness and increasing carbon content. However, toughness is reduced at the same time, and thus the material’s sensitivity during heat treatment and tool use becomes larger. All unalloyed tool steels are shell hardeners, that is, they only harden on the workpiece surface and not across the entire section. Complete hardening is only possible up to a diameter of 10 mm.

During operation, the surface temperature of the workpiece should not exceed 180 °C. Otherwise tempering phenomena are inherent which are associated with a decline in hardness.

Table 2.11 lists some frequently used unalloyed cold working steels as well as their hardness and typical applications.

Alloyed Cold Working Steels. The carbon content of alloyed cold working steels is between 0.18 and 2.30 %, therefore higher than that of unalloyed steels. In addition, they contain the alloying elements Cr, Mo, W and Mn, which contribute to a reduction of the critical cooling rate and thus to the favourable through hardenability of the materials as well as to the formation of carbides and thus to the increase of wear resistance [PÖHL99]. Also, they increase the tempering resistance and the high temperature strength. These steels as well can only be exposed to surface temperatures of up to 200 °C during operation (Table 2.12).

Hot Working Steels. Hot working steels are used for the chipless forming of steel, non-ferrous metals and their alloys under temperature far above 300 °C, frequently in a hot state. Thus, high demands are placed in terms of heat resistance, high temperature wear resistance, heat conductivity, toughness and

Table 2.11 Unalloyed cold working steels [MERK03]

Steel type	Hardness/HRC	Application purpose
C70U	57	Deburring tools, axes, cutting goods
C80U	58	Hot dies, hot rolls, machine cutting tools
C105U	61	Embossing and drawing tools, dies
C120U	62	Files, milling tools, band and bow saws

Table 2.12 Alloyed cold working steels [MERK03]

Steel type	Hardness/HRC	Application purpose
60WCrV8	58	Embossing, extrusion and shearing tools
90MnCrV8	60	Cutting, bending, deep drawing and embossing tools
X100CrMoV5	62	Cold pilger mandrels and cutting tools
X153CrMoV12	61	Cutting, thread rolling and pressing tools
45NiCrMo16	52	Embossing and bending tools

tempering resistance. The type of load determines the simultaneous presence of several or all of these properties. Essential for hot working steels is also their insensitivity to fire cracks, which results from a combination of toughness and heat conductivity [NN96].

Since in most cases the contact with the hot metal to be processed is intermittent and repeated at certain intervals, the inherent temperature changes result in an additional load that gradually leads to the formation of net-like cracks, called fire cracks [SPUR84].

In order to meet all these requirements, a large number of alloying elements are required that cause additional interactions among themselves, resulting in complex steels. Steels with the alloying components Cr-Mo-V and Ni-Cr-Mo-V are especially suited to meeting these requirements.

One essential property of these steels is a high hot hardness caused by a secondary hardening in the temperature range around 500 °C. This is due to additional carbide precipitations, which hinder plastic deformation of the material in this temperature range [MERK03].

A further important property of these steels is their high toughness, which is significantly higher than other steels that are applied within this temperature range. This attribute is the reason why these materials can also be applied in tools that are subjected to high loads such as forging dies. While hot working tools made of Cr-Mo-V steels are ideal for water cooling because of their thermal shock resistance, Ni-Cr-Mo-V steels are—due to their toughness—used for tools with abrupt and high compressive loads. Table 2.13 shows some frequently used hot working steels as well as their hardness and some typical applications.

High-Speed Steels. High-speed steels offer a good combination of high-temperature hardness, wear resistance and toughness. Especially the latter two properties have brought about their use predominantly for cold forming tools. The special properties of this steel group are based on the strong carbide formers W, Mo, V and Cr [BEIT01].

Table 2.13 Hot working steels [MERK03]

Steel type	Hardness/HRC	Application purpose
55NiCrMoV7	42	Forging dies, hot shear blades
32CrMoV12-28	46	Rod extrusion tools, dies
X37CrMoV5-1	48	Water coolable rod extrusion tools and dies
X40CrMoV5-1	50	Hot shear blades, rod extrusion tools

Table 2.14 High-speed steels [MERK03]

Steel type	Application purpose
HS 6-5-2	Punches, dies, fine blanking tools
HS 6-5-3	Press bushes, die inserts
HS 10-4-3-10	Mandrel

A distinction is drawn between high-speed steels fabricated by metallurgical melting processes and the more cost-intensive powder-metallurgically produced high-speed steels, which differ due to their finer and more uniform carbide distribution and their lack of segregation. This results not only in higher compressive strength but also in enhanced toughness properties [MERK03].

Table 2.14 lists some often used high-speed steels along with their hardness and typical applications.

2.7.2.4 Cemented Carbides

Cemented carbides are composite materials. They consist of a soft metallic binder phase such as cobalt or nickel and of carbides of the transition metals W, Ti, Ta, Nb. Carbides border between metals and ceramics. They exhibit some properties similar to metals, e.g. electrical conductivity, but are—as metallic hard materials—assigned to non-oxide ceramics [MERK03].

The hard materials are responsible for hardness and wear resistance. The task of the binder phase is to bind the brittle carbides and nitrides to a relatively solid body.

The advantages of cemented carbides are their good microstructural uniformity due to the powder-metallurgical production, their high hardness, compressive strength and high temperature wear resistance. Cemented carbides have the same hardness at 1,000 °C. as high-speed steel at room temperature. Furthermore, it is possible to produce cemented carbides with different properties by making targeted changes in terms of the hard material and binder contents [BEIT01].

The cemented carbide types used for forming purposes usually consist of tungsten carbide (WC) as a phase in a cobalt matrix (Co). The cobalt content is between 6 and 30 %, whereby the mixture ratio largely determines the properties of the cemented carbide. With increasing amounts of WC, the hardness, compressive strength and wear resistance increase. On the other hand, toughness, bending strength and buckling strength are increased along with the Co content.

Typical areas of application for cemented carbides in forming technologies are cutting tools, stamps, press bearing bushes and dies for both cold and hot forming, which must have high wear resistance and high compressive strength. Cemented carbides are especially often used for narrow-tolerance components, which are then produced in smaller series as well.

2.7.2.5 Ceramics

The material category ceramics includes all non-metallic, inorganic, temperature-resistant materials that are at least 30 % crystalline [SALM82, TIET94]. This does not however exclude the possibility of metallic and/or polymer components being present within a ceramic material as additives.

Besides artistic ceramics (e.g. porcelain), which are not used in metalworking, modern ceramic materials are classified into the two large groups “functional ceramics” and “structural ceramics” [WILL88]. Structural ceramics are used when high mechanical loads are expected. This is the case, for example, for indexable inserts in machining or for the balls of hip joint prostheses. Commonly used structural ceramics are either oxides, carbides or nitrides. Functional ceramics are used because of their special functional properties. Among these are good electrical insulating properties or heat conduction. High-performance ceramics are materials that can satisfy especially high requirements, including very high wear resistance and heat resistance. From a technical point of view, structural and high-performance ceramics are used for metal processing. They are summarized by the generic term of “technical ceramics” [SALM83, WILL88].

Technical ceramics are subdivided into the groups silicate ceramics, oxide ceramics, non-oxide ceramics and titanates. Table 2.15 lists some typical representatives of these ceramic groups.

Oxide and non-oxide ceramics are especially important for metal processing (forming).

Ceramics are usually manufactured according to the following schema:

1. forming process: ceramic powder and binder are pressed into a green body
2. green machining: the still soft green body is processed by near-net-shape machining
3. sintering: heat treatment at 1,200–2,200 °C to generate the actual ceramic
4. finishing: hard machining (grinding, lapping) is used to create the near-net-shaped ceramic.

For forming technological applications, the ceramics aluminium oxide (Al_2O_3), zirconium oxide (ZrO_2), silicon oxide (SiC) and silicon nitride (Si_3N_4) are of primary interest.

Table 2.15 Classification and examples of technical ceramics

Ceramic group	Ceramic examples		
Silicate ceramic	Steatite ($\text{Mg}_3(\text{OH})_2(\text{Si}_4\text{O}_{10})$)	Cordierite ($\text{Mg}_2\text{Al}_4\text{Si}_5\text{O}_{18}$)	Kaoline ($\text{Al}_2\text{O}_3 \times 2\text{SiO}_2$)
Oxide ceramic	Aluminium oxide (Al_2O_3)	Zirconium oxide (ZrO_2)	Magnesium oxide (MgO)
Non-oxide ceramic	Silicon carbide (SiC)	Silicon nitride (Si_3N_4)	Aluminium nitride (AlN)
Titanate	Calcium titanate (CaTiO_3)	Barium titanate (BaTiO_3)	Lead zirconate titanate (PZT)

Application Examples. Because of the many advantages associated with the use of ceramic tool materials in forming technologies, a number of areas of application have already been opened up. It is current state of the art, for example, in wire manufacturing that the rolls have a fully ceramic core. The benefit of ceramic tools is that the high wear resistance of ceramics is a necessary prerequisite for the effective application in this manufacturing process.

In wire forming, the tools employed are subjected to high mechanical loads and heavy wear depending on the composition, microstructure and surface properties of the wire. In the case of some wire materials, such as copper alloys, there are additional problems due to the propensity to adhesion between the tool and the wire [WAGE00]. In addition to their high hardness, the tribological properties of ceramics make them suitable for the use in industrial applications and in the sphere of forming tools in particular. Here, their non-metallic bond character and thus their small adhesive tendency in the case of friction pairings make them particularly effective. As a result the total friction losses as well as the tendency to cold welding in the case of mixed or dry friction are reduced. This advantage has been practically proven in the case of drawing rings made of silicon nitride [WAGE99].

Various research projects have and still do set out to investigate the applicability of ceramic tools in sheet forming. In one case, the use of silicon nitride in rotationally symmetric deep drawing made it possible to boost tool life by up to 300 % compared to conventional tool steel. Considering that such ceramics are still much more expensive, such an increase in tool life is also necessary to make their use economical [KLOC03b].

The properties of ceramic materials are advantageous not only in deep drawing, but are also useful in other sheet metal forming operations. One example is the form roller as it is encountered in the manufacture of tins when forming the container edge [WAGE99].

A similar application was executed for the manufacture of welded pipes. In this case, ceramic form or pressure rollers are applicable in the welding unit, since they are not only wear resistant but also have a high temperature resistance and cannot be heated by eddy currents in the case of induction welding [WAGE99].

Another important field for the use of ceramic tools is massive forming. Impact extrusion involves very high contact stresses and internal tool pressures, especially in the case of higher reductions of cross-section. This increases the formation of weldings between the workpiece and the tool. The advantages of ceramics with respect to wear resistance and their low propensity to adhesion can be fully utilized in this case as well. Experiences with ceramics have already been made even in the case of steel-forging, where the high temperature resistance of ceramics is utilized in addition to the aforementioned advantages [WAGE00].

2.7.2.6 Plastics

Plastics are also used as tool materials in forming technologies. Since compared to metals they can only take a small amount of mechanical and thermal loads, their

use is currently limited to the deep drawing of thin sheets in small to medium-sized series in which high compressive strengths are not necessary [FRAN99]. In this case, the advantage of a lower volume price and a more economical shaping process via milling or casting compared to steel can be exploited [DEIL03].

Both epoxy resins and polyurethane are used, the properties of which are modified partially by means of fillers.

2.7.3 Determining the Flow Curve and Materials Testing

Besides the determination of quality characteristic values and material data, materials testing also serves to test the suitability of materials for various forming processes. In the following, material data determination and suitability testing with the help of standardized test methods will be introduced in more detail. The most crucial material characteristic value in forming technology is the flow curve $k_f = k_f(\varphi, \dot{\varphi}, \vartheta)$ of the material to be formed. With it, stress distribution, the power and energy requirement of the forming process and the strength of the manufactured part can be derived. Further characteristic values include the Young's modulus E for describing elastic resilience, the strain hardening exponent n for representing strain hardening of the material (Sect. 2.7.3.1) and the anisotropy r , which describes the dependence of the material's properties on the direction of load (Sect. 2.7.1.1).

For a lasting shaping of the workpiece material, plastic flow must be initiated in the material and be maintained during the process [SIEB62]. Here, stress—required for bringing about plastic flow of the workpiece material in the case of a uniaxial state of stress—is called yield stress. If the active force is designated as F and the actual surface as A , the yield stress is:

$$k_f = \frac{F}{A}. \quad (2.55)$$

Yield stress is generally plotted over the true strain as a flow curve. The yield stress of uniaxial states of stress can be transformed to multiaxial ones using the yield criteria of *Tresca* and *von Mises* (Sect. 2.3). To this end, an equivalent stress σ_v is calculated, which is then compared with the yield stress k_f at an effective strain φ_v .

The flow curves of the unalloyed and alloyed steels and non-ferrous metals that are most important for cold forming are compiled in the flow curve atlas of metallic materials [DOEG86].

Flow curves are usually determined by means of simple material tests. In special cases, they can also be calculated from the chemical composition of the material [LEYK78]. In order to determine the flow curve, three basic tests are applied as a rule: the tensile test, the compression test and the torsion test. The method used to record flow curves should be selected as a rule such that stress and

strain conditions come as close as possible to those of the forming process to be designed. Since this requirement is very difficult to meet except for a few cases, often simple compression and tensile tests on round specimens are preferred for determining the flow curves of massive-formed materials. In sheet forming, the tensile test with flat test pieces as well as the flat crush test and the hydraulic cupping test are used.

2.7.3.1 Determining the Flow curve with the Tensile Test

A large number of standards exist for the tensile test (Fig. 2.51), and it is the most commonly used test to determine material data. One advantage of the tensile test is that it can be executed without friction. Furthermore, it is especially suitable for determining the Young's modulus E in the range of elastic elongation. In the case of stress beyond the elasticity limit σ_E , the material begins to yield and shows lasting deformation after the stress is removed from the specimen. Until the maximum tensile force is reached, the strain is equally distributed in the tensile specimen and is designated as uniform elongation A_g . Uniform elongation is generally expressed as relative strain respectively nominal strain ($\varepsilon = \Delta l/l_0$). After the maximum tensile force is reached, the specimen is constricted in the case of further stress. In the case of most metallic materials, this constriction begins already at relatively small true strains ($\varphi_g = 0.2 \dots 0.3$). Since the state of stress in the tensile specimen shifts from a uniaxial to a multiaxial one with the onset of constriction, the flow curve has to be extrapolated or determined using special calculation rules above this point. The tensile test is described for both massive and flat specimen types in the standards DIN 50125, DIN EN 10002-1, DIN EN 10002-5 and DIN EN 10045-1.

The tensile test on round specimens is primarily used to determine material data for massive forming. This is because the round specimen largely eliminates the effects of the manufacturing process.

Flat bar tension specimens are frequently used to determine material data for sheet metal materials. The advantage of this is that not only the flow curve but also the anisotropy characteristic values can be determined (Sect. 2.7.1.1). Moreover, the flat tensile test also measures elongation at break, which can be used as a measure for the formability of a sheet metal material.

The disadvantage is that the flat tensile test is restricted to lower true strains, as it only permits the recording of flow curves below uniform elongation. Evaluation in the constriction range is not possible with the usual methods, the more so as the constriction generally does not progress perpendicular to the specimen's axis [JAHN81].

Determining the Flow Curve using the Tensile Test with a Uniaxial State of Stress. When executing a tensile test, a round specimen, the dimensions of which are specified by DIN 50125 [DIN04a] is continuously loaded until fracture (Fig. 2.51). Since within uniform elongation there is a largely uniform load across

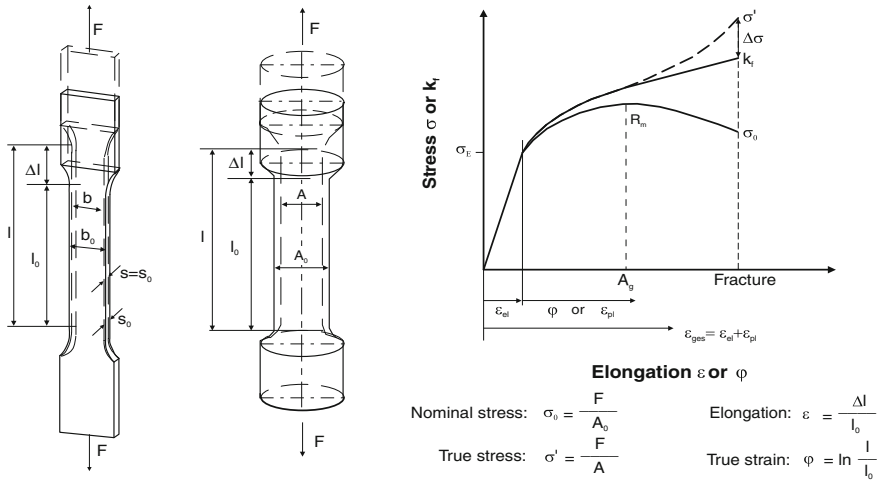


Fig. 2.51 Schematic stress-elongation profile from a tensile test on a metal without a pronounced yield point

the cross-section of the specimen, several relations are used to calculate yield stress in this range. The following is true for volume constancy:

$$l \cdot A = l_0 \cdot A_0, \quad (2.56)$$

which can also be represented as:

$$\frac{l}{l_0} \cdot \frac{A_0}{A} = 1 \text{ or } \ln \frac{l}{l_0} = \ln \frac{A_0}{A}. \quad (2.57)$$

The effective strain φ_v

$$\varphi_v = \ln \frac{A_0}{A}. \quad (2.58)$$

can also be represented as:

$$e^{\varphi_v} = \frac{A_0}{A}. \quad (2.59)$$

Thus the following is true for the yield stress k_f :

$$k_f = \frac{F}{A} = \frac{F}{A_0} \cdot e^{\varphi_v}. \quad (2.60)$$

For the forming velocity $\dot{\varphi}_v$, the following is valid:

$$\dot{\varphi}_v = \frac{d\varphi}{dt} = \frac{1}{l} \cdot \frac{dl}{dt}. \quad (2.61)$$

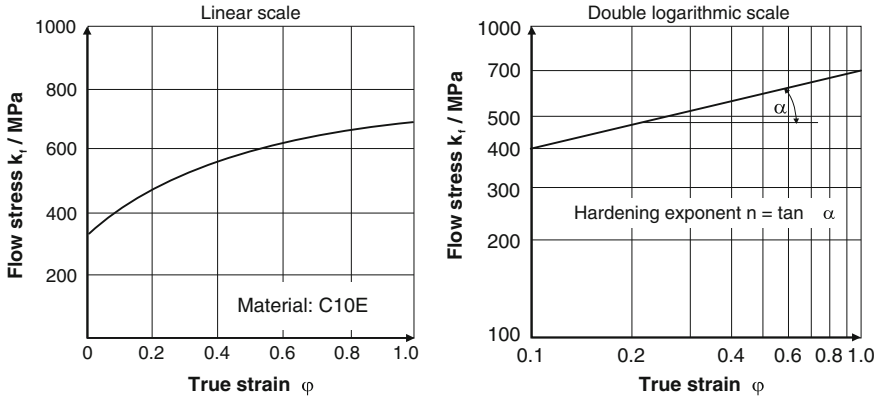


Fig. 2.52 Flow curve and solidification exponent n

Determining the Flow Curve using Tensile Strength and Uniform Elongation.

The flow curves of most unalloyed and low-alloy steels as well as Al alloys at room temperature can be described for deformations $\varphi < 1.0$ in good approximation by the power function

$$k_f = C \cdot \varphi^n. \quad (2.62)$$

This “Ludwik equation” [LUDW09] does not take the elastic portion into consideration and is only valid assuming that the material is not pre-strain-hardened.

The strain hardening exponent n , which is a measure for the material strain hardening occurring during forming, and the value C are material-specific constants.

If the flow curve is plotted in a double logarithmic representation, it becomes a straight line, the slope of which corresponds to the strain hardening exponent (Fig. 2.52).

According to Reihle [REIH61], the following relations are true:

$$n = \varphi_g \quad (2.63)$$

and

$$C = R_m \cdot \left(\frac{e}{n}\right)^n. \quad (2.64)$$

Here, e is the basis of the natural logarithm. To determine the flow curve, only the uniform elongation strain φ_g and tensile strength R_m need be established.

The uniform elongation strain φ_g (true strain) can be determined from the uniform elongation A_g (relative strain) in the tensile test as follows:

$$A_g = \varepsilon_g = \frac{l_g - l_0}{l_0} = \frac{l_g}{l_0} - 1 \quad (2.65)$$

and

$$A_g + 1 = \frac{l_g}{l_0} \quad (2.66)$$

resulting for φ_g in:

$$\varphi_g = \ln \frac{l_g}{l_0} = \ln(1 + A_g). \quad (2.67)$$

Here, the accuracy with which uniform elongation A_g is determined has a direct effect on the accuracy of the flow curve.

The uniform elongation can also be determined approximately by the formula

$$A_g \approx 2 \cdot A_{10} - A_5 \quad (2.68)$$

[KOST51]. So it is often possible to make a first approximation of the flow curve when one knows the elongation at fracture A_{10} and A_5 as well as the tensile strength R_m . The accuracy of the flow curve thus depends heavily on the accuracy of the manufactured test pieces.

Determining the Flow Curve Using the Tensile Test with a Multiaxial State of Stress

Determining the Flow Curve using the Tensile Test with a Multiaxial State of Stress. Above uniform elongation, the state of stress is no longer uniaxial, as the specimen now begins to become constricted. Taking constriction into account, yield stresses with true strains of up to $\varphi \approx 1$ can be calculated (Fig. 2.53). To this end, Siebel and Schwaigerer [SIEB48] developed for the constriction of a round specimen the following calculation rule, according to which the flow stress k_f is calculated as:

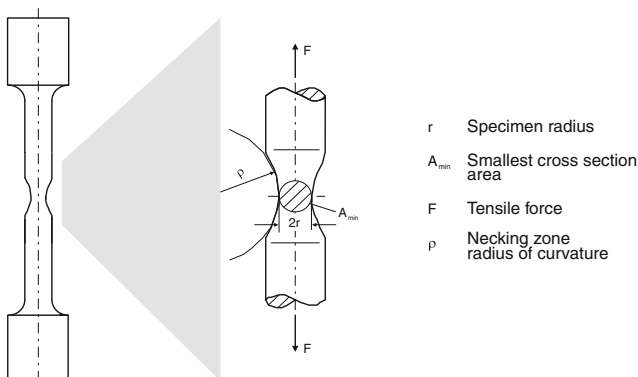


Fig. 2.53 Schematic representation of the constriction zone of a cylindrical tensile specimen

$$k_f = \frac{F}{A_{\min} \cdot \left(1 + \frac{r}{4\rho}\right)}. \quad (2.69)$$

Another possibility is to calculate the flow stress k_f in the case of the constriction of a round specimen with the following relation [BRID44]:

$$k_f = \frac{F}{A_{\min} \cdot \left(1 + \frac{2\rho}{r}\right) \cdot \ln\left(1 + \frac{r}{2\rho}\right)}. \quad (2.70)$$

The difference between both formulae is minor and in both cases the associated effective strain is calculated as follows:

$$\varphi_v = \ln \frac{A_0}{A_{\min}}. \quad (2.71)$$

However, this method requires that the constriction zone retains its circular cross-section. The largest possibilities of error in this method are the result of determining the radius of curvature ρ in the constriction zone and neglecting the effect of velocity, as there are higher strain rates in the constriction zone than in the other areas of the specimen. In determining the radius of curvature, the ratio r/ρ can be approximated as:

$$\frac{r}{\rho} \approx \sqrt{\ln\left(\frac{A_0}{A_{\min}}\right)} - 0, 1. \quad (2.72)$$

2.7.3.2 Determining the Flow Curve with the Compression Test

Higher true strains are obtained in the crush test than in the tensile test, since the deformability of metals is generally higher in the case of a hydrostatic compressive stress than in that of a hydrostatic tensile stress. Thus, it is especially practical for determining flow curves in massive forming with high true strains. In the process, a cylindrical specimen is continuously compressed between two level parallel compression paths (Fig. 2.54).

Cylinder Crush Test with a Uniaxial State of Stress. A “uniaxial” cylinder crush test presumes a uniaxial state of stress and homogeneous deformation. This is the case when the specimen remains cylindrical during upsetting. Due to frontal friction, material flow is obstructed on the front faces however, so that the specimen bulges convexly. It is hardly possible in that case to capture the effective strain φ_v exactly. Homogeneous deformation can be maintained up to effective strains of $\varphi_v \approx 0.8$ by reducing frontal friction with the help of a suitable lubrication (Fig. 2.54). In the case of optimal lubrication, the specimen maintains its cylindrical shape during the forming process, while insufficient lubrication leads to convex bulging. In this case, the state of stress becomes multiaxial, and, in the case

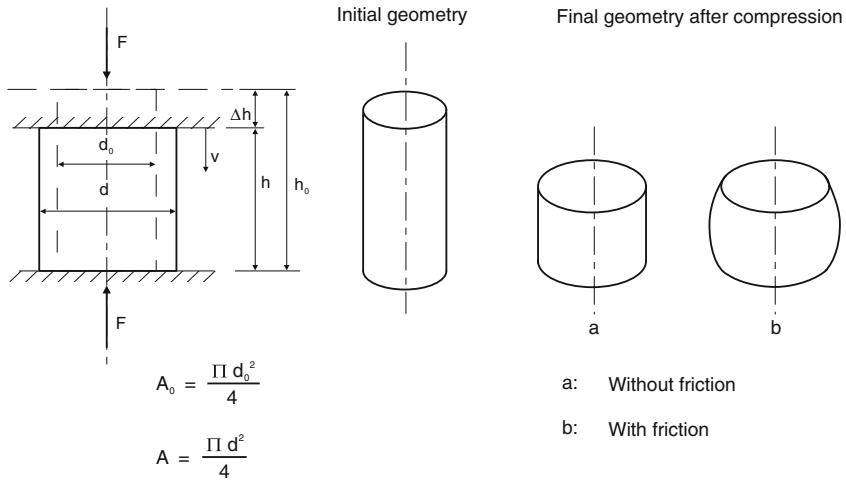


Fig. 2.54 Schematic representation of a cylinder compression test and the effect of friction on the test result

of a convex specimen shape, the yield stress k_f becomes larger than the resistance to forming, as the compressed surface is smaller than the average surface. Measures to reduce friction can include the use of plastic films or the turning of grooves into the front faces of the specimen, which then accommodate the lubricant. A deformation that is as homogeneous as possible can also be achieved by a discontinuous upsetting process, in which the specimen in the case of small amounts of bulging is brought back to its original shape by turning. The following laws are used to calculate the yield stress:

$$k_f = \frac{F}{A} = \frac{F}{A_0} \cdot e^{\varphi_v} \quad (2.73)$$

with

$$h \cdot A = h_0 \cdot A_0. \quad (2.74)$$

The following is true for the effective strain φ_v :

$$\varphi_v = \ln \frac{h}{h_0} = \ln \frac{A_0}{A} \quad (2.75)$$

and for the strain rate $\dot{\varphi}_v$

$$\dot{\varphi}_v = \frac{d\varphi}{dt} = \frac{1}{h} \cdot \frac{dh}{dt}. \quad (2.76)$$

Cylinder Crush Test with a Multiaxial State of Stress. Since homogeneous deformation of the compression specimen cannot be guaranteed in all cases, the yield stress can be determined by upsetting several specimens with the most varied

ratios of diameter d_0 to height h_0 . The results are then extrapolated to $d_0/h_0 = 0$ [SACH24]. Such an extrapolation is undertaken because the effect of friction decreases as the ratio of diameter to height becomes smaller. Thus, a ratio of zero corresponds to a frictionless upsetting process.

Another way to calculate yield stress in the upsetting of cylindrical specimens taking multiaxiality into consideration requires the undeformed specimen have a slenderness ratio of $d/h < 1$ [REIC51]. Calculation of the yield stress k_f is based on [SIEB48]:

$$k_f = \frac{\frac{F}{A_{\max}}}{1 - \frac{r_{\max}}{4\rho_a}}. \quad (2.77)$$

With a slenderness ratio of $d/h \geq 1$, the formula is as follows:

$$k_f = \frac{\frac{F}{A_{\max}}}{1 - \frac{r_{\max}}{4\rho_a} + \frac{\mu \cdot (d-h)}{3 \cdot h}}. \quad (2.78)$$

The effective strain φ_v is calculated from the maximum specimen front sides with

$$\varphi_v = \ln \left| \frac{A_0}{A_{\max}} \right|. \quad (2.79)$$

However, the friction coefficient μ (Sect. 2.8.2), the undeformed front lateral surfaces of the specimen A_0 and the front lateral surfaces A_{\max} of the deformed specimen must be known, as well as the radius r_{\max} of the largest cross-section after compression upsetting and the radius of curvature ρ_a of the bulged specimen. The latter can also be calculated approximately with the following formula:

$$\rho_a \approx \frac{h^2}{8 \cdot (r_{\max} - r)}. \quad (2.80)$$

Flat Crush Test. The flat crush test was developed in order to depict, also in one single test, the high true strains often reached in sheet metal forming processes and thereby to produce comparable flow curves. In this test, two opposing, flat punches are pressed into the specimen (Fig. 2.55). During the test, the compressive force is constantly measured at the corresponding height reduction. The loaded surface remains constant.

The width/height ratio of the flat specimen has to be $w/h > 6$ in order to assume a planar deformation. Under this assumption, the following is true for all ratios $h/a < 1$ with the yield criterion of Tresca [GREE51]:

$$k_f = \frac{F(\varphi_v)}{a \cdot b} \quad (2.81)$$

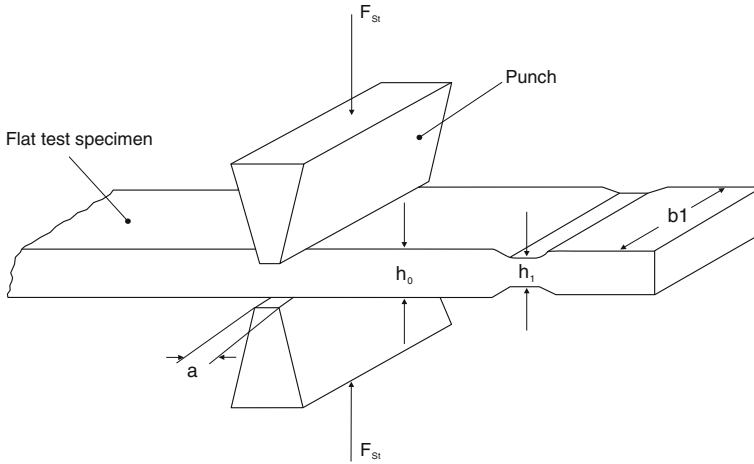


Fig. 2.55 Schematic representation of the flat compression test

with

$$\varphi_v = \ln \frac{h}{h_0}. \quad (2.82)$$

The yield stresses calculated with Eq. 2.81 are maximally 4 % too high, which has been verified experimentally. In general, higher true strains can be obtained in the flat crush test than in the tensile test. The selected thickness of the sheet metal cannot be too small, since otherwise the height reduction and thus true strain cannot be determined with sufficient accuracy. Moreover, the upsetting tools must be guided with high precision, since a lateral displacement decreases the contact surfaces and thus the upset volume. In comparison to the cylinder crush test, the results of the flat crush test are, with good lubrication, less affected by friction [KRAU62].

Taper Crush Test. Siebel and Pomp [SIEB27] have developed a crush test which avoids the effect of friction if the frontal surfaces of the specimen and the compression paths of the tools are conical. The cone angle must be chosen such that the radial shear stresses obtained are large enough to eliminate the frictional shear stresses. This requirement is met when the cone angle fulfils the following equation:

$$\alpha = \arctan(\mu). \quad (2.83)$$

The cone angle α is about 3° – 7° when upsetting steel at room temperature, which corresponds to a friction coefficient of $\mu = 0.08 \dots 0.125$. Since a homogeneous deformation can thus be assumed in the forming process, the same laws apply for the calculation of yield stress as for a crush test with a uniaxial state of stress (Eqs. 2.73–2.76). Since the frontal surfaces of the specimens are conical,

average heights are used for the heights h and h_0 . True strains of $\varphi_v \approx 0.5$ can thus be obtained without the specimen becoming bulged, making the deformation inhomogeneous. If larger true strains are to be reached, the specimen can be reduced in diameter until its original ratio of diameter to height is reached again. Re-upsetting can lead to true strains of $\varphi_v \approx 1.2$ with this method.

2.7.3.3 Other Tests for Determining Flow Curves

Hydraulic Cupping Test. In the hydraulic cupping test, which is especially suited to recording the flow curve of thin sheets, a sheet metal specimen of thickness s_0 whose circumference is firmly clamped is pressed into a usually circular die opening with a single-direction pressure (Fig. 2.56). The pressure, the depth of the outward bulge and the thickness of the sheet metal s_1 are measured on the pole of the cupped specimen. Fluids serve as the medium of load transmission. The sheet metal is formed in a pure stretch forming process, since the clamping precludes yielding. The bulging thus results in a reduction of the thickness of the sheet metal [PANK64].

With the help of the yield criterion of von Mises, the yield stress k_f can be calculated from the radius of curvature at the pole, the sheet metal thickness s_1 of the cupped specimen and the hydraulic pressure p [GOLO77]:

$$k_f = \frac{p \cdot \rho}{2 \cdot s_0} \cdot e^{\varphi} \cdot s \quad (2.84)$$

with

$$\varphi_v = -\varphi_s = \ln \frac{s_0}{s_1}. \quad (2.85)$$

With this process, the flow curve can be recorded up to a true strain of about 0.7, hence for a much higher range than in the tensile test. It is frequently observed that the flow curves obtained with the cupping test deviate from the data determined by the tensile test. The causes for this are the simplifications in the calculation (geometry, yield criterion) and the often high anisotropy of the sheet metal specimens, which cannot be specially taken into account in this method.

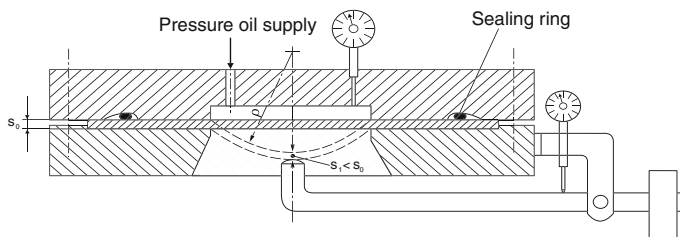


Fig. 2.56 Hydraulic cupping test

Often, the hydraulic cupping test is used to investigate the stretch drawing properties of thin sheet metals.

Torsion Test. In the torsion test, a cylindrical solid body is twisted by a torque around the longitudinal axis. With the measurement data of the torque and the torsion angle along with the specimen dimensions, the yield stress k_f and the effective strain φ_v can be calculated [DIET72]. Since the test is frictionless and can be executed at relatively low cost, it is good for determining flow curves in cold massive and hot massive forming up to high true strains.

Bending Test. In the bending test, a flat, rectangular specimen is bent. With the bending moment and the bending angle, the flow curve of the material can be determined. When calculating the flow curve, simplifications are applied that are only partially fulfilled. For example, instead of a uniaxial state of stress, there is actually a triaxial state of stress in the forming zone, which, among other things, leads to calculated yield stresses that are about 30 % below the values obtained in the tensile test. Thus, the bending test is in most cases not suitable for an exact flow curve determination [DIET72].

2.7.3.4 Comparison of the Methods Used to Determine the Flow Curve

The previous chapters have described the most important methods used to determine flow curves. Comparing the flow curves of a workpiece material recorded by different methods, considerable deviations can arise (Fig. 2.57). The cause of these deviations is primarily due to the individual processes, which have the following uncertainties:

- deviating testing approaches
- faulty measurements

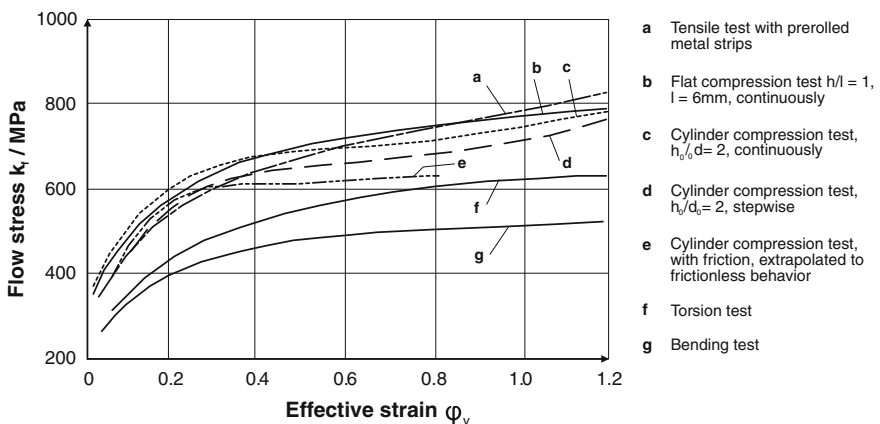


Fig. 2.57 Flow curves of the material C10 acc. to von Mises derived from different test methods [DIET72]

- requirements for test execution and test evaluation are not consistent
- inaccuracy of the method used to determine the reference value
- varying temperature and friction conditions in the different test methods
- varying changes of the test parameters during the test in the different test methods
- elastic resilience of the testing devices.

In addition, each test method involves varying test conditions with respect to

- anisotropy of the material
- microstructure of the material
- analytical errors concerning the material used
- temperature and frictional effects during the test.

These lead to deviations among the flow curves.

A comparison of the recorded flow curves shows that the cylinder crush test is affected by friction. Thus additional energy must be applied, which is reflected in the “higher” position of the flow curve. In addition, there is a clear increase in temperature in the entire specimen due to the forming process. This disadvantage does not arise in the case of the flat crush test, as in this case the heat generated can be diverted along the compression paths and the undeformed specimen areas. This advantage of frictionless test execution is accompanied by the disadvantage that deformation takes place inhomogeneously when the uniform elongation is exceeded. As a result, there is the possibility of errors in the calculation of the flow curves. The torsion test permits a simple variation of the strain rate and temperature in a frictionless test process, in which large true strains can be reached. However, complex test equipment is required. Furthermore, inhomogeneous deformation leads to lower yield stresses than those recorded, for example, in compression tests.

2.7.3.5 Sheet Metal Testing Methods

In order to predetermine the suitability of a sheet material for a certain forming operation, numerous model testing methods have been developed that, for example, simulate the load generated in principle in a stretch drawing, deep drawing or bending process. Since in practice many sheet forming processes represent a combination of deep drawing, stretch drawing and bending processes due to the variety of geometries, universally valid statements are not possible with the help of individual test procedures. For this reason, usually several testing methods are utilized in practice. The following will provide a short description of the most important ones.

Deep Drawing Test. To assess the suitability of sheet metals for deep drawing, cup deep drawing test methods are often used. In the case of the deep drawing test of Swift, cylindrical cups are drawn from sheet metal blanks with a gradually

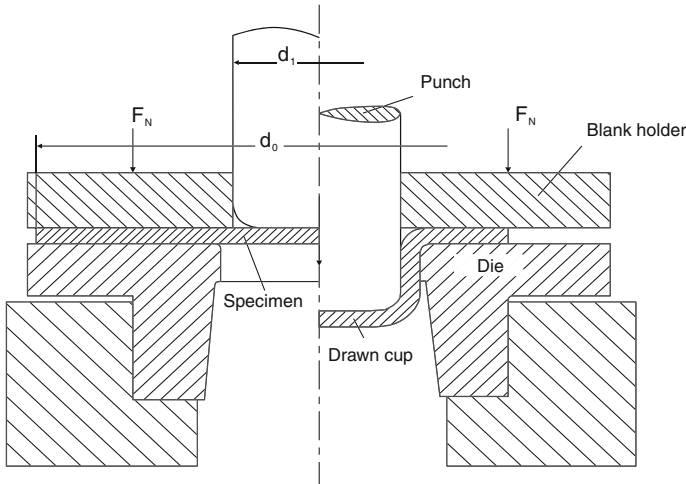


Fig. 2.58 Cup deep drawing (acc. to Swift)

increasing diameter at constant die diameter (Fig. 2.58). The characteristic value is the maximum drawing ratio β_{\max} , at which the drawability limit of the sheet metal is reached due to an imminent cup base fracture [TÖLK70]:

$$\beta_{\max} = \frac{d_{0\max}}{d_1}. \quad (2.86)$$

Since the maximum drawing ratio can only be determined with sufficient accuracy on the basis of a series of tests, this test procedure is associated with relatively high costs. Moreover, the results from the deep drawing test cannot simply be applied to the deep drawing with large tools, since the maximum drawing ratio obtained from the test is generally larger than it is in the case of operational forming. This is because the effects of friction in the area of the blank holder become increasingly apparent in the case of large tools.

Stretch Drawing Test. The Erichsen cup test has become an essential tool for testing the suitability of a sheet material for stretch drawing [HESS91]. In this case, a firmly clamped sheet test piece is dented to the point of fracture (Fig. 2.59). The central characteristic value is the Erichsen cupping value, the depth to which the punch can deform the sheet without cracking. In this process, the cupping is determined in a biaxial state of stress. Thus, it is a measure for the formability of sheets via stretch drawing. There is no correlation between the limiting draw ratio and the cupping value, so this test method is of little value for deep drawing processes.

Bending Test. Bending counts among the most frequently employed forming processes, as, in addition to well-known bending procedures (e.g. die-bending, roll forming) many other processes, such as deep drawing, are combined with bending processes.

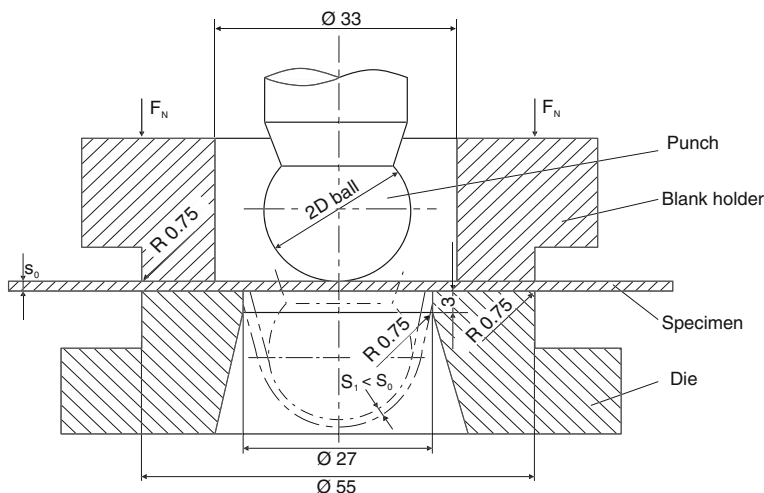


Fig. 2.59 Tool for the Erichsen cup test (acc. to DIN EN ISO 20482 [ISO03])

Among specific tests for the bending capability are the folding test (bending test) [KAEH92, ISO04b, EN01b] and, for nominal thicknesses of 0.3–3 mm, the to-and-fro bending test [PERE92a, ISO00].

As shown in Fig. 2.60, the bending test involves freely laying the test block on two rotatable rollers at a prescribed distance and bending it with a mandrel that is also exactly defined in its dimensions. The measure for the bendability of the sheet metal is the bending angle, the maximum of which can be reached without cracking on the tension side of the specimen. The elongation values obtained are larger in comparison to the tensile test, which can be derived from the supporting effect of the lower-lying “fibres”.

In the case of the to-and-fro bending test, the specimen is clamped on one side between clamping jaws and bend alternately towards the left and the right into a horizontal position (Fig. 2.61). The number of bendings that the sheet metal can endure until cracking or fracture is defined as the bending number N_b and is used as the measure for bendability. Here, one bending is defined as bending the specimen into a horizontal position and bending it back into a vertical position.

Determining Forming Limit Diagrams. Deformations made during the drawing of irregular sheet metal parts can be highly different with respect to size and type in different areas of the same drawn part. For this reason, it is impossible to describe process limits with a universally valid characteristic value such as the limiting draw ratio for deep drawing symmetrical parts [DANN83].

One way to represent the process limits of a drawing process with a plane state of stress is the forming limit diagram (Fig. 2.62). The forming limit diagram serves as a tool for the assessment of the forming properties of sheet metals with the help of measuring grids. The theoretical basis of the measuring grid method has already been described in Sect. 2.4.6.

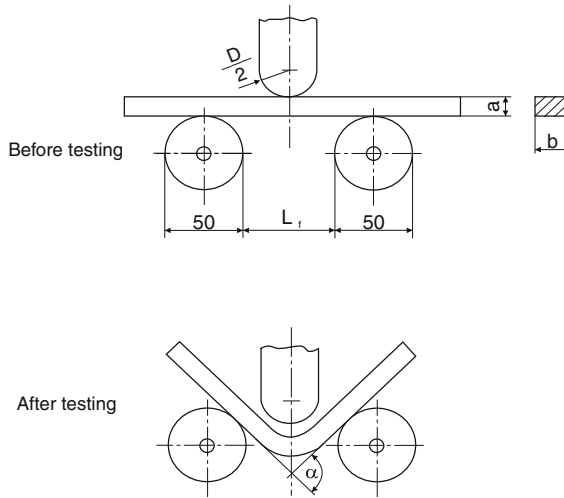


Fig. 2.60 Bending test (acc. to DIN EN ISO 7438 [ISO04b])

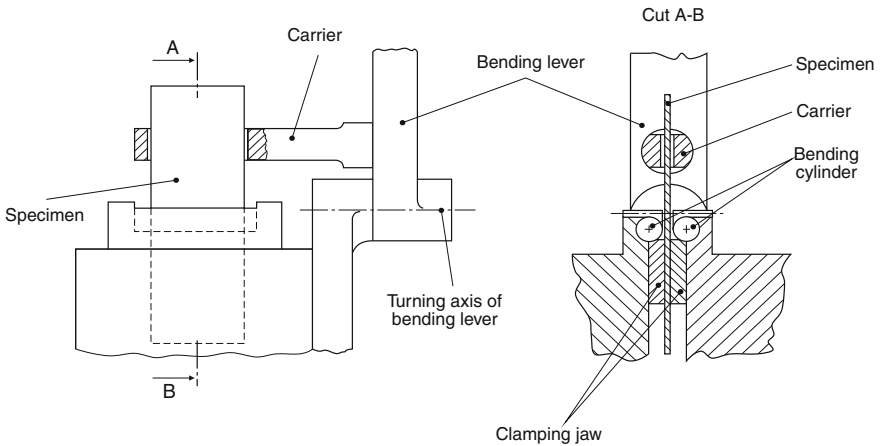


Fig. 2.61 To-and-fro bending apparatus for sheet metals, belts and strips (acc. to DIN EN ISO 7799 [ISO00])

The forming limit curve plotted in the diagram characterizes the combinations of both deformations φ_1 and φ_2 , in which the sheet metal material tends towards failure due to necking or cracking. Above the forming limit curve, shown as a solid line, the material fails. In addition to the limit curve, the diagram also indicates the states of “pure deep drawing” ($\varphi_1 = -\varphi_2$), “uniaxial tension” ($\varphi_1 = -2\varphi_2$), and “pure stretch forming” ($\varphi_1 = \varphi_2$). Since according to the definition, the second principal stress can never be larger than the first, pure stretch forming represents the natural limit of the diagram.

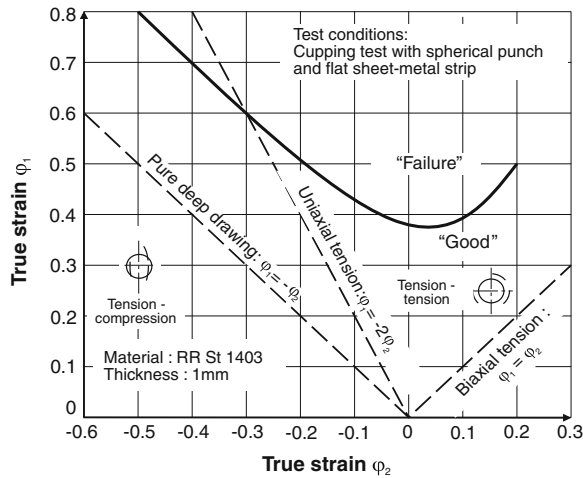


Fig. 2.62 Forming limit diagram [HASE77]

We can thus recognize critical areas by comparing the deformation distribution on a drawn part to be tested with the corresponding limit curve. With the help of this information, forming conditions such as the shape of the blank holder, blank holder force, lubrication, tool geometry (edge radii etc.) and the sheet blank size can be optimized so that a maximally uniform deformation distribution is obtained and load peaks are removed. With respect to cost effectiveness, it may then be possible to select sheet metals of lower quality but which can still safely sustain the deformations required.

Besides testing and designing new tools, deformation analysis is also often used in practice to monitor a running production. By determining the distance between the deformations of critical areas and the forming limit curve, which is a measure for production reliability, both differences in sheet metal quality and tool wear progress can be detected. This is important insofar as the geometry of a tool (die clearance etc.) sometimes alters considerably with progressive wear. The resulting new distribution of deformation is then frequently the cause for failure [SUY77].

If drawn parts are manufactured in several stages, one must bear in mind that the forming history (deformation path) also affects the position and shape of a forming limit curve [HASE80b].

Judging the forming suitability of different sheet metal materials is only possible to a limited extent with the help of forming limit diagrams. While materials with very different physical properties do also differ in their forming limit curves, the latter imperfectly reproduce the effects of the strain hardening exponent n and of perpendicular anisotropy r [LANG74]. It is thus possible that two sheet metal materials differing only in these two parameters have almost identical forming limit curves on the one hand but exhibit quite different deformation distributions after a drawing operation and as a result are not equally suitable for the forming process on the other hand.

In addition to the evaluation of cases of failed production parts, usually experimental test procedures are used in order to determine the forming limit curve. Among the most common processes are cupping tests with varying punch and blank shapes, the hydraulic cupping test as well as the tensile with notched specimens [HASE78]. They differ mainly by the shape of the specimen respectively blank as well as by the type of material load, whereby the resultant forming limit curves can deviate from each other considerably at times due to process-specific differences.

2.8 Tribology in Forming Technology

The term “tribology” was introduced in 1966 by an English commission and was derived from the words for “to rub” (tribein) and “theory” (logos) [JOST66]. Tribology is limited however not only to the study of friction, but also includes wear processes. It comprises the entire science and technology of surfaces acting upon each other under relative motion and thus aims for the scientific understanding of all types of friction, wear and lubrication as well as the technical application of tribological knowledge [GFT02].

2.8.1 *The Tribological System*

When observing tribological processes, it is important not only to take into consideration the individual bodies in contact but the entire tribological system and the collective load acting upon it (Fig. 2.63) [CZIC03].

The tribological system consists of bodies and counter-bodies (tool and workpiece in the case of manufacturing technology) as well as intermediate and surrounding media (lubricant and air as a rule). The sum of external load effects such as process forces, temperature or sliding speed makes up the tribological stress collective, which can be understood as the system input from a system's approach.

Within the system structure there are many influences at work, which effect the system's behaviour at exposure of the stress collective (Fig. 2.64). Besides the type of materials involved, the local load induced stress distributions, contingent on the microgeometry of the surfaces, has an important influence on the friction behaviour. In contrast to friction processes in bearing technology or gear drives, major plastic deformations of a friction partner (the workpiece) can arise during the forming process. These deformations are sometimes associated with considerable surface enlargements, so that the various influences on the system are subject to permanent change. This makes it difficult to capture the state of the system exactly.

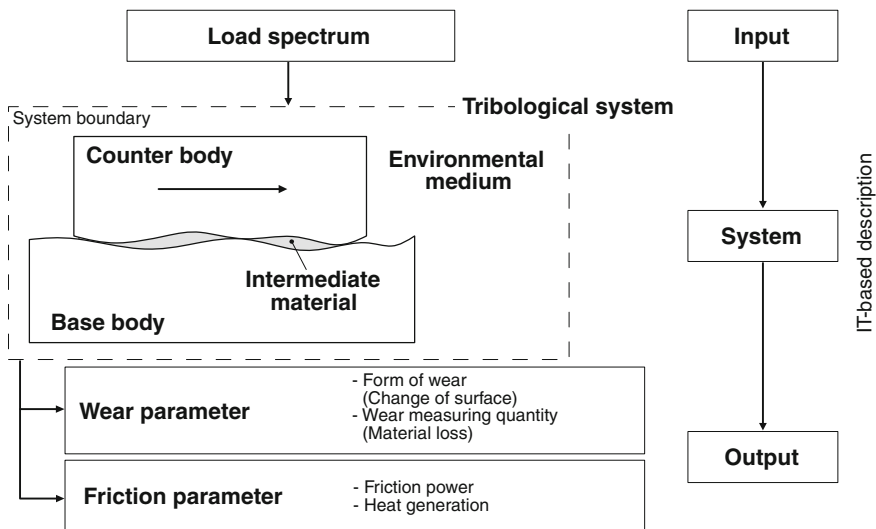


Fig. 2.63 The tribosystem and the system's approach

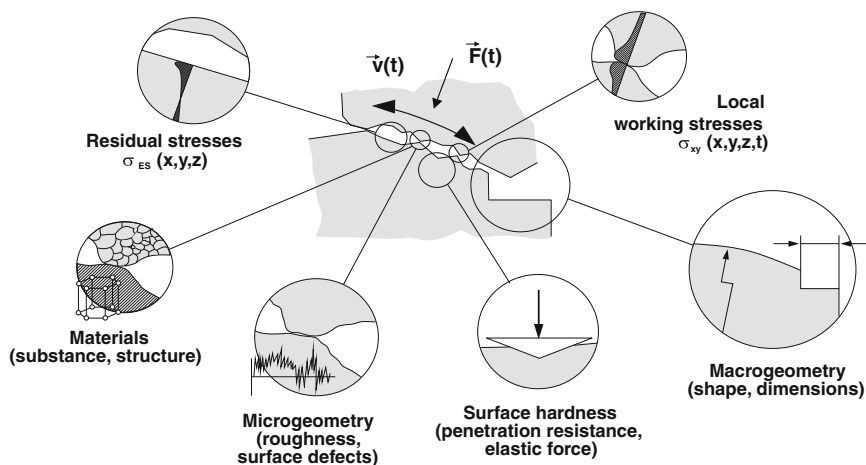


Fig. 2.64 Influences on the tribological system's behaviour within the system structure [FRIE97]

Both friction and wear are dependent on the structure of the tribological system and on the stress collective. They thus make up the system response or system output. Progressive wear and consequentially altered friction conditions retroactively affect both the system structure and the stress collective [CZIC03]:

- *friction, wear* = $f(\text{system structure, stress collective})$
- *system structure, stress collective* = $f(\text{friction, wear})$.

The tribological conditions within the system of a forming process have an effect on numerous characteristics of forming processes. Among these are:

- process limits
- cost-effectiveness
- workpiece quality
- impact on the environment and workplace
- resource conservation.

The aim of tribological process designs and optimizations is the improvement of one or more of the above factors. For example, changing the friction conditions can have a major effect on material flow. The latter determines the obtainable final geometry of the workpieces and thus the process limits as well. Furthermore, friction affects the process forces. A reduction of the process forces contributes to resource conservation due to a saving of energy. In addition, tool life is increased with lower loads, which has a positive effect on the cost-effectiveness of a forming process. One consequence of friction is tool wear, the type and characteristics of which affect the service life of the tools used (cost-effectiveness) and the surface quality of the forming parts produced. Many forming processes in manufacturing would not be economically viable at present without the tribological advances of the 20th century.

Given precise knowledge of the tribological conditions within a forming process, friction and wear can be influenced and minimized by carefully selecting the individual components of the tribological system. Essentially, this selection includes the tool materials being used, tool coatings and lubricants, which in turn codetermine the environmental friendliness of a process. In the following, the different types of friction and wear will be elucidated, as well as the potential ways to affect friction and wear by means of measures taken in terms of material and lubrication.

2.8.2 Friction

Friction occurs when there is relative motion between bodies in contact. We differentiate between two basic types of friction. External friction takes place between material areas of different bodies in contact. Internal friction involves contact between two substance areas within the same body. It arises within metallic bodies that are undergoing plastic deformation, leading to forming heat. What both types of friction have in common is that friction respectively the frictional force is directed against the relative motion [GFT02]. In the following, we will take a closer look at external friction.

2.8.2.1 Parameters Influencing Friction

A large number of parameters affect friction. Some of these parameters, such as the true contact surface or the state of lubrication, are difficult to capture formula-ically. Figure 2.65 shows different influencing parameters [LI95] affecting friction conditions which arise within a dynamically changing contact surface in the microscopic order of magnitude. Friction is thus a complex process, the analytical calculation of which is very difficult in the sphere of forming technology.

The predominant stress collective has a decisive influence on the magnitude of the frictional force. Forming temperature, strain rate and surface pressure between the body and counter body are essential parameters in this context. In the realm of mixed and boundary friction, which is encountered in forming technology, it is especially surface pressure—also called contact normal stress—that is of paramount importance.

The condition of the tribological system is a further source of influence. This includes factors such as surface finish and the chemical composition of the tool and workpiece. One very important factor is the surface finish of the tool. The influence of machining is so considerable that the frictional force has different values depending on the sliding direction relative to the machining direction. Apart from sheet metal forming, the type of machining process used on the contact surface of the body to be formed is significant only in the initial stage of forming. With progressive deformation, the surface smoothens and becomes a replica of the tool surface.

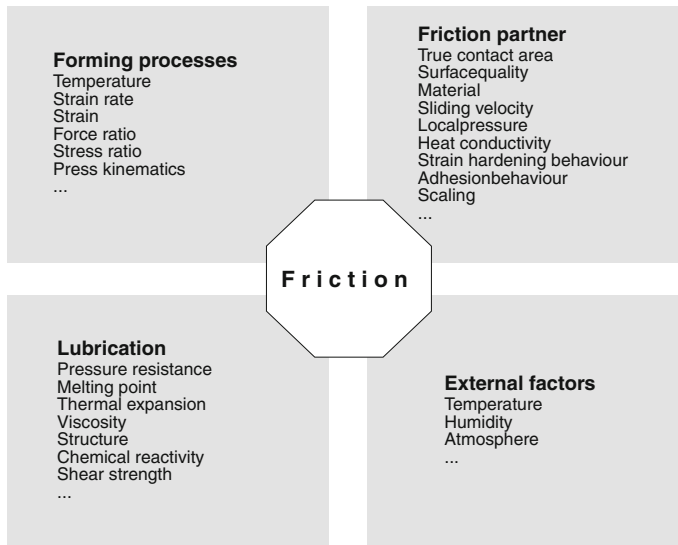


Fig. 2.65 Influencing parameters on friction [LI95]

The physical/chemical condition of the tool and workpiece surfaces has substantial influence on the force of friction. During the forming process, oxides and impurities are removed from the contact surfaces, causing an increase in friction and potentially an increase in the occurrence of wear phenomena. Thus, lubricants need to be employed. These ensure that the size of the frictional forces and the assault of wear on the tool remain within acceptable limits [LI95, RAED02].

2.8.2.2 Friction Laws for Movement Friction

Friction laws are mathematical/analytical approaches with which we can calculate the maximum transmissible frictional shear stress in a friction interface as a function of its main influencing parameters. In plasticity theory, two models have become established to describe the frictional shear stress τ_R —the Coulomb law and the shear friction law (Fig. 2.66). Newer approaches have adjusted the properties of these friction laws to the special requirements of forming technology and combine the advantages of both established models.

Generally speaking, greater accuracy in the calculation of forming processes is possible when the friction laws applied describe the reality more exactly and the characteristic values required for the calculation are all known. One must bear in mind that numerical values such as those that are valid for the friction of normal machine components should never be used to determine friction forces in the case of plastic deformation.

Coulomb Law. The first attempts to describe the underlying natural law stem from the work of Leonardo da Vinci in the 15th century [DAWN79]. Coulomb summarized these experiences in 1785 in a natural law named after himself [COUL85]. The Coulomb law describes the relation between the compressive

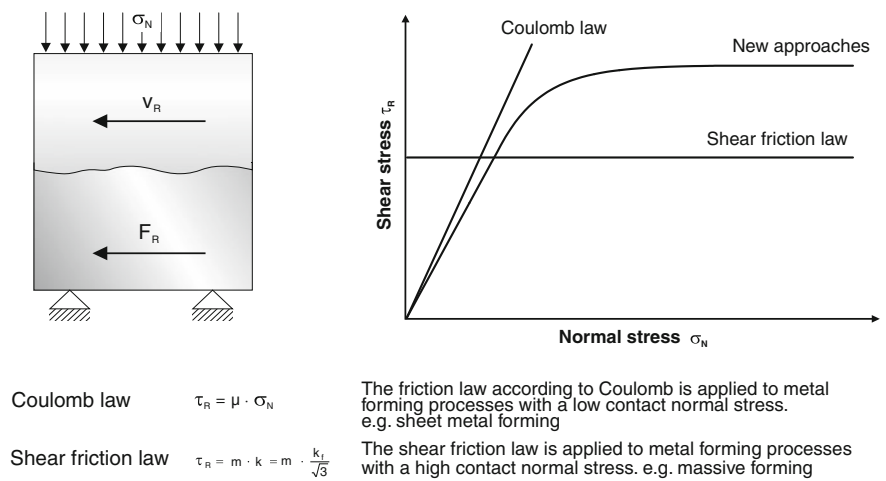


Fig. 2.66 Friction laws in forming technology

force F_N acting in the normal direction and the friction force F_R arising in the interstice in opposition to the direction of movement by the linear relation:

$$|F_R| = \mu \cdot |F_N|. \quad (2.87)$$

The proportionality factor is the friction coefficient μ , which is mostly viewed as constant throughout the duration of the friction process and along the friction surface. Thus, this friction law is based on the assumption that the force of friction is proportional to the load applied and independent of the contact surface and sliding speed. The normal force and friction force can be transferred to locally acting stresses by means of the following relation:

$$|\tau_R| = \mu \cdot |\sigma_N|. \quad (2.88)$$

Thus, the locally acting frictional shear stress τ_R is proportional to the contact normal stress σ_N .

If a relative motion arises in the contact surface of two bodies (workpiece/tool) under the condition that the contact normal stress σ_N is small compared to the flow stress k_f , then the frictional shear stress initially has a linear relation to the contact normal stress if the friction coefficient μ remains constant. Thereby the friction coefficient μ can arbitrarily be set to any positive constant value. A value of 0 describes a frictionless state. But if the frictional shear stress reaches the size of the shear flow stress k of the softer body, the softer body will react with shifting below the contact surface, and both bodies will adhere to each other in the contact zone. This condition is called static friction. The limiting friction coefficient at which adhesion initiates is calculated with $\mu_{limit} = k/|\sigma_N|$. With increasing normal stress, the frictional shear stress corresponds to $|\tau_{Rmax}| = k$, whereby k represents a function of deformation in the case of solidifying materials. The Coulomb law is no longer valid in this case, since it does not take an upper limit for frictional shear stress τ_{Rmax} into consideration.

Shear Friction Law. Another mathematical friction law used to describe friction is the shear friction law. This model assumes that the frictional shear stress τ_R must be linked with the shear flow stress k of the softer material with the relation

$$\tau_R = m \cdot k, \quad (2.89)$$

whereby the proportionality factor m is called the shear factor.

This law assumes that the frictional shear stress is constant and independent of the normal pressure. $m = 1$ results in the condition of adhesion, while $m = 0$ characterizes the frictionless state. With the shear factor $0 < m < 1$, the shear friction model is only a rough approximation, as there is no objective method for estimating the numerical value of m . By using the yield criterion of von Mises $k = k_f/\sqrt{3}$ with the flow stress k_f , we obtain the following relation for the shear friction model:

$$\tau_R = m \cdot \frac{k_f}{\sqrt{3}}. \quad (2.90)$$

Free Friction Laws. As opposed to two bodies that slide along each other, the surface of a counter body can tear open because of plastic deformation. In this way, the material from the inside of the plasticized material reaches the surface so that new particles are constantly participating in the friction process. Furthermore, the yield criterion shows that the frictional shear stress is only increased until plastic flow begins, so the friction coefficient is reduced in the case of high surface pressures and thus itself must be a function of surface pressure. This has been determined in numerous investigations, so the Coulomb law is only true for relatively small normal stresses, while the shear friction law is more suitable for high contact normal stresses [KLOC02b].

For this reason, Orowan [OROW43] suggested that the frictional shear stress τ_R should be calculated according to Coulomb's law in proportion to the contact normal stress σ_N in case of low contact normal stresses and that a constant frictional shear stress should be set equal to the shear flow stress k for high contact normal stresses. Figure 2.67 illustrates this law. One proven disadvantage of this approach is the discontinuous transition area, which insufficiently describes the actual conditions of friction.

Further studies have shown that the size of the friction coefficient is determined not only by the material combination but also by the geometry of the friction surface and by the physical and chemical influencing parameters active in the frictional interstice such as pressure, sliding speed and temperature. Dowden and Tabor [BOWD50] have shown that the Coulomb law is only valid as long as the true contact surface increases in proportion with the normal force. Shaw [SHAW63] pursued this problem and has formulated a friction law that describes a continuous transition (area 2) of frictional shear stress between low (area 1) and high contact normal stresses (area 3) (Fig. 2.67).

Building upon the work of Orowan and Shaw, Wanheim and Bay have developed a universal friction law as a combination of the Coulomb law and the shear friction law. This universal friction law describes on the one hand the continuous transition between both friction laws and on the other hand takes into consideration the true contact surface. In this way, the ratio between the true and the apparent contact surface becomes larger as the normal stress increases, and the

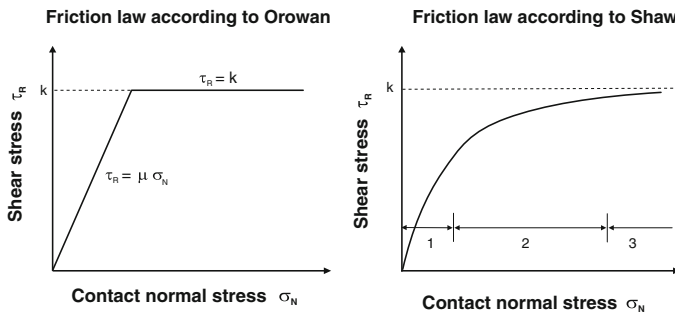


Fig. 2.67 Friction law acc. to Orowan and Shaw [OROW43, SHAW63]

ratio of friction shear stress to the shear flow stress proceeds asymptotically towards 1. This is described by the following relation:

$$\tau_R = f \cdot \alpha \cdot k \quad (2.91)$$

with

- τ_R frictional shear stress,
- f friction factor $0 \leq f \leq 1$,
- α ratio between true and apparent contact surface and
- k shear flow stress

Studies on the influence of the contact normal stress σ_N and shear flow stress k on the contact surface ratio α have shown that the course of α initially shows a linear increase and then approaches the value $\alpha = 1$ asymptotically [WANH87, WANH99]. The mathematical relation that describes this effect looks as follows:

$$\frac{\tau_R}{k} = \frac{\tau_R^*}{k} \cdot \frac{\frac{\sigma_N}{k_f}}{\frac{\sigma_N^*}{k_f}} \quad (2.92)$$

with

$$\frac{\sigma_N}{k_f} \leq \frac{\sigma_N^*}{k_f}$$

and

$$\frac{\tau_R}{k} = \frac{\tau_R^*}{k} + \left(f - \frac{\tau_R^*}{k}\right) \cdot \left[1 - \exp \frac{\left(\frac{\sigma_N^*}{k_f} - \frac{\sigma_N}{k_f}\right) \cdot \frac{\tau_R^*}{k}}{\left(f - \frac{\tau_R^*}{k}\right) \cdot \frac{\sigma_N^*}{k_f}}\right] \quad (2.93)$$

with

$$\frac{\sigma_N}{k_f} > \frac{\sigma_N^*}{k_f}$$

The friction stress τ_R and the normal stress σ_N are normalized with the shear flow stress k and the flow stress k_f respectively. The limits of proportionality for the frictional shear stress and the contact normal stress (τ_R^* , σ_N^*) are described by:

$$\frac{\tau_R^*}{k} = 1 - \sqrt{1 - f^2}, \quad (2.94)$$

$$\frac{\sigma_N^*}{k_f} = \frac{1 + \frac{\pi}{2} + \arccos(f) + \sqrt{1 - f^2}}{\sqrt{3} \cdot (1 + \sqrt{1 - f^2})}. \quad (2.95)$$

The friction model is based on contact tests between one smooth and one rough surface. Due to plastic deformation of the roughness peaks, the ratio α between the

true and the apparent contact surface is determined as a function of the normal stress σ_N and the friction factor f , which describes friction in the true contact surface ($0 \leq f \leq 1$). In the case of low normal contact stress, the roughness peaks are deformed without being influenced by neighbouring peaks. If α is proportional to the normal stress, the Coulomb law is valid. In the case of higher contact normal stress, frictional shear stress is increased along with the normal stress (Eq. 2.92). The frictional shear stress here progresses towards a constant value, comparable to the shear friction model. Figure 2.68 left shows the normalized dimensionless frictional stress as a function of the normalized normal stress with the friction factor f in accordance with the Wanheim/Bay friction law.

In the calculation of forming processes, often either the Coulomb law or the shear friction model is used. The Coulomb law overestimates the frictional shear stress between the workpiece and the tool very frequently however, since the applied normal stress is often so large (e.g. in massive forming) that the frictional shear stress becomes larger than the shear flow stress. In the case of low normal stresses, the shear friction model overestimates the frictional stress, since the friction is not dependent on the current state of stress between the workpiece and the tool, but only on the properties of the workpiece material.

A comparison between a real and a FEM-calculated compression test of a conical specimen without lubrication shows that calculating with a Wanheim/Bay friction factor with $f = 1.0$ describes the deformation of the cone better than the calculated deformation with a friction factor of $m = 0.85$ obtained in the ring compression test (Fig. 2.68 right). The explanation for this is that the shear friction model overestimates the actual friction on the upper side of the workpiece/tool contact surface due to the low contact normal stress, and therefore the material on the top does not flow as much in the radial direction. On the contrary, the shear friction model underestimates friction on the bottom of the workpiece/tool contact surface, since here the contact normal stresses are significantly higher. Thus, the material in this area flows much more in the radial direction in the simulation (Fig. 2.68 right). This is especially clear in those areas in which the contact normal stress takes on small values, i.e. when the normalized normal stress is $\sigma_N/k_f < 1$. Guérin et al. [GUÉR99] have implemented this friction law into commercial FE software. The implementation included two-dimensional and three-dimensional applications.

2.8.2.3 The Effect of Friction on the Process

Many forming processes are heavily influenced by friction. Increased friction causes a larger power and energy requirement, increases surface temperature and affects material flow and with it the distribution of deformation and strength in the entire forming zone. As a result of the higher power requirement, tool load is also increased, leading to a shorter tool life. In sheet metal forming, the maximum drawing ratio is influenced. In the case of excessive frictional forces, cup base

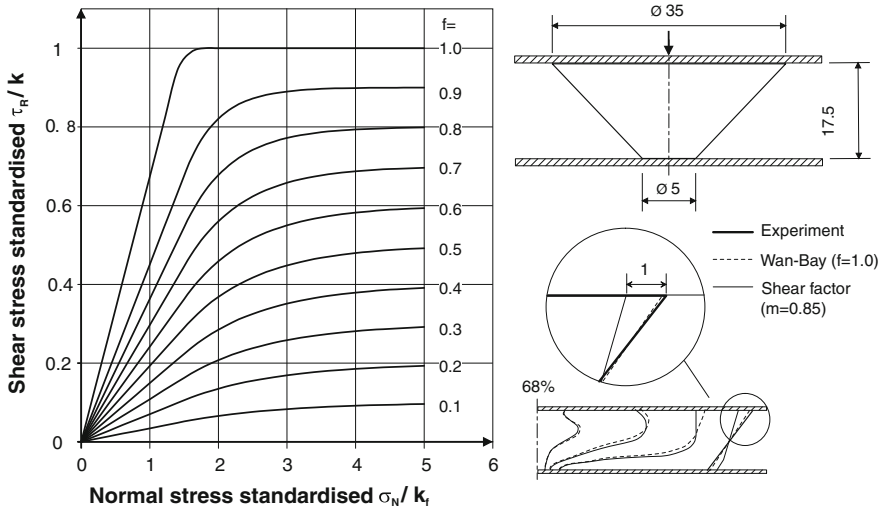


Fig. 2.68 Accuracy of the shear friction law and friction law according to Wanheim and Bay using the example of a conical test piece

fractures can occur. Moreover, the accuracy grade and surface quality of the workpiece can be significantly affected [KOPP99].

However, it is not justified automatically to consider friction merely from a negative light as something undesirable. In forming technology in particular, several processes absolutely require a certain amount of friction for the process to run stably, e.g. rolling (Sect. 3.5). Depending on the requirements of the application at hand, friction in forming technology thus represents a problem of either minimization or optimization.

The simplest example of how friction affects the forming output can be seen in the compression testing of a cylindrical specimen. Assuming frictionless compression, the specimen remains cylindrical during the entire process. The true strain tells a similar story as it remains constant within the cross-section of the specimen and increases with progressing deformation. If the compression process is subject to friction, the specimen bulges more and more with increasing deformation. The bulging is all the more apparent the higher the friction is between the workpiece and the tool. A cross-section through the compressed specimen shows the distribution of the true strain, which increases radially outwards along the contact surface between the workpiece and tool on the one hand and also increases in the axial direction on the other hand, so that the maximum true strains become arranged along the component diagonal.

In the case of reverse cup extrusion (Sect. 3.1.2.1), a variation of friction only leads to a small change in the component's geometry. Nonetheless, the process is heavily influenced by friction (Fig. 2.69). The evaluation of test series carried out with varying lubricants has shown that the punch force is strongly influenced by the lubricant. Dry contact surfaces lead to a high punch force. The friction laws

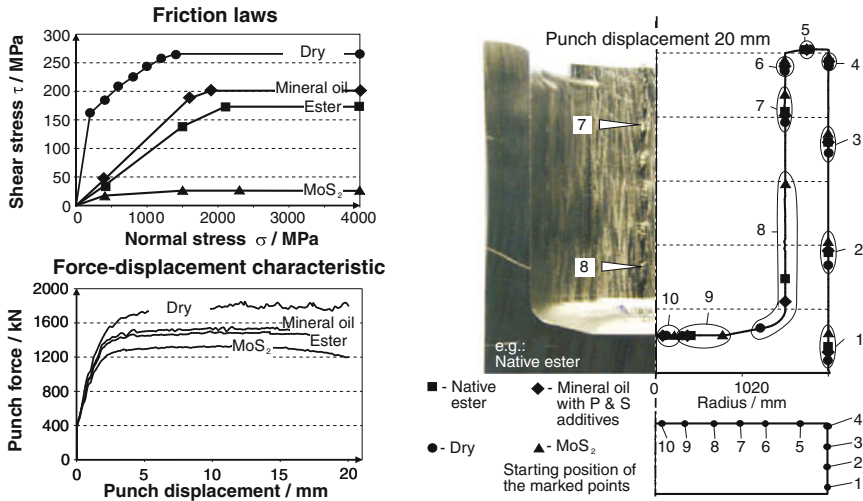


Fig. 2.69 Effects of different types of friction on the forming process using the example of reverse cup extrusion

shown in Fig. 2.69 were established by means of a combination of different test series with FEM simulations and approximately reproduce the actual course of frictional shear stress over contact normal stress. [KLOC04e] provides a detailed explanation of the procedure used to determine these laws.

When one considers surface enlargement during the forming process, one sees that high frictional shear stresses lead to minor displacements along the surface. To this end, in one experiment the surface of the initial test piece was equipped with markings (Fig. 2.69). After forming, the displacements of the points as a result of forming were evaluated. The result was that, in a forming process with dry contact surfaces, the displacement of the marking points relative to their initial coordinates is the smallest. This is especially clear in the case of marking point 8. While this point is shifted in a dry forming process maximally up to the beginning of the punch edge, in a forming process with a solid lubricant it is shifted up to half the height of the cup wall. These examples show that friction is a process-specific quantity which can have a decisive influence on the properties of the component and thus cannot be ignored.

2.8.3 Wear

In the case of constant load, the frictional stress of forming tools is accompanied by wear. According to worksheet 7 of the German Society for Tribology, wear refers to the progressive loss of material from the surface of a solid body from mechanical causes, i.e. contact and relative motion of a solid, liquid or gaseous

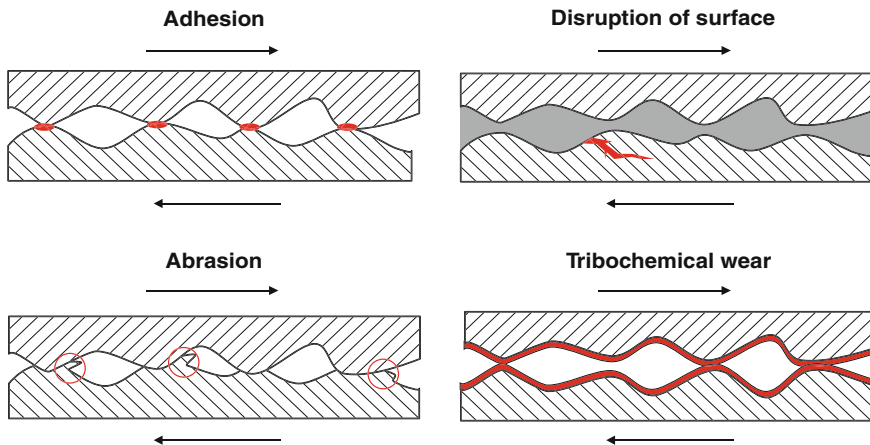


Fig. 2.70 Wear mechanisms in forming technology

counter body [GFT02]. In forming technology, wear is defined also as the transfer of workpiece material to the tool surface, which is commonly referred to as cold shut or wear due to scoring [LANG90a]. In addition to the possibility of cracks, tool fracture and plastic tool deformation, tool wear has a considerable influence on the life of forming tools. The tool life quantity is defined as the amount of produced workpieces till the end of tool life. This is reached when a required quality of workpiece, characterized by accuracy grade and surface quality, can no longer be maintained.

Wear is caused by the interaction of different mechanical and chemical processes. The basic processes involved in wear can be traced back to the following wear mechanisms [CZIC73]: abrasion, adhesion, disruption of surface and tribochemical reactions (Fig. 2.70).

Figure 2.71 shows some typical peculiarities of the wear natures produced by individual mechanisms with the help of selected scanning electron microscopic images. In most cases however, tool wear is the result of several mechanisms operating simultaneously. While the transfer of workpiece material can clearly be attributed to adhesion, material loss cannot always be clearly assigned to individual wear mechanisms.

It should be noted that a distinction must be made in the case of adhesive material transfer between two initiating mechanisms—adhesion due to interfacial bonding (adhesion in the classic sense) and mechanical clasp (Sect. 2.8.3.2). Figure 2.71 top left shows two examples that make the difference clear. The level areas with white points in the left image represent the surface of a polished, powder-metallurgical high-speed steel. The white points are the spherically formed carbides. The adhered workpiece material lies on this very smooth surface and adheres due to the formation of interfacial bondings on the surface. In the right image, a high-speed steel surface is also shown but in much lower magnification. In this case it is a turned surface and as such much rougher. The vertical grooves

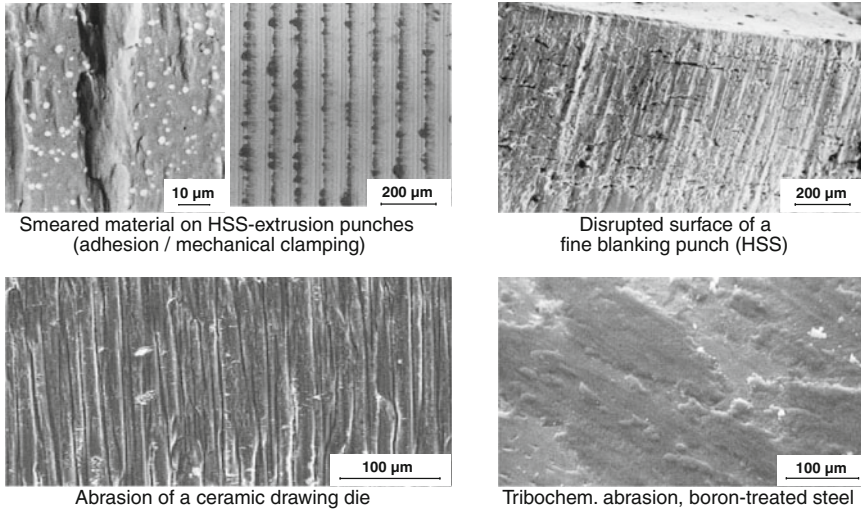


Fig. 2.71 Scanning electron microscopic images of typical forms of wear on forming tools caused by different wear mechanisms

can be easily seen. Workpiece material adheres to the raised transitions between the grooves. This material is sheared off by the elevations during the forming process and becomes mechanically anchored on the uneven patches.

2.8.3.1 Abrasion

Abrasion of the base body occurs in tribological contact classically when the base body is loaded by the roughness peaks of a harder counter body or by hard particles [BART00]. In forming technology, the tool is the base body, which due to the process is always harder than the workpiece to be formed, i.e. the counter body. Abrasive wear of forming tools is thus attributed to hard particles found in the frictional contact zones between the base and counter bodies. Among these are hard phases contained in the counter body material (workpiece material) such as the carbides of the alloying elements or intermetallic phases, as well as oxides (e.g. scale of forging blanks) or other compounds or impurities on the surface. The abrasive hard particles are pressed into the hard tool surface according to a kind of hydraulic principle. The position and shape of the abrasive particle is decisive [RAED02]: on the side of the workpiece, the particle is loaded with a relatively small pressure, which is maximally three times the value of the yield point of the softer material. If this particle has a small contact surface on the side of the tool, it exerts a corresponding amount of pressure there, since the equilibrium of forces must be maintained.

Even extremely hard tool materials such as cemented carbides or ceramics are subject to this wear mechanism, the results of which manifest themselves

microscopically in small furrows on the tool surface and material loss in the form of wear particles (Fig. 2.71 bottom left). The hardness of the abrasive particles in relation to the hardness of the tool material is decisive for the quantitative characteristics of abrasive wear. Beyond a certain hardness difference, there is a rapid increase in wear. The designation of low/high wear level is used for this [BERT00].

Depending on the material properties, different forms of abrasion can arise on the tool surface, individually or in combination [GAHR87]:

- **micro ploughing:** furrowing, plastic deformation of the base body with accumulations on the furrow edges, ideally without material removal
- **micro fatiguing:** separation of the material from the surface of the base body as a result of repeated micro ploughing
- **micro chipping:** formation of a “microchip” in front of the abrasively acting hard particle
- **micro fracture:** exceeding a critical load leads to cracking and thus to larger chippage, especially in the case of more brittle materials.

The wear particles originating from the mechanisms of micro chipping and micro fatiguing are harder than the base material of the tool, since they were subjected to plastic deformation before separation. These particles act abrasively in turn and can thus additionally enhance abrasive wear. It is therefore the task of lubrication to transport wear particles of any kind as quickly as possible from the contact zone between the tool and the workpiece.

2.8.3.2 Adhesion

Adhesive wear manifests itself in a transfer of material from the softer friction partner to the surface of the harder one. It originates under the effect of higher surface pressures between the base and counter bodies. Due to the extreme surface pressures and the friction combination of hard tool/soft workpiece, adhesive wear is of decisive importance in forming technology. In the case of adhesive wear, we differentiate between two initiating mechanisms—interfacial bonding and mechanical clasping (see also Fig. 2.71 top left and Sect. 2.8.3). Both mechanisms will be explained further in the following.

The wear mechanism of adhesion is, according to the classic definition, initiated by the formation of interfacial bonds when non-metallic surface layers like oxides tear open in tribological contact and are removed. This results in a purely metallic contact between the materials of the tool and the workpiece [RAED02].

On the workpiece side, enlargement of the surface with progressive plastic deformation is responsible for tearing open the oxide layers. On the tool side, local load peaks on roughness peaks lead to elastic material deformation, which also leads the brittle oxide layers to becoming torn open. Moreover, it is possible that the oxide layers are abrasively removed.

At the points of metallic contact, interfacial bonds can finally be formed under the high surface pressures. These interfacial bonds are also known as “cold welding” or “scorer”. The mechanism involved is adhesion, to which all chemical bonds can contribute that can also bring about the inner cohesion of solid bodies. Among these are the strong primary valency bonds (ionic bonds, covalent bonds, metallic bonds) as well as the relatively weak secondary valency bonds (van der Waals bonds).

These interfacial bonds can be stronger than the cohesion inside the soft workpiece material, so that separation of the bond generally takes place inside the workpiece material via shearing. In this way, the workpiece material is permanently transferred to the tool surface (Fig. 2.71 top left, left image).

In numerous investigations, attempts have been undertaken to discover connections between the general tendency to adhesion and the basic material properties of different metals. The basic insights gained from this can be summarized in rules of thumb, which however are only valid for pure metals and only partially:

- The adhesive tendency of metals is reduced with increasing hardness [SIKO63].
- The adhesive tendency is reduced as a function of the lattice structure in the order fcc- bcc-hexagonal [BUCK68, HABI68]. The reason for this lies in the different number of glide planes, which effect the formation of true contact surfaces.
- The strength of adhesion is reduced in the order b-group metals—noble metals—transition metals [CZIC68]. This is founded in the differing electron configuration and the associated capability to form certain types of bonds.

Furthermore, adhesive wear is in many cases initiated by mechanical claspings. In this case, due to the high pressures arising during the forming process the soft material of the workpiece is pressed into surface defects (grinding grooves, burrs, coating defects etc.) of the tool and sheared off the workpiece by relative motion (Fig. 2.71 top left, right image). In this way, workpiece material also remains on the tool surface, bringing about in turn a metallic contact which in this case is between the workpiece material adhered to the tool surface and the workpiece itself.

Adhesive wear has different technological effects. Heavily roughened tool surfaces are the first result, resulting in turn in grooves on the workpieces. If the surface quality of the workpieces is exceeded to an impermissible extent, the end of the tool life has been reached. Mechanical reworking (e.g. grinding or polishing), or in some cases chemical treatment (e.g. in the case of aluminium buildup weldings), can remove these undesirable material transfers.

Furthermore, the buildups of workpiece material also causes local overloads of the tool surfaces in the case of repeated tribological load. These locally excessive and time limited stress peaks promote the mechanism of the disruption of the surface (Sect. 2.8.3.3). Thus, spontaneous cracking can occur that lead eventually to pitting-like disruptions from the tool surface.

Potential measures against adhesive wear are extremely numerous. In order to prevent the development of interfacial bonds effectively, one must separate the metallic surfaces of the tool and the workpiece (see Sects. 2.8.4 and 2.8.5). In order to prevent mechanical claspings, an optimal finishing processing of the tool surfaces is necessary. In many cases therefore, polished tools are employed since they lay themselves open for attack by mechanical material claspings to only a small extent.

2.8.3.3 Surface Disruption

Surface disruption is based on fatigue and crack initiation of the areas near the surface, brought about by tribological alternating loads in the surface layer zone of both contact partners, leading to material separation [CZIC03]. It is a wear mechanism brought about by the cyclical rollover and tangential and normal multiple loads on the same surface areas.

Surface disruption has certain similarities with fatigue and the fracture of massive components. Accordingly, fatigue is determined by the load amplitude and number of cycles. We differentiate in general between short-term and long-term fatigue. In the short-term fatigue range, load amplitudes are on the level of tensile strength. In these cases, cracking and fractures can develop after a very short amount of time. On the contrary, long-term fatigue is characterized by long tool life and low load amplitudes and represents the technologically most desirable variant of fatigue. The process of long-term fatigue on surfaces can, as opposed to short-term fatigue, be subdivided into the following phases [SUH73]:

- generation of dislocations below the tribologically loaded surface (tool surface),
- accumulation of dislocations,
- formation of crystallographic defects and submicroscopic “voids”,
- merging of the voids into cracks parallel and perpendicular to the loaded surface and
- generation of wear particles when the cracks reach a certain critical length.

Surface cracks and platelet-shaped wear particles are the result (Fig. 2.71 top right). In order to obtain as many load cycles as possible without surface disruption (or high tool life quantities), the load amplitude must be kept as low as possible. In the case of surface fatigue, peak loads occur on the surface warping. Among these are, for example, roughness peaks or grinding grooves or burrs remaining from the tool manufacture. In analogy to the mechanism of adhesion via mechanical claspings, the result is the need for forming tools with surfaces of extremely low roughness. But even in the case of ideally smooth surfaces, buildup workpiece material transferred by the wear mechanism of adhesion to the tool surface can form imperfections that have a load-concentrating effect.

2.8.3.4 Tribochemical Wear

The tribological loading of both friction partners induces frictional energy into the surface areas of the contact partners. This generates chemical reactions between the base and counter bodies, intermediate material and the surrounding medium, in which surface layers of altered chemical composition form on the base and counter bodies, usually with significantly altered material properties (Fig. 2.71 bottom right). Brittle-hard reaction layers can only reduce tribologically induced stresses to a limited extent and are removed by brittle disruption when a critical thickness is reached, whereas softer reaction products are continuously regenerated and abrasively removed [FINK32, QUIN62]. Both kinds of removal of chemical reaction products from tool surfaces are designated as tribochemical wear. Loss of material from the tool surface is common to both of them.

Tribochemical reactions can generally be accelerated by different processes [HEID75, THIE67]:

- removal of reaction-inhibiting surface layers
- acceleration of the transport of the reaction participants
- enlargement of the reactive surface
- temperature increase as a result of frictional heat
- generation of surface atoms with free valencies as a result of lattice distortions resulting from plastic deformation processes.

In forming, all five of these processes take place simultaneously. In addition to the friction energy mentioned, dissipated forming energy and potentially process heat (such as is required for forging) also lead to further temperature increases on the tool surface. Chemical reactions between the tool and the surrounding or intermediate medium thus arise in all forming processes, even if they differ considerably with respect to their magnitude or technological effect. We will briefly list two examples to elucidate this:

- The surfaces of forging tools are exposed to high temperatures. As a result, increased oxidation (reaction of the base body and the surrounding medium) takes place compared to room temperature. As a result of thermal and mechanical activation, these occur especially on microcontact areas (roughness peaks). Disruptions of the resulting oxide islands result, resulting in turn in undesirable loss of material from the tool in the form of wear particles.
- In cold forming, lubricants are often provided with reaction layer-forming additives. The reaction layers are generated continuously and again removed and per definition contribute to tribochemical wear. This is intentional in this case however and is accepted in order to prevent adhesive wear via the surface-removing effect of reaction products (e.g. iron chloride in the case of chlorinated oils, Sect. 2.8.4.4), as adhesive wear has a much stronger effect.

2.8.4 Lubrication in Forming Technology

Lubrication is extremely important in forming technology. Very different materials are used to prevent tool wear and to work against the effects of friction. Due to the exceedingly high tribological loads, many forming processes are not even executable without special lubrication techniques.

In most applications, liquid lubricants based on minerals or synthetic oils or natural oils serve as the base lubricants. These base lubricants are also called base oils (Sect. 2.8.4.3). However, pasty, fatty and solid substances or foils are also employed, as these have an increased surface-separating effect or, in the case of solid lubricants, can withstand higher temperatures such as those that are found in forging (Sect. 2.8.4.5). In order to obtain a technologically effective lubricant, different additives must be mixed into the base oils, emulsions or greases (Sect. 2.8.4.4). In many cases, the lubricants can be applied to the workpieces directly. In the case of complicated processes, cold massive forming in particular, often it is necessary to apply a lubricant carrier layer, which then itself receives the lubricant (Sect. 2.8.4.2).

Work sheet 2 of the German Society for Tribology [GFT91] provides an overview of the lubricating media suitable for forming. This guideline also contains information regarding the type of application that is best suited for the respective lubricant.

The reason for the above mentioned diversity of lubricants used in forming technology has to do with the array of process-dependent tribological loads with respect to mechanical tool load and relative velocity between the tool and workpiece surfaces. From hydrodynamic states of lubrication, as sometimes found in the blank holder area of deep drawing tools, to extreme conditions of boundary friction in massive forming, the entire spectrum of lubrication states is thus covered by all individual forming process (Fig. 2.72).

2.8.4.1 Forming Lubricant Requirements

The most important tribological function of a lubricant consists in separating the surfaces of the tool and workpiece, thereby shifting the friction conditions from the boundary friction area in the direction of hydrodynamic friction (Fig. 2.72). Optimal friction conditions are the prerequisite for good workpiece surfaces as well as minimal forming forces and thus for a low mechanical load and low tool wear.

A further tribological function consists in the removal of heat from the lubrication gap. This function is of particular importance above all in forging processes. By spraying the forging die between every working stroke, it is guaranteed that the tool material does not overheat and prematurely fail due to softening and oxidative wear. But high temperatures are encountered in the case of “cold” forming as well. In the reverse cup extrusion of soft-annealed case-hardening steel 16MnCr5 for

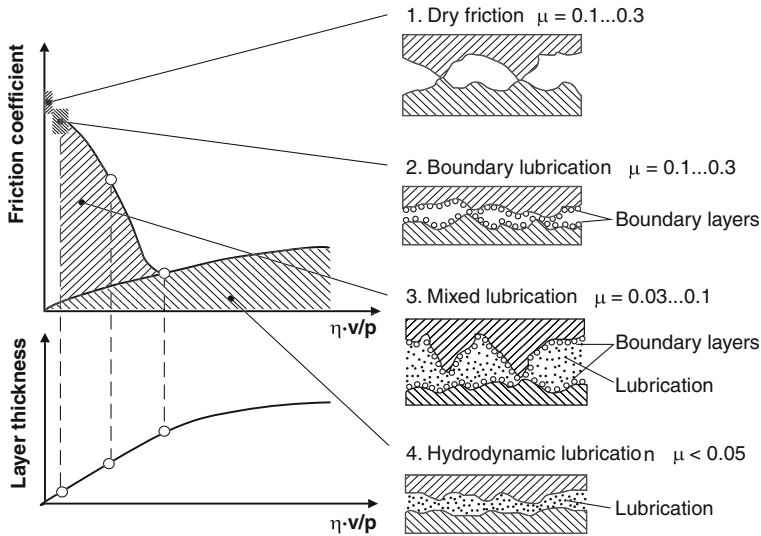


Fig. 2.72 Stribeck diagram for different states of lubrication, with η dynamic viscosity, v sliding speed, p pressure/surface pressure [CZIC03]

example, contact temperatures of more than 350 °C can arise, in the case of stainless steel even more than 500 °C [RAED02, STEE99]; similar temperatures are found in fine blanking.

Yet in addition to the tribological properties of lubricants (reduction of friction and wear as well as heat removal), lubricants must also perform many other tasks and meet a large number of requirements. Figure 2.73 gives an overview of the requirements of forming lubricants. Each requirement can be met in a different way, as will be shown in the following by means of describing individual lubricants and their functionality.

2.8.4.2 Release Agent and Lubricant Carrier Coatings

In cold forming operations, in which enhanced surface enlargement of the workpiece is to be expected, the material to be formed is equipped with a lubricant carrier layer (conversion coating) in chemical baths. Conversion coatings are crystalline, highly porous salt layers that originate via chemical conversion with the base material and are firmly fused to it. The task of these layers is to separate the metallic surfaces of the tool and workpiece even in the case of major surface enlargements and to serve as a tie coat or conversion partner for the lubricant to be applied.

Besides extrusion, conversion coatings are also utilized for wire, tube and profile drawing and sometimes in sheet metal processing, e.g. in the case of difficult wall ironing operations [MANG83]. While bulk solids are coated by

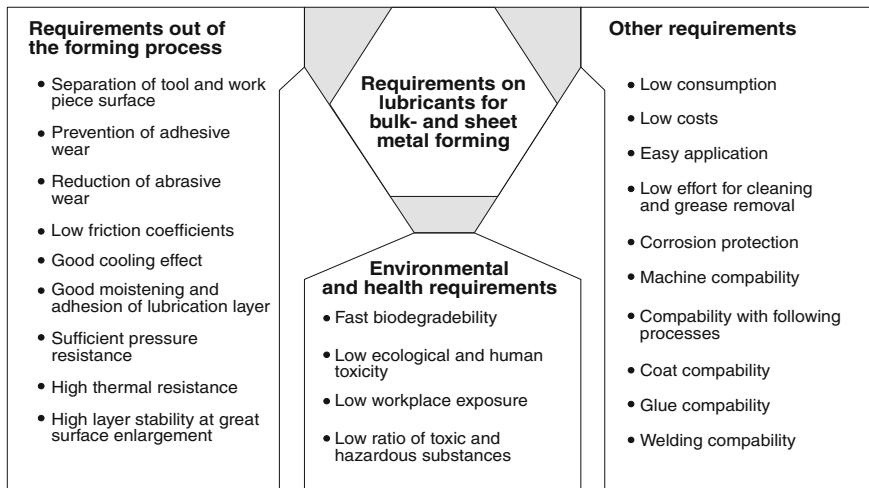


Fig. 2.73 Requirements for lubricants for massive and sheet metal forming

immersion in multi-chamber systems, tunnel machines tend to be used for wire and sheet metal.

Especially important are metal phosphate and metal oxalate coatings which are used for the extrusion of high-strength chrome and/or nickel steels [MANG83, LANG90a, NITT04a]. Zinc phosphating is the most common pretreatment method for steel extrusion parts. However, sometimes manganese phosphate or zinc manganese phosphates are also used. For the extrusion of high-strength aluminium materials, very often calcium aluminate coatings are also employed in addition to zinc phosphates [NITT04a]. Titanium alloys are equipped with titanium fluoride coatings.

Zinc phosphate coatings are stable to about 400 °C, while oxalate coatings already begin to disintegrate after 140 °C [MANG83]. For a short time however, both can withstand much higher thermal loads in forming processes.

As an example, let us briefly consider zinc phosphating. First of all, it is important that the blanks have a consistent, homogeneous surface quality, as present-day phosphating facilities are highly automated. In order to obtain this, the blanks often undergo a form of mechanical pretreatment such as peeling, sand-blasting or shot peening [BAY94].

To better fix the phosphate coating on the workpiece surface, first iron atoms are removed from the composite by means of a pickling process using sulphuric, phosphoric or hydrochloric acid. After rinsing, actual film-forming begins. The phosphating solution involved consists of a phosphoric acid solution of the primary zinc phosphate. First there is a pickling reaction of the workpiece surface with the free phosphoric acid. This alters the solution equilibrium at the workpiece/solution interface; the primary zinc phosphate in the solution breaks down into poorly soluble tertiary zinc phosphate and free phosphoric acid. The poorly

soluble tertiary zinc phosphate is deposited on the workpiece surface as a crystalline film, while the iron atoms released from the surface react with the solution to form Fe-III phosphate. The latter collects at the bottom of the phosphating bath and has to be disposed of as phosphate sludge.

General tips on phosphating metals, also regarding chipless shaping, can be found in DIN EN 12476 [EN01a]. More recent developments in conversion treatment have been focused on reducing the use of chemicals and lubricants, diminishing processing times and lowering process temperatures during the coating process in order to make the process more environmentally friendly and cost-efficient [KÖNI93a].

The form of the film structure depends on how long it spends in the phosphating bath. Figure 2.74 clarifies the effect of the phosphate film structure on the extrusion process.

While the characteristic of the phosphate film has indeed an influence on friction and thus press force, however it itself does not have any properties that reduce friction [MANG83]. Rather, it provides, depending on the porosity of its structure, an extremely large surface, which is an ideal tie coat for additional lubricants of various kinds. The better the layer fulfils its function as a lubricant carrier, the better the lubricants can perform.

Depending on the expected process temperature, suitable lubricants can include oils, different soaps and polymer dry films, or solid lubricants like molybdenum disulfide (MoS_2) or graphite [LANG90a, MANG83, NITT04b]. Extrusion oils with different high pressure additives are preferred for the manufacture of screws, bolts, nuts and small parts on automated multistage presses.

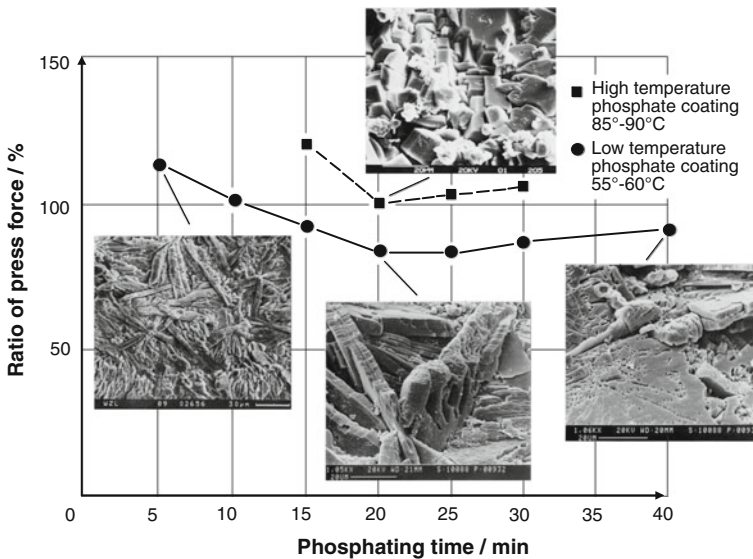


Fig. 2.74 Effect of the phosphate film structure on the press force in the extrusion of helical gears

Soap lubricants are of particular interest for most extrusion and drawing processes, as the fatty acid in the soap can react with the zinc phosphate film in hot, aqueous solution to form highly friction-reducing zinc soap (e.g. zinc stearate in the case of stearic acid). This reaction has two advantages:

- good bonding of the lubricant to the carrier layer and
- the resulting zinc soap has a higher melting point than alkali soaps (sodium soaps).

These soaps are functional until about 200 °C. An important disadvantage of these lubricants is that the soap film cannot endure greater surface enlargements of the workpiece and tears open. This results in the dreaded metallic contact between tool and workpiece, which the still existing phosphate layer can no longer prevent. In the case of more difficult forming processes and higher temperatures, solid lubricants such as molybdenum disulfide (MoS_2) and graphite thus tend to be utilized (Sect. 2.8.4.5).

In some cases, polymer dry films are used instead of MoS_2 , as they allow a further increase in performance compared to MoS_2 [NITT04b]. This is of interest for near-net-shape applications, which require optimal mould filling. Certain components can be produced with the use of polymer films even without zinc phosphating and soap. Cold massive forming without a zinc phosphate film is also significantly aided by the use of CVD and PVD coatings [RUPP97].

2.8.4.3 Oils, Greases and Emulsions

Liquid and fatty lubricants are those based on oil and water. Alone they generally have no sufficient wear/friction-reducing effects for forming applications. Oil and water serve as base substances for lubricants in forming technology and thus as carriers for additives or solid lubricants. In order to obtain a lubricant that is technologically attractive and meets all requirements, additives and/or solid lubricants must be added in emulsified, dissolved or dispersed form (Sects. 2.8.4.4 and 2.8.4.5).

Greases. Oils in their pure state are often called base oils. By adding soaps (e.g. sodium soap), solid greases (e.g. wool grease), solids (e.g. chalk), gelling agents (e.g. silica gel) or polyureas, thickened products can be produced that are called greases or pasty substances [MANG01]. Greases are frequently employed because of their rheological properties or for the stable introduction of solid materials that cannot precipitate in grease. The consistency and tribological properties of greases depend heavily on the base oil used, the thickening system and the additives and/or solid lubricants mixed in.

Emulsions. Both oils and greases are often used in the form of emulsions. In the case of emulsions, one liquid is dispersed in another. That is, one liquid is in droplet form (disperse or internal phase) and is surrounded by another liquid (continuous or external phase) [MANG01]. Depending on the type of dispersion, a

distinction is drawn between oil-in-water (OW, oil/grease as the disperse phase) and water-in-oil emulsions (WO, water as the disperse phase). The advantage of emulsions is the enhanced cooling effect resulting from their heat conductivity being five times higher than that of oil and the three times higher heat capacity of water. In the case of hot forming processes, there is also the more rapid vaporization of water, which also has a cooling effect. Moreover, when emulsions are used, the need for oil—which is significantly more expensive than water—is much smaller. However, the higher cost of maintenance and upkeep is a disadvantage, since emulsions are susceptible to contamination from bacteria and fungus as well as to frost. Essential for the quality of an emulsion is that the water used be of consistent quality, as water can fluctuate greatly with respect to pH, ion content and the microorganisms it contains. It is also true for emulsions that their performance depends greatly on the base oil used as well as its additive content.

Viscosity. Probably the most important characteristic value of oils and emulsions is viscosity. As a rule, it is labelled as kinematic viscosity ν at 40 °C in mm²/s (SI-unit) or cSt (centistokes) and describes the fluidity of liquid substances [MANG01]. Forming technology covers a wide range of viscosity, from low-viscous, thin oils (e.g. residue-free vapourizing punching and drawing oils, $\nu \approx 3$ mm²/s) up to extremely viscous, hardly flowable oils (e.g. oils for mandrel lubrication in pipe manufacture, $\nu \approx 1,000$ mm²/s) [MANG83].

Viscosity changes as a function of temperature and applied pressure [MANG01]. Viscosity-temperature behaviour (VT behaviour) is described by the viscosity index (VI). The higher the VI given for a certain lubricant is, the less its viscosity drops with increasing temperature. Viscosity-pressure behaviour (VP behaviour) on the contrary is characterized by a viscosity-pressure coefficient α [GOLD01]. A high α value stands for a high increase in viscosity with increasing pressure.

Since viscosity is also a measure for the carrying capacity of a lubricant film, a reduction of viscosity under increased temperature has a negative effect in most forming processes, while the tendency to increase viscosity with increasing pressure is a positive one. Favourable lubricant behaviour is thus indicated by high values of VI and α .

Mineral Oils. Base oils are classified as mineral oils, synthetic oils and natural oils [HUBM94, MANG83, MANG01, SEID04]. Mineral oils are, as before, still the most important group with the greatest market strength.

Depending on the properties desired, different components of mineral oil are used, called raffinates. Paraffinic or naphthenic mineral oil raffinates are used, aromatic oils on the other hand to only a very limited extent. Aromatic mineral oils do have properties that are attractive for forming, as they have a very good VP behaviour and the high solubility for additives, but they frequently contain carcinogenic compounds. While paraffin oils, quantitatively the most important group, have the best VT behaviour and lowest dissolving power for additives, aromates are the exact opposite. Napthenes represent the compromise between VT behaviour and dissolving power. Table 2.16 provides an overview.

Table 2.16 Evaluation of the properties of different mineral oils with respect to forming processes [HUBM94, MANG83]

	VT behaviour	VP behaviour	Wettability	Dissolving of additives	Dispersing power	Evaporation
Paraffin	+	—	—	—	—	+
Naphthene	○	○	○	○	○	○
Aromates	—	+	+	+	+	—

Synthetic Oils. The most important synthetic oils are polyolefins, alkyl benzenes, polyglycols and carboxylic acid esters [HUBM94, MANG83, MANG01]:

- Polyolefins have properties similar to paraffinic mineral oils. Especially common are polyalphaolefins, which depolymerize at high pressures or temperatures. That means that their viscosity may sink with use, but they are ideally suited for forming parts that have not been degraded prior to thermal postprocessing.
- Alkyl benzenes as a whole are very similar to aromatic mineral oils and thus provide similarly good dissolving power for additives. Their absolute lack of sulphur makes the use of these materials especially attractive.
- Polyglycols are water soluble in most cases, often oil soluble simultaneously. Compared to emulsions, they thus make more stable oil-water mixtures available. These materials are of interest for solid lubricant dispersions for hot and warm forming because of the possibility of using aqueous oil-based dispersions. Compared to water-based dispersions, they thus provide an enhanced lubricative effect, and compared to oil-based dispersions, a greater cooling effect.
- Synthetic carboxylic acid esters are fabricated by esterifying natural fatty acids (obtained from natural fats, e.g. rapeseed oil) or synthetic carboxylic acids (oxidation of mineral oils). Their greatest advantage is their polar character, leading to a very adhesive lubricant film and a very good lubricative effect in the mixed friction range.

Natural Oils. In the last several years, natural oils have become increasingly important due to their improved biodegradability compared with mineral oils [AHLR04, GERB03, KLOC04c]. Although they have many favourable properties, they have not become dominant because of their high prices and variable quality. The saturated and unsaturated fatty acids (e.g. oleic acid) contained in natural oils and different ester compounds (e.g. triglyceride) exhibit polar groups that become deposited on surfaces via adsorption, thus greatly aiding lubricant film adhesion and stability. In their pure form, they thus lead to significantly lower friction coefficients than pure mineral oils (Fig. 2.75). They are also frequently superior to mineral oils containing additives [KLOC04e]. Native fatty acids and ester compounds are therefore often used as additives (polar additives) in lubricants based on mineral oils. Furthermore, they are distinguished by a better VT behaviour than mineral oils and a much lower degree of vaporization. Since most forming

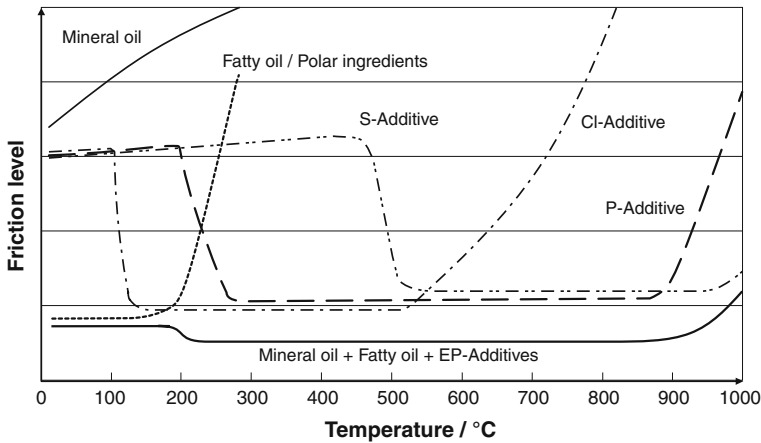


Fig. 2.75 Qualitative profile of the friction coefficients for different base oils and additives over temperature [HORL89, MANG83, SCHU04a]

processes work without circular lubrication but rather with loss lubrication, their low ageing stability is of a little importance in forming technology.

2.8.4.4 Additives

Forming lubricants, including oils, greases and emulsions, are generally provided with additives. A distinction is drawn between stabilizing additives such as oxidation, hydrolysis and foam inhibitors, emulsifiers and surface-active additives [BART94, MANG83, MANG01]. Among the latter are included anti-corrosion additives as well as friction and wear reducing materials. Surface-active friction/wear-reducing materials have the greatest effect on the respective forming process [ULLM04]. What they all have in common is that they reduce the friction coefficient to a greater or lesser degree and protect the surface from wear. The biggest difference is in their mechanisms of action (physisorption, chemisorption and chemical reaction), of which one or more are active simultaneously. Depending on the type of tribological conditions dominant in the lubrication gap, each additive varies in terms of how well it can be used or combined with lubricants. Figure 2.75 shows the friction-reducing potential of different liquid lubricants and additives over temperature.

It is difficult to subdivide additives into different classes, and this is undertaken in various ways in the literature. In the following, we will differentiate between polar agents and EP additives.

Polar Agents. The most important polar agents are natural fats (ester compounds like triglycerides), fatty acids, synthetic carboxylic acids and carboxylic acid esters, fatty alcohols, fatty acid amides and amines and metallic soaps [ULLM04]. They deposit themselves to a great extent on metallic surfaces via

physisorption, creating van-der-Waals bondings between the polar molecular end and the metal surface. In this way, they influence the wetting behaviour of the lubricants and, already at room temperature, form friction-reducing and slightly wear-protective films of the thickness of one molecular length. At temperatures above 100 °C, the polar bonds begin to be released, eliminating the friction-reducing effect (Fig. 2.75). Moreover, fatty acids are capable of reacting with the surfaces of metallic materials. This results in metallic soaps that also have a friction-reducing effect and are stable to about 200 °C.

Extreme Pressure (EP) Additives. The EP additive group is needed for difficult forming processes when the use of additives with polar materials is no longer sufficient. The metallic surfaces newly created during forming react with the EP additives during the process to form shear-soft reaction layers that prevent undesirable metallic contact between the tool and workpiece. Under mechanical load, these films are easily sheared off and thus have a friction-reducing effect (Fig. 2.75). The reaction layers are thus constantly built up and rubbed off again, consuming the EP agents.

The class of EP additives is dominated by three especially common material classes [HORL89, KORF94, MANG83, MANG01, SCHU04a, ULLM04]:

- **Sulphur-containing additives:** The most effective and commonly used reaction layers are sulphidic. The reaction of metallic surfaces with sulphur contained in oil takes place at high temperatures (generally above 500 °C) and leads to very stable and temperature-resistant separating layers. The effectiveness of sulphur carriers is based on the fact that they become deposited on the metal surface through physical adsorption and separate sulphur via chemisorption, which then reacts with the metal to form a sulphide. Sulphurized oils are produced by the addition of pure sulphur powder (also called flower of sulphur, which also has the properties of solid lubricants), sulphurized fats (e.g. sulphurized fatty acid esters) or by sulphurized hydrocarbons (e.g. alkyl polysulfides) and contain between 10 and 50 % sulphur. The particular additives used differ with respect to polarity (physisorption capability), which increases from hydrocarbon to fat, sulphur activity (chemisorption capability) and sulphur content, which is reduced from hydrocarbon to fat. In order to cover a wide range of applications therefore, often different sulphur carriers are used in combination.
- **Phosphoric additives:** Phosphoric additives partially cause a phosphatizing of the surfaces of both tool and workpiece. By means of its synergy with sulphur carriers, they are being used nowadays increasingly in combination as a substitute for chlorinated paraffins [WÜNS02]. The most important phosphorous additives are phosphoric acid esters. In the phosphate part of the molecule, oxygen can be replaced by sulphur, resulting in thiophosphates, of which previously zinc dialkyldithiophosphates were preferably used. They are utilized in almost all lubricant areas and are being increasingly substituted by zinc-free compounds. In the case of these materials, there is not only phosphatizing but also the release of reactive sulphur, so that sulphidic separating layers are also obtained. The stability of the phosphate films created is very limited in the high

pressure range, which is why phosphorous carriers are often not labelled as EP additives but rather merely as AW (anti-wear) additives. Besides their wear-protective effect, they often function as oxidation and corrosion inhibitors.

- **Chloric additives:** The most important group of chlorine-containing additives are the oily, usually highly viscous chlorinated paraffins with chlorine contents between 35 and 70 %. Their effect is based on a similar mechanism as is seen with the sulphur additives (physisorption—chemisorption—reaction). They have a friction-reducing and wear-protective effect from their mere presence alone, being very polar compounds. When the activation temperature ($>100\text{ }^{\circ}\text{C}$) is reached, an iron chloride layer is formed consisting of iron(II) and iron(III) chloride, which is stable up to a maximum temperature of $670\text{ }^{\circ}\text{C}$ (melting point of iron(II) chloride). Different information is provided in the literature regarding their exact workings and thermal limits of use. A good description can be found in [SCHU04a]. Chlorinated paraffins bring about extremely low friction coefficients. The latter is of interest especially for processing high-alloyed Cr-Ni steels, since in this case polar additives can only bring about a small reduction of friction. Despite their excellent tribological effect and relatively low price, their use is rapidly declining at present. The reason for this is the ban on short-chained chlorinated paraffins (10–13 C atoms) in Europe since December 31st, 1999 because they were found to be toxic, carcinogenic and difficult to degrade [AHLR04, NN95]. Medium and long-chained chlorinated paraffins may indeed still be used, but are suspected to break down into short-chained chlorinated paraffins during use. Their disposal is expensive, since dioxin is formed when they are burned. Moreover, the hydrochloric acids freed during consumption often cause corrosion problems for the parts produced along with associated high cleaning requirements. Nonetheless, they are still used for some forming processes, e.g. in the case of difficult deep drawing operations of austenitic, stainless steels or in certain fine blanking processes [KLOC03c, KLOC04d]. Substitute products are often less effective, much more expensive or frequently entail a rearrangement of downstream cleaning stages.

Passive Extreme Pressure Additives (PEP). This class of additives is characterized by very good high-pressure properties without a chemical reaction with the metal surface taking place, such as is the case with sulphur-containing or chloric additives. They are called passive extreme pressure additives (PEP) for this reason. Typical representatives of this class are overbased sulphonates. These compounds contain, besides conventional petroleum sulphonate (calcium, sodium), the corresponding carbonate in very fine distribution, so that the entire mixture appears as an amorphous liquid. The carbonates function as a solid lubricant and bring about at least a partial physical separation of the tool and the workpiece. In this way, the pressure absorption of the oils is heavily increased. At the same time, overbased sulphonates provide good corrosion protection and act as acid scavengers.

2.8.4.5 Solid Lubricants

It is impossible to find a generally binding definition for dry or solid lubricants, terms which the literature often uses synonymously. Fundamentally, a classification can however be made into structurally effective, mechanically effective and chemically effective solid lubricants. Furthermore, it is possible to subdivide the solid lubricants used in the metalworking industry according to their chemical character into organic and inorganic solid lubricants. In the following, we will look at the solid lubricants that are common in forming technology along with their properties [HORT01, KORF94, LANG90a, MANG83, SEID04, ZIBU04]:

Solid Lubricant Powder. Among the most important of all solid lubricants are the structurally effective inorganic lubricants. The most significant representatives of this group are graphite, molybdenum disulfide (MoS_2) and hexagonal boron nitride (hBN, not to be confused with the cutting material cBN). These are used both in cold massive forming as substitutes for soap at higher temperatures as well as in forging in suspensions with water or oil. Moreover, they are also used in greases. Their structure consists of superimposed multilayered platelets that can withstand high pressures and large true strains. The layers in the platelets shift against each other, but this does not tear open the lubricant film. MoS_2 can be used up to about 400 °C, graphite up to about 700 °C and hBN up to about 1,000 °C. At higher temperatures, oxidation sets in.

In cold forming, the good lubrication properties of graphite and MoS_2 are bought at a high price, which is about 15 times more than that of soaps and thus places economic limits on a broader use. Solid lubricants can be applied on previously phosphated workpieces by tumbling, dipping in suspension and by a combination of phosphating/oxalating and coating.

Forging processes work primarily with graphite. The advantages of hBN come to play at temperatures above 600 °C, where hBN has a lower friction coefficient than graphite. The disadvantage of hBN is its high cost.

Titanium iodide (TiI_2) and chrome chloride (CrCl_3) have properties similar to molybdenum disulfide.

Plastic Foils. Plastics are used in various forms as foils and strippable paints and as additives in liquid and pasty lubricants. Their use is limited predominantly to the manufacture of decorative sheet metal forming parts made of stainless noble steel, aluminium, copper and bronze materials, where they significantly improve the friction conditions and protect from undesirable grooves. Foils are applied or glued to the sheet metal, while strippable paints are applied in liquid form and then dried. PVC, PE and PP are examples of suitable materials. Thickness ranges between 10 and 50 μm . Both paints and foils are employed only in combination with other lubricants, since they generally tear during the forming process, though they can withstand an elongation of up to 300 %.

Dry Lubricants. “Dry lubricants” are also being increasingly used. A distinction is drawn between “dry lubes” and “hot melts”. The former are quickly volatilizing suspensions that are applied at room temperature and leave behind a solid film after drying that often contains combinations of diverse polymers and

waxes as well as PTFE (Teflon). The waxy hot melts on the other hand are applied in a heated form (60–80 °C), often already just after cold rolling as a corrosion inhibitor. In many application examples, their properties are the same as or better than those of oils with high amounts of additives, making them a more environmentally friendly alternative in sheet metal forming or in the extrusion of aluminium.

Prepainted Sheets. In more recent developments in sheet metal forming, pre-painted sheet metals are being used to an increasing extent because of the savings potential in painting as well as because of the enhanced corrosion protection. The paint layers often have a positive influence on friction conditions during forming and thus can be included among the dry lubricants.

Salts and Glasses. When forging, especially in the case of some bar extrusion processes and when forging special materials like nickel-titanium alloys, salts or glassy materials can lead to tribological improvements. Their effect is based on the formation of a highly viscous lubricant film above the melting temperature of these materials. They are often sprayed on as a suspension in organic carriers and water. Salts are provided in aqueous solution as well.

Soaps. Some authors also include soaps, such as the often-used, water-soluble and reactive sodium stearate, along with the solid lubricants, since they have a solid character at room temperature. However, sodium stearate is applied in most cases in aqueous solution, e.g. as a soaping on phosphated press blanks. In the extrusion of non-ferrous metals, especially pure aluminium and aluminium alloys, metallic soaps like zinc stearate or zinc behenate or cadmium stearate are used in powder form. They are applied on the blanks by “tumbling”, i.e. the blanks are put in large revolving drums along with the soap powder, resulting in a solid lubricant film on the blanks. Metallic soaps are also required in order to thicken greases based on mineral oil or synthetic oils (colloidal dispersion of metallic soap and hydrocarbon oil) or serve as polar additives in liquid lubricants.

Soft Metals. Finally, the literature also includes soft metals such as Pb, Sn, In, Ag and Au among the solid lubricants. They are used as highly adhesive metallic coatings (e.g. tin for drawing steel bushes) when other kinds of lubrication are uneconomical. The resulting frictional shear stress depends directly on the shear strength of the soft metal and on the strain hardening of the soft metal to be expected in the process temperature.

2.8.5 Tool Influences

In addition to the lubricant used, the tool material also has a decisive influence on the forming tribological system. The tool material and especially the characteristics of its edge zone and surface determine the resistance of the tool to wear and affect the friction conditions in the lubrication gap.

2.8.5.1 Influence of the Tool Material

Section 2.7.2 described the tool materials that can be used in forming technology as well as their properties and areas of application. In order to keep the assault of wear at bay as much as possible, it is important that one also bears the tribological material properties in mind when selecting material. Depending on the primary mechanism of wear, corresponding material properties can be exploited for wear reduction [ESCH04, FINZ03, FÜLL04, GEIL04, SCHR04]:

- **Abrasion**—The hardness of a material is a measure of its resistance against abrasive wear (Sect. 2.8.3.1). From the standpoint of abrasive wear protection therefore, the active elements of forming tools subjected to friction should be as hard as possible. The hardness of tool materials increases in the following order: plastics—cast—quenched and tempered steel—cemented carbide—ceramics. Besides the selection of material, heat treatment is also important in this context, as it determines the ultimate hardness of the tool. In the case of forging dies, a high required red hardness is also important. For tool steels, hardness is determined primarily by the carbide-forming alloying elements (Cr, W, Mo, V) and the carbon content. Tungsten, molybdenum and especially cobalt result additionally in an increase in red hardness.
- **Adhesion**—The assault of adhesive wear and the formation of interfacial bonds is among other things affected by the electron configuration of the friction partner materials respectively their alloying elements (Sect. 2.8.3.2). We also refer in this context to the mutual solubility of the friction partners. In connection with the development of adhesion therefore, this indicates the potential of two materials to form common interfacial bonds. The more different the material character of the tool and workpiece materials is, the lower the probability of adhesive wear. For example, especially strong adhesive wear by austenitic, stainless noble steels cannot be prevented by using tool steels with high chrome or nickel contents. Cemented carbide and especially ceramic tools on the contrary reduce adhesion; yet they are only usable under special conditions because of their susceptibility to cracking [FÜLL04].
- **Surface disruption**—Prerequisites for high resistance to surface disruption are both good toughness properties and high mechanical and thermal (especially for forging dies) fatigue strength of the tool material. These properties can suppress cracking (Sect. 2.8.3.3). Toughness is enhanced by means of alloying elements such as cobalt or nickel. Furthermore, the danger of cracking can be diminished by minimizing inclusions and defects in the tool steel and by means of a surface that is as smooth and groove-free as possible. In addition, crack propagation can be hindered with a fine-grained microstructure. Powder-metallurgically manufactured steels are especially important in this context.
- **Tribochemical wear**—Tribochemical reactions arise due to the reaction of the tool material with the lubricant and/or the oxygen in the surrounding air. Wear originates when the reaction products are rubbed off of the tool surface (Sect. 2.8.3.4). Thus, the tool material must be as oxidation-resistant and as inert as

possible. Furthermore, high heat conductivity leads to a more rapid removal of heat, reducing surface temperatures. This generally decelerates chemical reactions. A certain amount of tribochemical wear is unavoidable however; indeed, it is even desirable if reactive EP additives are being used. Most wear-protective additives are designed for the surfaces of metals. When changing from uncoated to coated tool steels respectively to cemented carbide or ceramic tools, we must therefore check whether the additives are still effective. In the case of cemented carbides, one must also guarantee that the lubricant does not bring about any cobalt erosion. Even ceramic materials are subject to a certain amount of chemical attack. Si_3N_4 ceramics, for example, can react with water to form SiO_2 and NH_3 , resulting in extremely thin friction-affecting films [KAJD98].

For coated tools, it is essential that the tool material (in this case also called substrate material) has a sufficient supporting effect, i.e. strength, and that it is not subject to plastic deformation. Therefore, a high compression yielding point is required [ESCH04, EVER04]. In principle, it is indispensable for a consistent, faultless layer structure that one ensures flawlessly machined substrate surfaces with a poreless surface structure. Roughness values of $R_z < 1 \mu\text{m}$ are to be recommended, while visible grinding grooves and burrs are to be avoided.

In addition, one must ensure that tool manufacture affects the edge zones as little as possible. White layers from eroding or grinding processes are not permissible. This is especially true for surfaces to be coated. In hard machining, any reduction of hardness under the influence of heat is also impermissible.

2.8.5.2 Modification of the Tool Rim Zone

With the help of surface technology, we can affect the tribological properties of forming tools in a specific way by changing the composition of the tool rim zone or by coating the tool. Manipulation of the rim zone involves the targeted treatment of the upper edge layer of a workpiece in order to create certain properties. A distinction can be made in this context between pure heat treatment, thermochemical pretreatment or thermomechanical pretreatment. Careful heat treatment that is adapted to the respective tool steel is indispensable. Thermochemical pretreatment is an additional measure with which the wear resistance of forming tools can be increased and the effect of tool coatings can be influenced positively. This includes, among some other methods, case hardening, nitriding, borating, or chromizing [LANG90a, LUIG93]. What all variants of thermochemical surface treatment have in common is that the chemical composition of a material is intentionally altered by one or several elements diffusing into the material or out. Thermochemical surface treatment can be used to realize the following properties within the tool rim zone:

- increase in hardness,
- increase in high temperature strength,

- increase of the supportive effect against tool coatings,
- material modification to decrease adhesion.

The most common procedure, nitriding, involves a diffusion saturation of the edge layer of a workpiece with nitrogen in order to increase hardness, wear resistance, fatigue strength or corrosion resistance. The presence of elements that form special nitrides can, for example, bring about a higher edge hardness than can case hardening. However, the disadvantage is the steeper decrease in hardness towards the inner workpiece. After nitriding, the rim zone consists of an upper nitride layer (compound layer) and an underlying layer composed of nitrogen-enriched mixed crystals and precipitated nitrides (diffusion layer). Generally we distinguish between gas nitriding in an ammoniac gas flow at 500–550 °C, salt bath nitriding in cyan salt baths at about 520–580 °C and plasma nitriding at 450–550 °C. In the recent past, plasma nitriding, which is easy to combine with plasma-guided coating processes and requires shorter nitriding periods than gas nitriding, has become especially economical. This process is used in order to realize continuous distributions of hardness between the base material and the hard material coatings applied on it. Here, the nitride layer assumes the function of a supportive layer, while the hard material layer applied upon it takes over the actual function of wear protection. The disadvantage of gas nitriding is the long period of time required for nitriding, which can be shortened by glow discharging (plasma nitriding), which ionizes the nitrogen.

Other methods include carburetion, carbonitriding, borating and vanadizing. The advantages of these methods can partially be derived from the indications given in [Sect. 2.8.5](#) concerning the influence of alloying elements. For example, in [BARN04], a reduction of material transfer via borating is observed in the case of non-lubricated hammer forging, while nitriding leads to more material transfer than with an untreated tool. In lubricated experiments, nitrided, carbonitrided and borated upsetting paths diminish wear (material loss) compared to untreated paths in a similar way. [HUSK02] proposes a duplex treatment (plasma nitriding followed by PVD coating) as an effective measure for increasing both wear resistance and the fatigue strength of cold extrusion tools.

2.8.5.3 Tool Coatings

Since tool wear largely depends on the properties of the tool surface, it is obvious that the properties of the surface should be intentionally influenced. Modern thin-film technology gives us the possibility of improving the surfaces of forming tools with CVD and PVD processes by applying supporting layers in a targeted way [ESCH04, EVER04, VDI92]. The high hardness of the hard material layers thereby obtainable provides increased resistance against abrasive wear, while their non-metallic material properties lead to a reduced tendency to adhesion.

However, the use of tool coatings also has a drastic effect on the forming process as a tribological system, since the, as a rule, metallic surface of the tool is

replaced by a non-metallic and much harder one. This means a huge change in the physical and chemical processes involved in tribological contact, i.e. during the forming process, affecting the mechanisms of friction and wear. While wear is heavily limited by coatings as a rule, only a few coating systems are capable of reducing friction.

Coating Methods. The most important methods of coating are CVD (chemical vapour deposition) and PVD (physical vapour deposition) as well as their variants. With them, extremely different wear-protective and sometimes friction-reducing hard material coatings of a few μm thickness can be created. Volume 1 of this series contains a detailed description of these methods [KÖNI02]. Besides them, there are still other methods such as galvanic or galvanicochemical coating (e.g. hard chrome coatings) as well as plasma spraying. Large tools are often weld-clad or laser-treated (e.g. laser-beam cladding, surface alloying). These procedures are also used in the repair of large tools.

Layer Properties. The properties of a coating are characterized by defined values. An overview and exact indications on the execution of the most important test methods are provided in the various sections of DIN 1071 as well as in VDI guidelines 3198 and 3824 [DIN94, DIN03a, DIN03b, DIN04a, ISO04a, VDI92, VDI01] (Table 2.17).

Further characteristics include residual stresses, the exact chemical composition across the thickness of the layer, heat properties and surface energy. Beyond these, the tribological properties of coatings can be tested in many different experimental tests (Sect. 2.8.7). The importance of these coating properties for its function will be described in the following.

The coating thickness is generally between 1 and 5 μm . In the case of CrN, coating thicknesses of up to 10 μm are possible. Thicker coatings often have excessive residual stresses and tend to crack under elastic elongation, flaking off as a result. We refer to the so-called “egg-shell effect” or adhesive coating failure when the layer completely detaches from the substrate, and to cohesive coating failure when only some areas of the layer flake off without exposing the substrate. The inclusion of “relaxation layers” can decrease residual stresses, making it possible to generate larger coating thicknesses (up to about 15 μm).

In order to keep coating wear low, high hardness (protection from abrasive wear) and as possible a low Young’s modulus (high ductility, protection from

Table 2.17 Important values for characterizing hard material coatings and associated test methods

Quantity unit	Coating thickness μm	Hardness HV 0.05	Young’s modulus MPa	Adhesion class or critical load L_c in N
Range	1–5	1,700–4,200	2,000–5,000	1–4 respectively 10–90
Typical test methods	Light microscopic measurement at calotte cut	Microhardness or universal hardness	Universal hardness	Rockwell C test or scratch test

cracking) are required [RAED02, RENT97]. This contradictory ratio of Young's modulus and hardness can be obtained by means of multilayer technology (see below). The adhesion of a layer is determined qualitatively in indenter or scratch tests and is not directly transferable to forming process behaviour. Basically however, a high adhesion class is required, especially in the case of high local tool loads. Buildups can be influenced by the selection of the coating material (Sects. 2.8.3.2 and 2.8.5.1).

Furthermore, hard metal coatings possess other properties that affect their performance, but which usually cannot be determined by a standard characterization. Roughness is indeed sometimes indicated, but it depends primarily on the roughness of the substrate and thus does not characterize the coating but the coating-substrate composite. Nonetheless, it should be as low as possible in order to prevent local overloads at the roughness peaks. Tools to be coated should thus not exceed a surface roughness of 1 μm . Profile methods are used to determine roughness. Porosity, which should be kept as low as possible for reasons of high-load behaviour and protection against tool corrosion, is also rarely indicated.

Heat properties are important when high process temperatures are to be expected (e.g. forging, cold massive forming or fine blanking with a high number of strokes). As a rule, low temperatures are desirable in order to minimize thermal alternating load on the layer and thermal load on the lubricant. This can be obtained with high values of heat conductivity, thermal capacity and layer density [RAED02].

Often, good wettability of the tool surface by the respective lubricant is also required. Wettability can be evaluated in "contact angle measurements". In these, droplets of reference liquids are added to the coating in order to cite the angle between the droplet surface and the coating surface as a measure for wettability. With this method, the polar and disperse surface energies of solids and liquids can also be determined, which is indicated in mN/m [BOBZ00].

The properties of tool coatings are essentially a function of the following influences:

- coating method,
- layer material,
- layer construction and internal structure,
- substrate material and pretreatment.

Coating Materials and Internal Structure. Figure 2.76 lists the layer materials that can be used for PVD and CVD coatings. We distinguish between oxide, nitride, carbide and boride coatings. Detailed descriptions of different layer materials can be found in VDI guideline 3824-1 [VDI02]. Carbon layers have distinctive properties, differing fundamentally in their behaviour from the others. They are treated separately in VDI guideline 3840 [VDI04]. Most common are nitride and carbide layers as well as those based on C_xN_y . Inside monolayers, they form columnar crystallites, the structure of which depends on the parameters of the coating process and on the substrate and its pretreatment (Fig. 2.76 bottom left)

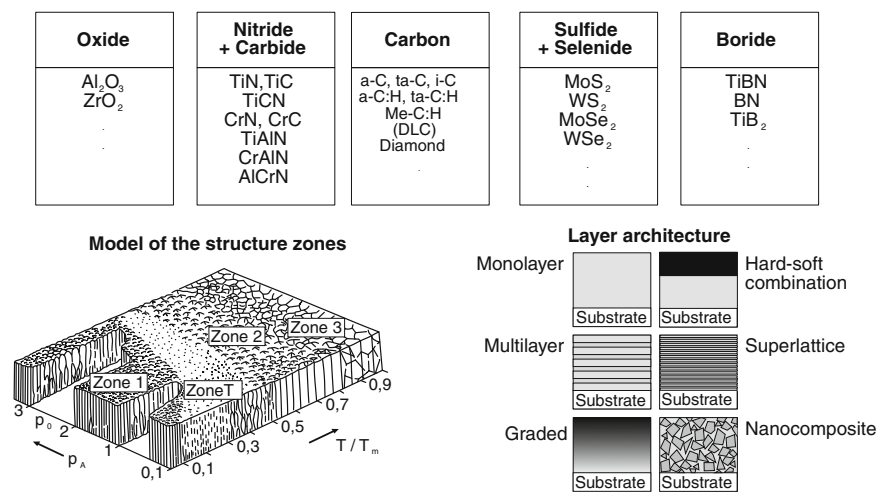


Fig. 2.76 Materials, structure and architecture of CVD and PVD coatings

[HAEF87]. The characteristics of the crystallites influence the mechanical properties of the layer, porosity, microtopography and wetting behaviour.

Nitride and carbide layers are often implemented as multilayer coatings or in recent times as nanolayer (or superlattice) coatings to increase ductility (Fig. 2.76 bottom right). In the latter case, the thickness of a single layer is only 5–20 nm, while the thickness of the entire coating is a few μm [BOBZ04]. So-called nanocomposite layers represent another variant with improved mechanical properties compared to monolayers. Their structure resembles those of cemented carbides, i.e. a hard phase is embedded in a somewhat softer matrix, also a hard phase. The hard-soft combinations and graduated layers consist on the surface of friction-reducing materials generally containing high amounts of carbon.

Carbon layers have a unique role within coating technology. Amorphous diamond-like carbons (DLC) are extremely wear-resistant and highly low-friction coatings deposited with CVD or PVD methods. The properties of these layers can be varied within broad limits depending on the manufacturing process, deposition conditions and composition. Depending on the amount of the predominant bond-type (sp^2 - or sp^3 - hybridization), the hydrogen content and the content of metallic and non-metallic doping elements, we obtain properties ranging between graphite-like and diamond. The exact designation of all variants along with an overview of their properties is specified in VDI guideline 2840 [VDI04].

Application Areas of Tool Coatings. Particular coatings are more or less appropriate for various forming processes. Figure 2.77 shows a rough classification. The extremely attractive low-friction, adhesion-reducing carbon coatings are especially suited for forming processes in which the tool surfaces are subject to only moderate mechanical loads. Hitherto they have mostly been employed in sheet metal forming processes (e.g. deep drawing or hydroforming) and in

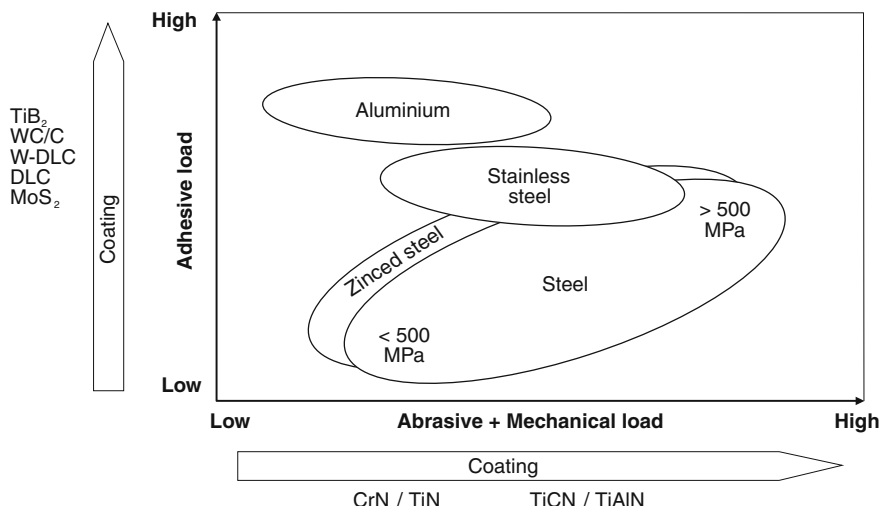


Fig. 2.77 Application areas for tool coatings in forming technology

aluminium processing [HORT01, KLOC04d, WEBE04]. For example, the use of amorphous carbon coatings led to significant tool life increases in the manufacture of caps for aluminium beverage cans. For the workpiece material aluminium in particular, boride layers (TiB and TiBN) are also of interest [HORT01]. If extremely low loads are to be expected and minimal friction coefficients are required, MoS₂ coatings as monolayers or as the top layer in multilayer coatings are an interesting alternative.

The adhesive strength of friction-reducing layers is often insufficient in the case of larger tool loads. In the areas of highest tool loads, multilayer coatings fit for heavy loads like TiCN, TiAlN, CrAlN and recently AlCrN (increased aluminium content compared to CrAlN) are used [EVER04, RAED02, RENT97]. These may not necessarily reduce friction, but they lead to significantly higher tool life quantities. The layers most suited to heavy loads are deposited nowadays using CVD methods on the basis of TiCN systems. The CVD coating here has the advantage of having greater adhesive strength.

In die forging tests, wear was reduced with a multilayer coating of type TiN-TiCN-TiC by a factor of three compared to plasma-nitrided dies and by a factor of two compared to TiN-coated dies [BARN04, DOEG01]. Similar CVD multilayer coatings are to be recommended for shearing electrical sheets and offer the possibility in cold massive forming of working without a zinc phosphate layer [RUPP97, TOUS00].

Yet in the case of moderate abrasive and adhesive loads, TiN is still a standard coating with high industrial acceptance. CrN is also used in the case of moderate loads when adhesive load is significantly more predominant or when increased temperature resistance is required [RUPP97]. TiAlN however—fit for heavy loads

and usually implemented as a multilayer or nanolayer coating—has the highest thermal stability (up to 800 °C).

For all coatings, one must bear in mind that the properties of coatings with the same name but made by different manufacturers can deviate considerably due to the variables mentioned above. Furthermore, when changing from uncoated to coated tools, one must check whether the lubricant used is suitable for the respective coating. As a rule, coating tools allows for a reduction of lubricant additives and/or lubricant amounts.

2.8.6 Effects of Topography

Even if the friction conditions in forming technology generally are in the range of mixed and boundary friction, in many cases of mixed friction local hydrostatic and/or hydrodynamic effects are nonetheless active that can sometimes have a positive influence on friction and wear (Fig. 2.72). Such effects arise when depressions are formed on the tool or workpiece surface in which lubricant is enclosed. These are called closed lubricant pockets, whereby a distinction is made between macroscopic pockets (e.g. in the case of sheet concavities in the flange area when deep drawing) and microscopic pockets (roughness/microtopography). Open pockets on the other hand can be so defined, that the lubricant contained in them can escape to neighbouring pockets or on the transition between the tool contact surface and free workpiece surface.

The lubricant enclosed in the pockets is compressed and exposed to high pressures due to the high contact normal stress in the lubrication gap, resulting in the formation of a hydrostatic cushion. This is especially the case when the affected pockets are on the surface of the workpiece [NEUD04]. During the forming process, workpiece surfaces are smoothened, reducing the volume of the pockets and heavily increasing the pressure in the lubricant. In the case of relative motion, hydrodynamic effects also become active on the flanks of the pockets. The most important influencing variables are as follows:

- size and geometry of the lubricant pockets and pockets flanks
- distribution of the lubricant pockets on the surface (stochastic or deterministic)
- ratio of closed to open lubricant pockets (especially in the case of miniature components in microforming [TIES02])
- viscosity and compressibility of the lubricant
- the stress collective, especially contact normal stress and relative velocity.

To calculate the effects of topography on friction, it is important that one uses meaningful three-dimensional surface parameters that permit a more extensive description of topography than simple roughness characteristics. Numerous new parameters and metrological methods have been developed for this in the last several years [PFES97, WAGN96].

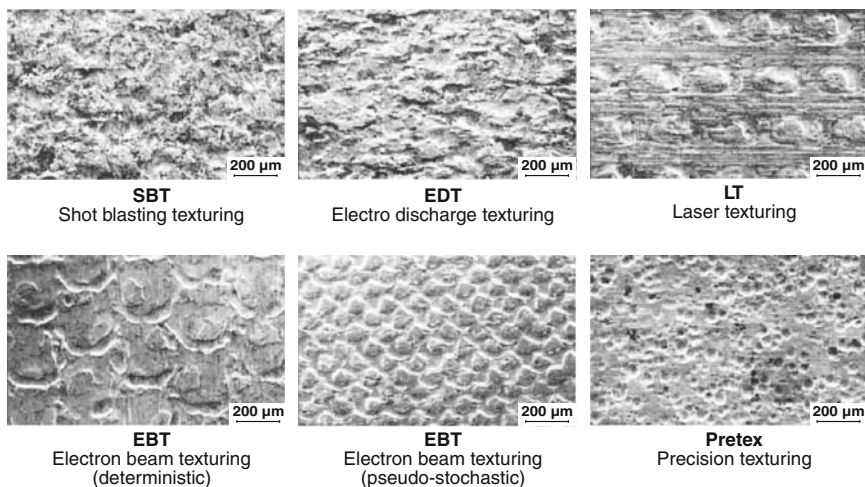
The following will explain the most important examples for the intentional integration and exploitation of surface microtopographies.

2.8.6.1 Surface Microtopography of Sheet Metal Materials

In sheet metal forming procedures, especially deep drawing, mixed friction conditions are frequently predominant, in which case lubricant pockets can be formed on the sheet metal surface. Here, the rather long-wave microtopography of the initial sheet metal plays a decisive role, while the far more short-wave topography of zinc coatings has a much smaller effect [BÜLT96].

The microtopography of the base sheet metal material is determined in the manufacturing process. After cold rolling and annealing, the sheet is lightly post-formed with so-called skin pass rolls (degree of skin-pass 0.5–1 %), so that the surface of the skin pass roll can be transferred as a negative to the sheet metal surface [NEUD04, STAE98].

The various types of texturing differ therefore in the processing of the roll surface. The concept of texturing in this context should not be confused with the texture of the workpiece material. For some years now, a variety of different methods exist for the modification of roll surfaces. The most common fine sheet metal texturings that can thereby be created are listed below and have been tested for their tribological properties in many investigations (Fig. 2.78) [DINK97, STAE98, WAGN96]:



Source: LFT

Fig. 2.78 SEM images of textured thin sheets [NEUD04]

- **MF**—mill finish (no texturing): ground skin pass rolls; hardly any lubricant pocket effects (depending on the drawing direction); improvements via cross-grinding possible; implementation declining [NEUD04]
- **SBT**—shot blasting texturing: roughening the roll surface by bombardment with a blasting agent accelerated by a shot blasting wheel [PANK90]
- **EDT**—electro-discharge texturing: roughening the roll surface in a spark-erosive process; less roughness and higher number of peaks as in SBT [HEBE87]
- **LT**—laser texturing (since 1982 [CRAH82]): pointwise fusing of the roll by means of a pulsed CO₂ laser; deterministic formation of small craters [CRAH82]
- **EBT**—electron beam texturing: similar to LT; fusing takes place by means of an electron beam; consistent, deterministic formation of ring-shaped craters; superimposition of craters leads to pseudo-stochastic distribution [DOLV91]
- **PRETEX**—precision texturing: application of an electrolytically generated, structured hard chrome layer; process control during coating leads to the formation of hard chrome droplets; stochastic distribution of calotte-shaped packets in the sheet metal [ZIMN98].

Texturing does not necessarily lead to friction coefficients that are lower than those of MF surfaces. However, they do shift the appearance of tool wear to higher surface pressures [STAE98].

2.8.6.2 Surface Topography of Materials for Massive Forming

Depending on the size of the workpiece, either wire or rod-shaped semifinished products are used as the starting material in massive forming. In cold forming, these are generally provided with a lubricant carrier layer, which is applied in the case of wire before and in the case of rods after the detachment of a blank (Sect. 2.8.4.2). Before applying these layers, the materials are often subjected to mechanical surface treatment, which influences the topography of the surface [BAY94].

It has been shown that blasting treatment (e.g. sand or shot blasting) leads to improved adhesion of the lubricant carrier layer compared to scalping, which due to the roughening of the surface in addition to the cleaning effect of the jet. But even without the use of carrier layers, the topographies created lead to improved friction conditions compared to fully untreated raw material. This can be attributed to the lubricant pocket effect.

2.8.6.3 Surface Topography of Forming Tools

In addition to the surface topography of workpieces, the formation of the tool surface also affects friction and wear. The essential difference is that the topography of tools is subject to significantly fewer changes. Those that nonetheless occur result less from plastic deformation, but are rather the result of tool wear.

Effect of Tool Finishing on Topography. Firstly, the tribological properties of a tool are influenced by the tool finishing process. In terms of wear, as a rule polished tools may be evaluated positively (Sects. 2.8.3.2 and 2.8.3.3).

It is also possible to create lubricant pockets by means of diverse blasting methods (e.g. shot blasting). These rarely used methods may indeed be used to strengthen the rim zone of tools and to induce compressive residual stresses, which can have positive effects on surface disruption. Since however blasting also involves a significant topographical alteration, the tool's tribological behaviour is also influenced.

Influence of Tool Coatings on Topography. While the roughness characteristic values of tool surfaces are only rarely significantly altered in most coating processes, layer microtopography does play a role in the interaction of surface and lubricant. For example, lubricants on the surface of columnar PVD layer crystals are much more adhesive than those on completely smooth layer surfaces. This can improve the effect of the lubricant (Fig. 2.76).

This effect can be exploited especially in the case of monolayers and multilayer coatings with relatively large single layer thicknesses, since the columnar layer structure can be created particularly prominently in this case. The lubricant penetrates into the hollow spaces between the crystallites and is thus borne into the action interstice between the tool and the workpiece. Depending on the selection of parameters in the coating process, the layer structure and its effects can vary. This was shown in [GERB02] using the example of CrN coatings.

Effect of Laser Processing on Topography. In some newer applications, laser-textured tools are being used in both massive and sheet metal forming [NEUD04, POPP04]. Similarly to the texturing of skin pass rolls for textured sheet metals, small pits are introduced into the tool surface by means of an excimer laser. These pits then serve as lubricant pockets in the forming process (Sect. 2.8.6.1). In principle, texturing can be carried out for all tool materials. In the case of coated tools, we differentiate between pockets introduced prior to and after coating [POPP04].

The pointwise laser remelting of tool surfaces is a special case. Here, hard material powder (e.g. TiC) is added to the surface of the tool and “implanted” into the surface using a laser beam [STEI99]. The implanted areas remain intact under tribological load, while the surrounding areas are reset by wear. The result is a self-sustaining surface structure.

Fundamentally, the same hydrostatic and hydrodynamic effects are found at the lubricant pockets as is the case with sheet metal materials, only that the shape of the lubricant pockets is not altered by plastic deformation during the forming process.

In exchange, workpiece material is squeezed into the pockets during the forming process, reducing the volume of the pockets and leading to an increase in pressure in the lubricant. This process can however also have a negative effect if the workpiece material is sheared off at the pocket flanks and remains in the pockets. On the other hand, it is advantageous that wear particles that can lead to abrasion during tool contact are collected in the pockets [POPP04]. While surface

quality is hardly affected in sheet metal forming, small elevations remain behind in the case of massive-formed components due to the imprinting of pocket geometries into the workpiece surface.

Overall, only in some cases an increase in tool life and a reduction of friction is possible by laser texturing forming tools.

2.8.7 Tribological Test Methods in Forming Technology

Tribological test methods are used in forming technology in order to test the tribological properties of materials and intermediates at little expense. Since it is often not possible for reasons of process reliability to test new tribologically effective products in everyday operation, simply designed experimental setups are used to help inspect those products. Tribological metrological and test engineering distinguishes between several task areas:

- experimental simulation of forming processes to discover friction and wear mechanisms
- determination of friction and wear parameters for the sake of process design and calculation
- comparison of materials and intermediates for process optimization
- quality surveillance and control of tribotechnical materials and lubricants.

In order to obtain meaningful test results that are applicable to real forming processes, it is important that the tribological conditions in the test process model those in the real process well. This requires material, kinematic and thermal similarity between the test and the forming process that is as close as possible. The test results are thus more or less relevant depending on the model test's degree of abstraction compared to the actual tribological system [GFT02]. Results from different experimental setups can deviate from each other considerably.

2.8.7.1 Equipment for Lubricant Testing

There are many simple standardized procedures for the general tribological testing of lubricants, whereby the highly abstracted tribological systems in the test devices used do not simulate a particular application. They serve rather to assist in the development of new lubricants in the selection of promising formulations and in quality assurance for existing products. A rough classification of lubricants with respect to additive content and wear protective effect is also possible with these processes. In some cases, a friction coefficient can also be determined, which cannot be used in the calculation of forming processes due to lacking applicability. Figure 2.79 provides an overview of the most important methods.

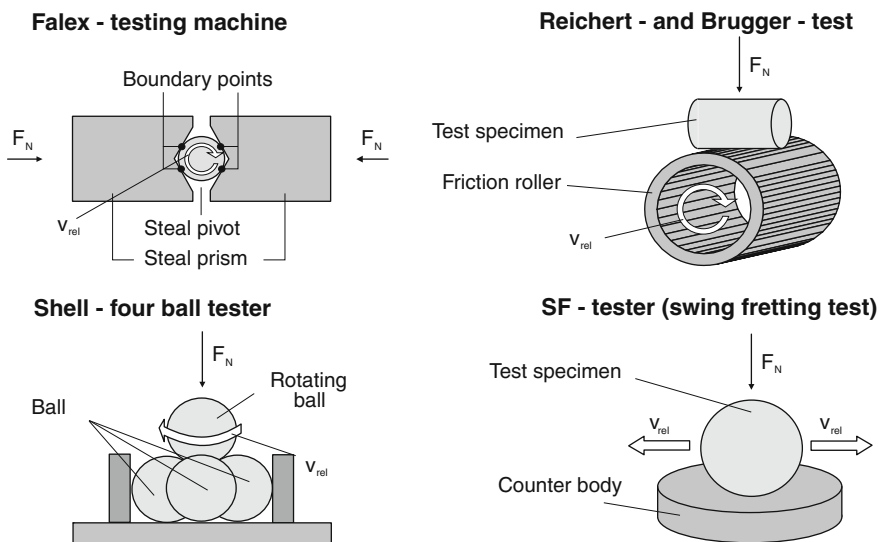


Fig. 2.79 Schematic representation of different lubricant test equipment [DIN77, DIN00, DIN04b]

These test methods differ not only with respect to geometric and tribological conditions but especially with respect to the response characteristics of particular additives (Fig. 2.80) [SCHU04a].

With respect to forming technology, the biggest disadvantage of these test methods is that the results obtained are not applicable to the tribological systems of forming processes. They are thus not suitable for selecting lubricants for particular applications. This is because both the tribological system components, which are usually manufactured from roller bearing steel 100Cr6, and the stress collective (surface pressure, relative velocity, temperature) are largely standardized and hardly correspond to those of forming processes. Only the SRV test provides the possibility of varying a large number of load parameters. But here too, it is impossible to take surface enlargement into consideration, which takes place in many forming processes. Nonetheless, the results of these standard tests are often the only tribological data provided by the lubricant supplier.

For a targeted choice of particular lubricants for particular forming processes therefore, further test methods must be used that approximate the tribological conditions in a better way (Sects. 2.8.7.3 and 2.8.7.4). In the following, the most common methods and devices used in lubricant testing will be briefly explained [SCHU04a]. It should be noted that in all of these processes, standard test objects (base and counter bodies) made of 100Cr6 are used. In this way, the results of the tests can be compared, yet they are generally not transferable to forming processes.

Falex Testing Machine. A soft steel pin rotates under load in an oil bath between two hardened steel prisms. The revolutions per minute (290 min^{-1}) is held constant; the load is increased in three stages. Contact of the test object takes

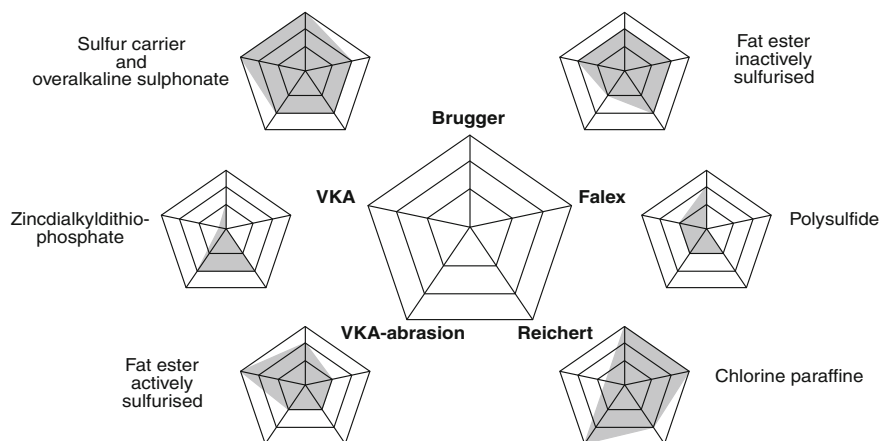


Fig. 2.80 Response characteristics of different wear-protective additives in various lubricant test equipment [SCHU04a]

place at four points in line contact. The test determines the scuffing load (fracture of the shaft at the predetermined breaking point) or, surviving all three load points, the wear on the steel pin.

Shell four ball tester. The lubricant is tested with a four ball system consisting of a rotating ball sliding on three balls identical to it [DIN77]. The test forces can either be increased gradually until the balls fuse, or, under constant test force, the calotte diameter of the three stationary balls is measured after a predetermined test time. Methods based on this standard function to determine characteristic values for lubricants with active substances that should allow for high surface pressures in the mixed friction range between surfaces in relative motion.

Reichert's Fretting Scale. In the case of this friction testing device, a firmly clamped test roller is pressed with a double lever assembly on a revolving slip ring, the lower third of which is submerged in the liquid to be tested. The revolutions per minute of the motor and of the slip ring revolving directly with it are set such that constantly enough liquid can enter the contact point (fretting location) between the test roller and the slip ring. Depending on the pressure absorption capacity of the liquid on the test roller, ground areas appear on the slip ring (elliptical wear marks), the size of which depends on the bearing capacity of the test liquid. The sharply delineated wear area allows for exact measurement, which is beneficial for an exact determination of the load bearing capacity of the test liquid. The pressure absorption capacity is the larger the smaller this wear mark is after a certain run time or distance (100 m of the circumferential path of the slip ring).

Brugger Lubricant Testing Device. To carry out a test run, a certain small amount of the lubricant to be tested is applied to the friction roller, and a cylindrical test piece is pressed against the still stationary roller with constant force. The test begins when the friction roller is set in rotational motion. The duration of the test is 30 s. According to Brugger, loading capacity, measured in N/mm^2 , is the

quotient of the pressing force of the test piece on the friction roller and the size of the wear area on the test piece [DIN00].

SF (Swing Fretting) Tester. The metrological principle is that an upper test piece (ball—point contact, standing cylinder—surface contact, lying cylinder—line contact) is moved in an oscillating manner on a ground or lapped surface (bottom test piece—counter body) [DIN04b]. The substance under investigation is located between the test pieces. The friction coefficient is recorded throughout the entire test period. In addition, the lubricant and galling mark can either be optically evaluated, or the galling mark can be measured. The big difference of SF testing from other test methods in the mineral oil industry is that a large number of parameters can be altered. Not only the test force (surface pressure) but also the test temperature, frequency of oscillation, amplitude (path traversed by the upper test piece) and the test time can be adjusted. Also, it is possible to select within a wide spectrum both the material of the test pieces as well as their geometries. In this way, tool coatings can also be tested. This variety of variables makes it possible to adjust the test conditions so that the actual process for which the lubricant was developed can be simulated as well as possible.

2.8.7.2 Devices to Test Coatings

Since coating technology is much younger than lubricant technology, it has been subject to significantly less standardization. In practice however, besides investigations for layer characterization (Table 2.17), often simple friction tests are carried out in order to determine the Coulomb friction coefficient against steel or wear behaviour.

The friction coefficient is carried out in simple pin-disc or ball-disc tribometers. A cylindrical pin or a ball, as a rule consisting of 100Cr6, is pressed with a defined pressing force against a coated disc rotating with a defined rotation speed. The result is the average friction coefficient after a test period of several minutes or hours. Furthermore, conclusions can be drawn concerning the run-in behaviour of the layer with the help of the course of the friction coefficient. With most layers, the friction coefficient decreases with time and continues towards a constant minimum. Not until advanced layer wear occurs the friction coefficient goes up again. In the case of adhesive or cohesive layer failure, the test is prematurely aborted.

Moreover, by measuring the galling mark, information can be obtained regarding the worn volume, given as a wear coefficient. The volumetric wear coefficient V_s is defined as the magnitude of the wear volume of the loaded surface divided by the effective glide path and the effective normal force. This is specified with the unit m^3/Nm . Sometimes planimetric wear (cross-sectional area of the galling mark) or gravimetric wear (mass loss) are also evaluated.

In some cases, the calotte grinding method in accordance with DIN V ENV 1071-6 is applied [DIN02]. The resulting abrasive wear coefficient cannot be

compared with that resulting from the pin-disc or ball-disc test, since the frictional load is different in kind.

In addition the flexibly applicable SF test can be used for the examination of tribological properties of coatings (Fig. 2.79) [DIN04b].

2.8.7.3 Test Procedures for Massive Forming

In order to test tribotechnical materials and lubricants under the demanding conditions of massive forming processes, a number of model tests have been developed with which the most varied massive forming processes can be simulated. The transferability of the test results is especially important in the area of massive forming, since it is difficult to reproduce the tribological conditions with sufficient precision. In massive forming, one must take into consideration, in addition to the consideration of the characterizing tribological system magnitudes of surface pressure (contact normal stress), relative velocity and temperature, the enlargement of the workpiece surface, which also influences the mechanisms of friction and wear to a decisive degree.

Figure 2.81 provides a comparison of typical cold massive forming process with some common model tests [LANG81a]. A comparison of the characterizing tribological system magnitudes is helpful in selecting the right model test. Figure 2.81 shows this using the example of relative surface pressure p_{\max} in relation to the initial yield stress k_{f0} .

It is clear that it is impossible to reproduce all cold massive forming processes equally well in model tests. Especially the extremely high requirements of reverse cup extrusion can not be met with these model tests. In this case however, it is possible to reproduce the process itself under laboratory conditions, in which case it is completely possible to make simplifications that reduce expense. For example, [RUPP97] suggests “free cup extrusion”. This is a reverse cup extrusion process without a die. One cup is not inserted into one single workpiece, but rather several cups side by side are inserted into a wire with a rectangular cross-section or in a semi-finished rod. With this model test, the major surface enlargement of the actual cup extrusion process, about 5 times that of the ring upsetting test, can be well approximated. In addition, [GRÄB83] proposes draw pressing (simultaneous reducing and drawing of a bar). This process is also characterized by relatively high surface pressures, relative speeds and surface enlargements, though not as high as in free cup extrusion.

Supplementing Fig. 2.81, Table 2.18 shows, next to the relative surface pressure, the values of maximum relative velocity v_R between the tool and workpiece in relation to the velocity v_0 of the forming tool as well as the surface enlargement A_1/A_0 of the workpiece [GRÄB83]. In contrast to the investigations in [LANG81a] (Fig. 2.81), here surface pressure p_{\max} is not related to the initial yield stress k_{f0} but to the average yield stress, which takes into account the strain hardening of the workpiece material.

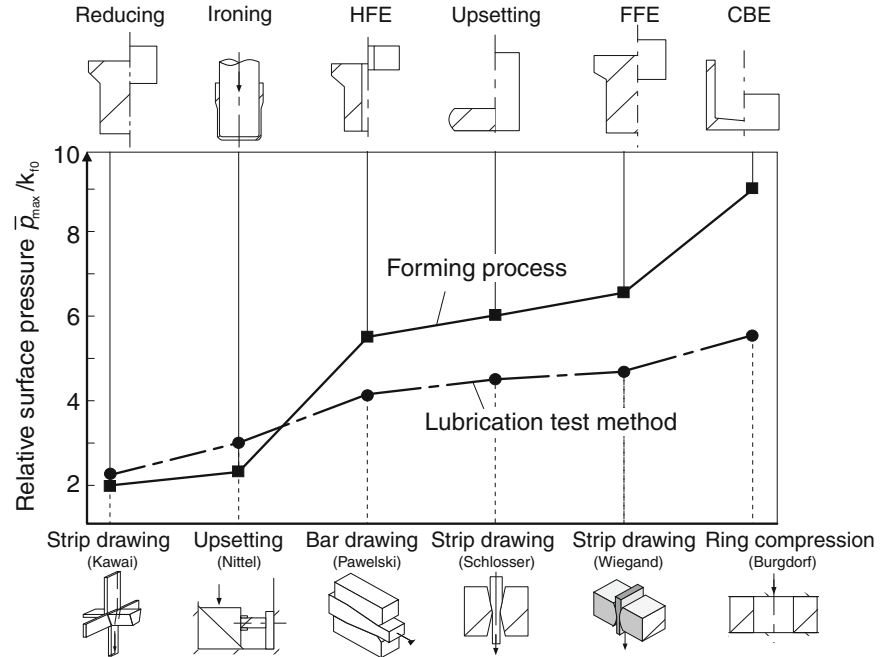


Fig. 2.81 Comparison of relative surface pressures in forming processes and model tests (acc. to Lange) [LANG81a]

Table 2.18 Comparison of characterizing tribological system magnitudes for different processes and model tests in massive forming [GRÄB83, RUPP97]

Process/model test	\bar{p}_{\max}/k_{fm}	v_R/v_{WZ}	A_1/A_0
Reducing	1.4	1.5	1.2
Ironing	1.6	2.3	2.2
Upsetting	3.4	2.4	4.5
Hollow forward extrusion (HFE)	3.2	5	4
Solid forward extrusion (SFE)	3.8	5.7	2
Cup reverse extrusion (CRE)	5.2	6.3	11
Strip tension (Kawai)	1.6	1.5	1.5
Strip tension (Wiegand)	1.6	—	—
Strip tension (Schlosser)	1.8	2	2.0
Rod tension (Pawelski)	1.9	1.5	1.5
Beveled upsetting (Nittel)	1.9	2	2.4
Ring upsetting (Burgdorf)	1.7	2	1.8
Draw pressing (Gräbener)	2.8	2.6	2.5
Free cup extrusion (Rupp)	4.3	—	9

Although, in comparison to draw pressing or free cup extrusion, it has limitations with respect to tribological load, ring upsetting as a test procedure is a good compromise between applicability, reproducibility and expense. It is thus very common and is often cited in the literature for determining friction coefficients for different states of lubrication [HORL89, KLOC04e, LI95]. For this reason, ring upsetting will be explained in more detail in the following.

The ring upsetting test has been known since the 1960s and permits a reliable experimental determination of friction values (friction coefficient μ and friction factor m) at low cost [BURG67]. It is suitable for investigations of both cold and hot forming. The ring-shaped specimen consists of a cylindrical body with a hole in the center (Fig. 2.82 top left). This specimen is compressed axially between two level, parallel upsetting panels, whereupon the geometry is measured and compared with the starting geometry.

During upsetting, a neutral surface can be formed between the inner and outer diameter with which the limit radius r_s is designated. The limit radius divides the specimen into areas of opposed material flow (Fig. 2.82 bottom left) [BURG67]. If there is a lot of friction, the inner diameter becomes smaller and the outer diameter larger. In the case of little friction, the neutral surface radius r_s is shifted inwards and the inner diameter becomes larger. The friction shear stresses in the contact zone bring about an outward curvature of the free external lateral surface (bulging), while the internal lateral surface bulges inwards or outwards depending on the direction of material flow.

The size of the ring specimens must be adjusted to the available press. Limitation of the maximum pressing force simultaneously entails limitation of the starting cross-section of the specimen. To determine the permissible starting cross-

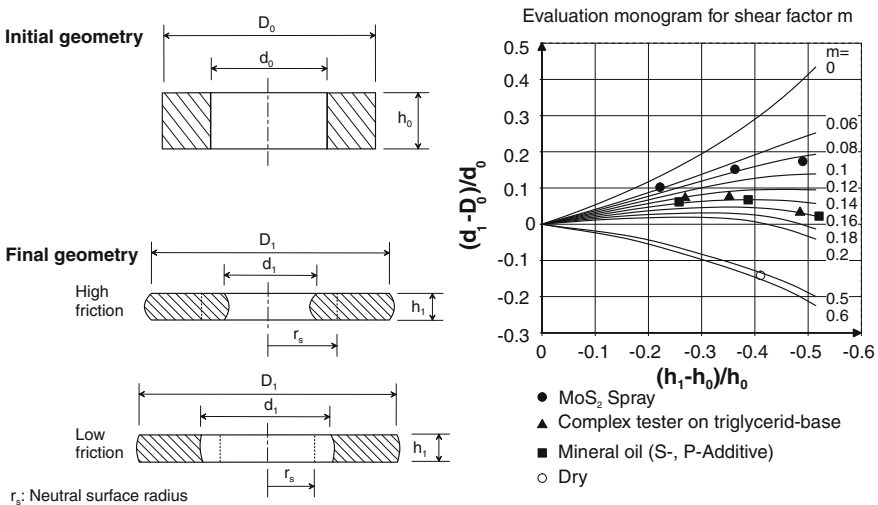


Fig. 2.82 Specimen geometry in ring upsetting and a monogram calculated via FEM simulation for the evaluation of ring upsetting tests; shear factor m for different lubricants [KLOC04e]

section, we assume that the largest height reduction occurring in the ring upsetting test is $\varepsilon_h = 0.5$ [BURG67]. Furthermore, a maximum allowable deformation resistance (yield stress) after a deformation of 2,000 MPa should not be exceeded. For a 200 t-press, the starting cross-section may not be larger than 500 mm². In order to prevent unsymmetrical deformations, the aim should be a wall thickness that is as large as possible or a large ratio of D_0/d_0 . On the other hand, the inner diameter should not be too small, which can cause the hole to close. Height is limited upwards by buckling problems and downwards by an unnecessarily high deformation resistance.

Considering the marginal conditions mentioned, a ring geometry with an outer diameter of 20 mm, an inner diameter of 10 mm and a height of 7 mm has proved suitable [BURG67]. The upper and lower edges must in every case be plane-parallel to each other.

In order to determine friction values for executed experiments, so-called evaluation monograms are required, which can be obtained in different ways, e.g. with the upper bound process or with the help of FEM (Sects. 2.4 and 2.5) [LI95]. When calculating the ring upsetting process, the shear factor m in the action interstice is varied between zero and one. Alteration of the inner diameter, reacting sensitively to the friction, is calculated and represented as a function of the shear factor in an evaluation monogram (Fig. 2.82 right). For a ring upsetting test with an unknown friction coefficient or shear factor, these can be taken from the diagram once the inner diameter has been measured.

The monogram in Fig. 2.82 right shows results from ring upsetting tests with different states of lubrication, in which the above mentioned ring geometry was used [KLOC04e]. It should be taken into consideration that the determined friction coefficients are not absolute values but average values across the entire contact surface between the specimen and the tool that were also determined along the entire path traversed.

2.8.7.4 Test Procedures for Sheet Metal Forming

For the evaluation of friction conditions between the tool and sheet metal material, different model tests have been developed with which the effects of various lubricants and the surface condition of the sheet metal can be investigated.

Strip Drawing Test. The most important model test for determining and assessing friction conditions in sheet metal forming is the strip drawing test. Strip drawing tests are carried out either with or without baffle. In the case of the strip drawing test without baffle, the “flat path test”, a metal strip is drawn through two friction pads that are pressed together with a defined normal force. The resultant frictional force on the metal strip is recorded with a metrological device, with which the Coulomb friction coefficient is determined. Instead of simple flat pads, it is also possible to integrate different shape elements into the friction pads for the flat path test. These days, both the simple blank holder area as well as draw beads are incorporated—the former with flat friction pads, the latter with corresponding

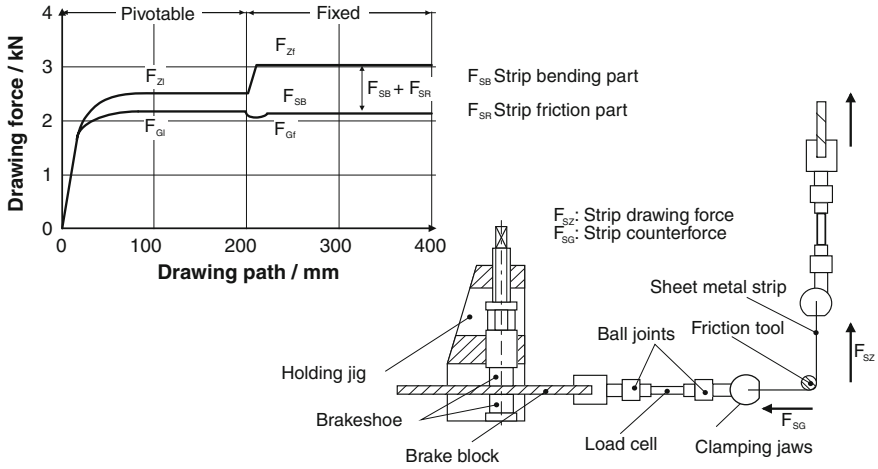


Fig. 2.83 Strip drawing test [WITT80]

shape elements in the friction pads. The strip drawing test with baffle shown in Fig. 2.83 serves to help investigate friction conditions on the die radius of deep drawing tools [WITT80]. In this short test procedure, a strip of the sheet metal material under investigation is drawn with a defined strip drawing force F_{SZ} over a cylindrical forming head, which represents the die radius. The required strip counterforce F_{SG} is applied with a holding device and measured with a force-measuring sensor.

The strip drawing force F_{SZ} consists of the sum of the counter-holding force F_{SG} , a force caused by friction F_R and a force required for bending the metal strip F_{SB} (Eq. 2.96):

$$F_{SZ} = F_{SG} + F_R + F_{SB}. \quad (2.96)$$

To determine the friction coefficient with the help of the Eytelwein equation (Eq. 2.98) however, the strip drawing force F_{SZ} must be reduced by the bending component F_{SB} . To determine its magnitude, a metal strip is pulled over a rotatably mounted forming head. In this way, the friction component disappears, and the bending component can be determined by measuring the drawing and counter-holding forces:

$$F_{SB} = F_{SZ} - F_{SG1}. \quad (2.97)$$

With the forces F_{SG} and F_{SZ} measured with a stationary forming head, the strip friction coefficient is:

$$\mu_{SZ} = \frac{2}{\pi} \cdot \ln \frac{F_{SZ} - F_{SG1}}{F_{SG}}. \quad (2.98)$$

The device developed by Pawelski is a variation on the classic strip drawing test [PAWE64]. In this case, friction measurements can be carried out under large specific surface pressures and large plastic deformations (Fig. 2.84).

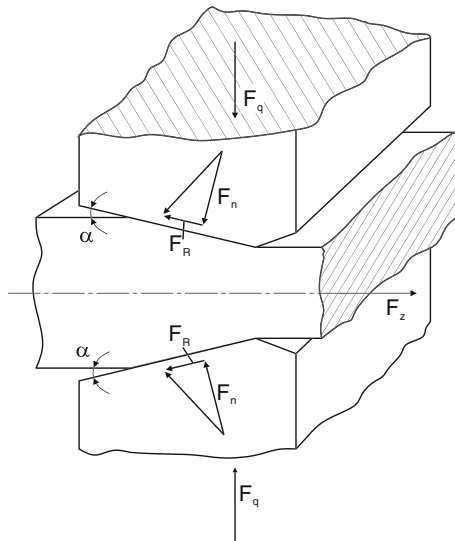


Fig. 2.84 Schematic representation of a test design for determining the friction coefficient in ironing [PAWE64]

The Coulomb friction coefficient μ is calculated from the drawing force F_z , lateral force F_q and the die clearance aperture angle α . It is an average value across the entire width of the test piece. For the friction coefficient we have:

$$\mu = \frac{\frac{F_z}{2F_q} - \tan \alpha}{1 + \frac{F_z}{2F_q} \cdot \tan \alpha}. \quad (2.99)$$

To determine the friction coefficient μ , only the condition of static equilibrium is used, while material equations for the elastic or plastic behaviour of both friction partners are not introduced into the calculation.

Ironing Test. With this test, it is possible to judge the quality of different lubricants used for ironing processes. To achieve this, the friction coefficient μ arising on the ironing ring is calculated from the particular forces active during ironing (Fig. 2.85). In order to obtain constant force conditions, an annealed cup that has already been ironed to a consistent wall thickness is used. While the punch force can be determined with a customary force-measuring device, the horizontal force is determined by means of the strain of the ironing ring with the help of an equation from elasticity theory. The test thus requires relatively high metrological

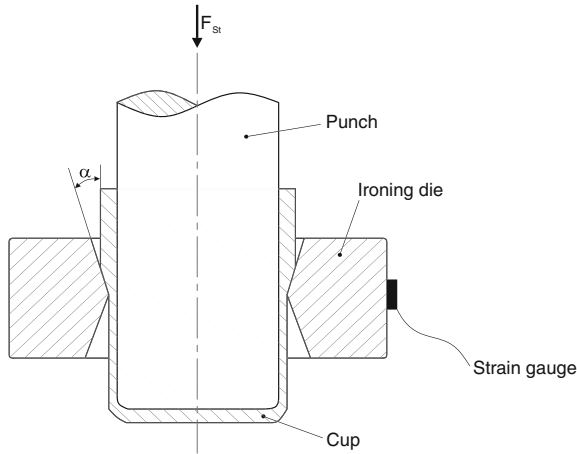


Fig. 2.85 Schematic representation of the test design used to determine the friction coefficient in ironing [SIEB54]

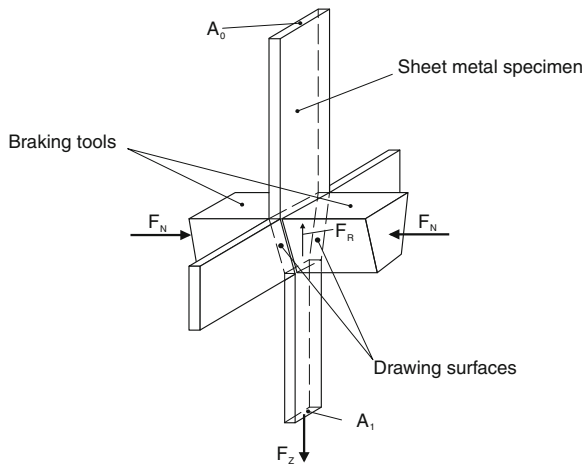


Fig. 2.86 Schematic representation of the test design used to determine the friction coefficient in the wedge draw test [REIH59]

expenditure (force and strain measurement). Making simplifying assumptions, the following determination equation is true for the friction coefficient at the ironing ring:

$$\mu = \frac{\frac{F_{St}}{2F_h} - \tan \alpha}{1 + \frac{F_{St}}{2F_h} \cdot \tan \alpha} \quad (2.100)$$

Wedge Draw Test. In the wedge draw test according to Reihle [REIH59], a metal strip is pulled through two tapered drawing surfaces, whereby the starting cross-section A_0 is reduced to the final cross-section A_1 (Fig. 2.86). The frictional force F_R is measured in the drawing direction at both brake components, which are pressed on the test strip with a normal force F_N . These load conditions are similar to those encountered in the flange when deep-drawing a cylindrical hollow body. We obtain the frictional coefficient with:

$$\mu = \frac{F_R}{F_N}. \quad (2.101)$$



<http://www.springer.com/978-3-642-36771-7>

Manufacturing Processes 4

Forming

Klocke, F.

2013, XX, 516 p., Hardcover

ISBN: 978-3-642-36771-7